Reduction of seawall overtopping at the Strand

by
George Bishop Roux

Thesis presented in fulfilment of the requirements for the degree of Masters of Science in the Faculty of Civil Engineering at Stellenbosch University

Supervisor: Mr Geoff Toms

March 2013

UNIVERSITEIT·STELLENBOSCH·UNIVERSITY
jou kennisvennoot • your knowledge partner

M.Sc. Eng. Thesis

(Port & Coastal Engineering)

Prevention of overtopping at the Strand

George Bishop Roux

Declaration

I declare that the entirety of the work contained herein is my own, original work, that I am the owner of the copyright thereof (unless to the extent explicitly stated otherwise) and that I have not previously in its entirety or in part submitted it for obtaining any qualification.

Date: 2012/12/01

Abstract

The Strand is located within False Bay and frequently encounters large quantities of wave overtopping over the coastal defences. This results in the damage of property and infrastructure and causes streets to be flooded. Physical modelling tests were done by a consultancy firm to determine a solution by making use of a recurve structure at the back of the beach.

This study is an expansion of the previous physical modelling that was done and focuses on several factors that were not tested by the consultancy firm that could have an influence on the overtopping rate and provide additional information on the recurve design. These tests were: (i) the effectiveness of the proposed recurve wall design in reducing overtopping was compared to a vertical wall; (ii) the influence that modifications to the beach profile such as the beach slope, beach width and beach level have on the overtopping rate; and (iii) the sensitivity of overtopping to changes in wave period was tested. The information gathered from these tests was used to propose a possible solution for the Strand.

Numerical modelling was done with Delft3D-Wave to determine the wave height at the back of the beach using a nested grid. The waves at the Strand are depth limited and therefore very sensitive to changes in water level. By altering the beach level the model showed how the significant wave height at the back of the beach changes. First estimates of overtopping were determined using the relevant empirical calculations from the EuroTop Manual 2007 for a vertical seawall. No estimate could be made for the recurve wall since it did not fall in the valid range of the equations.

From the physical modelling it was found that the overtopping reduced significantly from a vertical to a recurve seawall by a factor of about 50% depending on the wall height. All the prediction methods tested proved to be accurate in estimating the overtopping when the ratio of freeboard to significant wave height was ≤1.83. For non-breaking wave conditions the beach profiles that were gently sloped (1:50) and wide produced more overtopping than the beach profiles that were steep (1:10) and narrow. Increasing the beach level only decreased the overtopping if the water depth was shallow enough to cause the waves to break before they reached the back of the beach. Overtopping was found to increase with longer wave periods until the wave period became too long and the waves broke offshore which resulted in the overtopping decreasing.

Possible solutions to overtopping were proposed based on two beach levels and the implementation of a recurve seawall. Revised crest levels for the wall were made along the length of the beach for both the 1:20 and 1:100 year water levels.

Opsomming

Die Strand is in Valsbaai geleë en ervaar dikwels baie oorspoeling deur golwe bo-oor kusverdedigingswerke. Dit lei tot skade aan eiendom sowel as aan infrastruktuur en veroorsaak dat strate oorstroom. Fisiese modelleringstoetse is deur ’n konsultasiefirma gedoen om ’n oplossing te probeer vind deur van ’n teruggebuigde struktuur aan die agterkant van die strand gebruik te maak.

Hierdie studie is ’n uitbreiding van die vorige fisiese modellering wat gedoen is en fokus op verskeie faktore wat nie deur die konsultasiefirma getoets is nie. Dit kan moontlik ’n invloed op die oorspoelingstempo hê en verskaf bykomende inligting oor die ontwerp van die terugbuiging. Hierdie toetse is: (i) die doeltreffendheid van die voorgestelde ontwerp van die teruggebuigde strandmuur in die vermindering van oorspoeling word vergelyk met ’n vertikale muur; (ii) die invloed wat veranderinge aan die strandprofiel soos die helling van die strand, die wydte van die strand asook die strandvlak op die oorspoelingstempo het; en (iii) die sensitiwiteit van oorspoeling op veranderinge in golfperiode is getoets. Die inligting wat uit hierdie toetse verkry is, word gebruik om ’n moontlike oplossing vir die Strand voor te stel.

Numeriese modellering is met Delft3D-Wave gedoen om die golfhoogte aan die agterkant van die strand vas te stel deur van ’n genestelde ruitenet gebruik te maak. Die golwe by die Strand word deur diepte beperk en is dus baie sensitief vir veranderinge in die watervlak. Deur die strandvlakke te verander het die model getoon hoe die betekenisvolle golfhoogte aan die agterkant van die strand verander. Die eerste beramings van oorspoeling is bepaal deur van die relevante empiriese berekenings uit die EuroTop-handleiding 2007 vir ’n vertikale strandmuur gebruik te maak. Daar kon geen beraming vir die teruggebuigde muur gemaak word nie aangesien dit nie binne die geldige bereik van die vergelykings val nie.

Uit die fisiese modellering is daar vasgestel dat oorspoeling noemenswaardig met ’n gemiddeld van ongeveer 50% verminder is, afhangend van die muurhoogte. Al die voorspellingmetodes wat getoets is was akkuraat in die beraming van die oorspoeling wanneer die verhouding van vryboord tot betekenisvolle golfhoogte ≤1.83 was. Vir nie-brekende golftoestande het strandprofiele met ’n lae helling (1:50) en wat wyd was meer oorspoeling tot gevolg gehad as strandprofiele wat steil (1:10) en nou was. ’n Verhoging in die strand se vlakke het die oorspoeling slegs verminder indien die diepte van die water vlak genoeg was om die golwe te laat breek voordat hulle die agterkant van die strand bereik het. Oorspoeling is gevind om te vermeeder met verlengde golflengte tot dat die golflengte só lank geword het dat die golwe in dieper water begin breek wat aanlieding tot verminderde oorspoeling gegee het.

Daar word moontlike oplossings vir oorspoeling voorgestel gebaseer op twee strandvlakke en die implementering van ’n teruggebuigde strandmuur. Voorgestelde golfkruinvlakke vir die muur is al langs die lengte van die strand gemaak vir beide die 1:20- en 1:100-jaar watervlakke.

Acknowledgments

It would not have been possible to have completed this thesis without the guidance and support of the people around me. I would therefore like to express my sincerest thanks and gratitude towards the following persons:

1. My supervisor, Geoff Toms, for his continued guidance and advice throughout this study.

2. James Joubert for his help with the numerical modelling using SWAN as well as the data he provided for this study.

3. PD Naidoo & Associates for providing physical modelling results which were used in this study.

4. Marius Rossouw from the CSIR for advice regarding wave peak periods for False Bay as well as guidance with regards to the numerical model set-up that was used in this study.

5. Roelou Malan from the Somerset West Municipality for the guided tour of the Strand in order to show the information regarding the coastal defences which are currently in place.

6. Marilie van der Walt for proofreading this thesis.

7. My parents for their love and support throughout my studies.

Table of Contents

List of Figures

List of Tables

List of symbols

B_r	Horizontal distance of parapet from the wall
c_{pl}	Plunging coefficient
C_r	Reduction factor for crest
c_s	Surging coefficient
d_{n50}	Median rock diameter
E	Wave energy
g	Gravitational acceleration
G_c	Crest width
H	Local wave height
H_{mo}	Spectral significant wave height
H_o	Deep-water wave height
H_s	Significant wave height
$H_{2\%}$	Wave height exceeded by 2% of waves
h	Water depth at the toe of the structure
h_c	Freeboard
h_r:	Height of the parapet
h*	Impulsiveness parameter
k	Reduction factor for parapet
L_0	Deep-water wave length
L	Local wave length
n	Ratio of c_g to c
P	Permeability coefficient
P_c	Height of the vertical part of the wall from SWL
q	Overtopping rate
R	Runup
R_c	Freeboard
$R_{2\%}$	Runup exceeded by 2% of waves
S	Wave steepness
T_p	Peak period
T_{mo-1}	Spectral wave period
U	Energy flux
α	Probability density function scale parameter
ξ	Location parameter (extreme value distribution)
ξ_o	Surf similarity number or Iribarren number

$\xi_{m-1,0}$	Modified breaker parameter
β	Angle of the sea bottom or the structure
γ_b	Berm factor
γ_β	Oblique wave attack factor
γ_f	Roughness factor of the slope
κ	Cumulative distribution function shape parameter
ρ_s	Rock density
ρ_w	Water density
Δ	Relative mass density

List of acronyms

AMS	Annual Maximum Series
CRESS	Coastal and River Engineering Support System
EVA	Extreme Value Analysis
FSS	Flaring-Shaped Seawall
HAT	Highest Astronomical Tide
LAT	Lowest Astronomical Tide
LLD	Land Levelling Datum
MHWN	Mean High Water Neap
MHWS	Mean High Water Spring
ML	Mean Level
MLWN	Mean Low Water Neap
MLWS	Mean Low Water Spring
NCEP	US National Center for Environmental Prediction
NN	Neural Network
PDS	Partial Duration Series
SLR	Sea Level Rise
SWAN	Simulating WAves Nearshore
SWL	Still Water Level

1. Introduction

1.1 Background

Overtopping can cause significant damage to coastal properties and endanger people's lives. It is a significant problem in the Strand area which is located on the shoreline of False Bay in an area which encounters frequent overtopping.

Figure 1: Overtopping during August 2008 (Cape Town Gazette, 2008)

During 24 August 2005 a low pressure system measuring below 940 hPa in the southern Atlantic Ocean was semi-stationary for 4 days. This increased the time available for wave generation in the area and sent waves towards False Bay which arrived on 26 August. During this time a low pressure system was also located just south of False Bay and was travelling relatively slowly. The waves were measured with a Waverider buoy at Slangkop which is shown in Figure 25. The combination of the two systems resulted in a significant wave height of 10 m and a peak period (T_p) of over 18s (Hunter, 2005).

The storm caused the flooding of several roads due to overtopping and coastal infrastructure was severely damaged. A seawall, located in the area, was dilapidated and too weak for the

severe conditions which were imposed upon it. Three years later another large storm hit False Bay and again caused significant overtopping at the Strand. These conditions will worsen over time if rising sea levels occur.

Figure 2: Beach Road in the Strand during August 2008 (Cape Town Gazette, 2008)

After the storm conditions of August 2008 emergency coastal protection measures were required as a solution along a small section of the Strand which suffered the most during the storm. A rubble slope structure was placed in front of the existing vertical seawall to construct a composite vertical seawall. This has proved to be successful in the prevention of overtopping but this solution decreased the already narrow sand beach and it was only implemented for a small section along the Strand beach which experienced the most severe overtopping.

Physical modelling tests were done by a consultancy firm to find a solution by making use of a recurve structure and composite seawalls at the interface between the beach and the promenade, further referred to as the “back of the beach”. From the previous study several factors have been identified that were not tested. These could have an influence on the overtopping rate. This study is an expansion of the previous physical modelling that has been done and examines these factors in order to provide additional information on the effectiveness of the recurve wall design in this location.

The focus of the additional physical modelling tests is on (i) the effectiveness of the proposed recurve wall design in reducing overtopping compared to a vertical wall; (ii) the influence that modifications to the beach profile such as the beach slope, beach width and beach level have on the overtopping rate; and (iii) the sensitivity of overtopping to changes in wave period.

1.2 Objective

This study will determine how to reduce overtopping at the back of a beach by making use of seawalls and focusing on the Strand as a case study.

1.3 Literature study review

In the literature study several processes and characteristics of waves are explained to give insight into wave runup and overtopping. Thereafter an overview of the guidelines for overtopping is presented as well as the current methods that are used to prevent overtopping and the associated formulae for these methods are discussed. These include formulae for vertical seawalls, parapets/recurve walls, flaring-shaped seawalls, rubble mounds and composite vertical seawalls. The stability formula for the rock armour units is also provided for shallow water conditions.

The factors that influence the future rate of overtopping such as sea level rise, storm surge and wind and are presented as well as how they affect the overtopping process. An overview of the available methods in determining the extreme value analysis of the site conditions is discussed. The site conditions of the Strand were used in this study for both numerical and physical modelling.

Numerical modelling is discussed with a focus on SWAN and Delft3D-Wave which were used to determine the wave conditions in False Bay as well as the Strand.

For this study physical model tests were required in a wave flume and important issues regarding physical modelling are presented. The different hydraulic criteria, scaling ratios and model set-up are highlighted.

1.4 Methodology

An overview of the location of the Strand, current coastal defences, beach maintenance and problematic areas along the beach is provided to gain insight into the current circumstances of the Strand and to highlight the problems that the area faces.

Site conditions for the Strand are used in numerical modelling to determine the wave and water level conditions at the toe of the defensive structures which are located at the back of the beach. The site conditions of the Strand are determined from wind, wave and tidal data around the False Bay area. An extreme value analysis is performed on the wave and storm surge data in order to determine the different return periods for the wave and water levels.

The numerical modelling of the nearshore wave conditions is done by making use of Delft3D-Wave. The grid set-up, bathymetry and input parameters are discussed. The influence of beach changes, wind direction and wind speed are also investigated. The modelled wave height distribution at the back of the beach along the Strand is compared to the areas along the Strand beach that were identified as being problematic to determine the accuracy of the model.

The first estimates of overtopping could then be made by making use of empirical equations in order to determine the associated overtopping for the vertical wall and for a recurve wall, and to determine the main factors that influence the overtopping rate.

Physical modelling is used to find the effectiveness of a recurve wall compared to a vertical wall in reducing overtopping. Possible adjustments to the beach profile are tested to determine if overtopping could be further reduced by means of beach maintenance. The sensitivity of overtopping to changes in wave period is then looked at. The results of these tests are then discussed.

Physical modelling is also done to determine if the trends shown in the empirical calculations and the physical modelling are consistent. The physical modelling results are compared with empirical calculations, overtopping prediction methods and previous physical modelling results that were done by a consultancy firm. The overtopping results of freeboard level tests and beach level tests from the previous physical modelling are compared to the results of this study to determine if similar trends can be identified. The prediction methods that are used include the neural network overtopping software and the CRESS overtopping tool. Trends in the results are highlighted and discussed.

Based on the results of the numerical and physical modelling tests in this study, recommendations are made for the beach level and the recurve wall crest levels associated with different return periods. The recommended crest levels are determined by taking into account the effectiveness of the recurve wall in reducing overtopping as well as the wave height distribution along the Strand.

2. Literature review

2.1 Overtopping

Water that passes over a sea defence system is known as overtopping and is a major concern for coastal engineers. If the overtopping rate is great enough it can endanger people's lives and cause significant damage to surrounding structures.

Overtopping can occur in several different ways. The largest amount of overtopping occurs in conditions when the wave runup levels are high enough so that water can flow over the defensive structure. This continuous sheet of water is known as 'green water'. Overtopping can also occur when a wave hits a vertical structure such as a seawall which can send a column of water up and over the structure. Another form of overtopping is when a wave breaks on the defensive structure and causes water to splash over it, either by its own momentum or aided by onshore winds.

Figure 3: Wave overtopping at Kalk Bay harbour during August 2005 (Hunter, 2005)

Figure 3 is a photo taken at Kalk Bay during a storm in August 2005. Kalk Bay is located on False Bay and shown in Figure 25. The photo shows severe overtopping at the harbour breakwater. The person shown in the photo was a tourist who was washed off the breakwater by overtopping moments after the photo was taken (Hunter, 2005).

Several manuals have been published over the years to assist designers by offering guidance on how to determine overtopping volumes. The EuroTop Manual (Pullen et al.

2007) was published to replace the previous manuals on overtopping and runup such as the EU Overtopping Manual (1999), the TAW 2002 Technical Report on Wave Runup and Wave Overtopping at Dykes (Van der Meer, 2002), and Die Küste 2002 (EAK, 2002). The EuroTop Manual is a combination of the different manuals and calibrated many of the overtopping formulae by making use of the database from the EC CLASH project.

This literature review gives insight into wave conditions, ways to reduce overtopping, tools developed to predict overtopping, factors that influence overtopping, numerical modelling of nearshore waves and the physical modelling of overtopping.

2.2 Waves

Waves are generated by wind blowing across the surface of the sea. The wave height and period are determined by wind duration, speed and wave-wave interactions. The wave height can increase up to the point where it reaches maximum wave steepness before breaking. Waves undergo transformation as they gain and lose energy and change direction as a result of refraction, shoaling, diffraction, dissipation due to friction, breaking, additional growth due to wind, wave-current interaction, and wave-wave interactions (USACE, 2006). These processes affect wave propagation from the offshore deepwater region outside False Bay, towards the shallow water region around the Strand inside False Bay.

2.2.1 Refraction and shoaling

Wave propagation creates an orbital velocity field under the surface of the wave which extends to a depth of $L_o/2$ in deep water where L_o is the deepwater wavelength. When the depth is less than $L_o/2$, the orbital velocity field motion extends to the bottom and interacts with it. This causes changes in the wavelength, wave height (h), celerity (c), wave group velocity (c_g) and the direction of propagation.

Shoaling occurs when the waves enter shallow water and slow down. The energy flux (U), also known as the wave power, remains constant and compensation is made for the reduction in wave group velocity by an increase in wave height. This is shown with the following equations for two locations with different water depths and working from the assumption that no energy dissipation occurs (Bosboom & Stive, 2012).

$$U = Enc \qquad \text{Equation 1}$$

$$E = 1/8\rho_w g H^2 \qquad \text{Equation 2}$$

Therefore

$$U_1 = U_2 = H_1^2 n_1 c_1 = H_2^2 n_2 c_2 \qquad \text{Equation 3}$$

E: Wave energy

g: Gravitational acceleration

H: Wave height

n: Ratio of c_g to c

ρ_w: Water density

U: Energy flux

Refraction takes place in areas where waves propagate through depth contours at an angle. The sections of the wave crest that are located in deeper water travel faster than those in shallower water. This causes the wave crest to turn towards the depth contour.

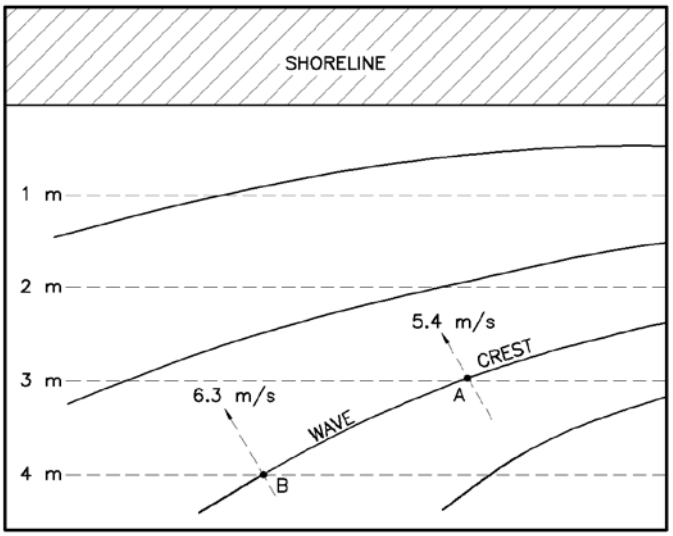

Figure 4: Wave refraction (USACE, 2006)

2.2.2 Wave breaking

Waves start to break when they reach maximum wave steepness or when the particle velocity associated with wave propagation exceeds the wave celerity. The characteristics of breaking waves in shallow water are described by the breaker type.

2.2.2.1 Wave steepness

In deep water, wave height can increase only up to a point where it reaches a maximum wave steepness (S) before breaking. It is generally accepted that for deep water, wave steepness is limited to 1/7. The wave steepness parameter is used to determine when waves start to break and is used to describe the characteristics of the breaking waves, known as the breaker type.

$$(S) = (H/L) \qquad \text{Equation 4}$$

As a wave approaches the shore, the length of the wavelength (L) decreases and the wave height (H) increases due to shoaling. This causes the wave steepness (S) to increase and the maximum wave steepness limit also changes. Miche (1944) determined a wave breaking equation based on Stokes wave theory relying on wave steepness. The equation is valid for both shallow and deep water and can be used to determine the water depth (d) at which breaking occurs. The 'b' in subscript indicates breaking conditions.

$$\left(\frac{H_b}{L_b}\right) = 0.14\tanh\left(\frac{2\pi d_b}{L_b}\right) \qquad \text{Equation 5}$$

In shallow water the equation for the breaker index is simplified to:

$$H_b/d_b \approx 0.88 \qquad \text{Equation 6}$$

The limit for wave breaking shown in Equation 6 is slightly different from solitary wave theory which is a non-linear wave theory valid for shallow water, in which the wave breaker index changes to approximately 0.78 (Bosboom & Stive 2012). Several studies have been done on the variability of the breaker index and Kaminsky & Kraus (1993) determined that the breaker index could range between 0.6 to 1.59 and has an average of 0.79.

2.2.2.2 Breaking type

Breaking waves can be divided into four wave conditions: surging, collapsing, plunging and spilling wave conditions (USACE, 1984).

- The crest of surging breakers remain unbroken as the wave moves towards the shore and the face of the wave experiences minor breaking as it travels up the beach.
- The crest of collapsing breakers also remains unbroken and the lower part of the face of the waves steepens and then falls.

- The crest of plunging breakers curls forwards and falls onto the base of the wave in the direction of the shoreline. This action produces large splashing.
- The crest of spilling breakers is unstable and falls down the face of the waves resulting in foamy water.

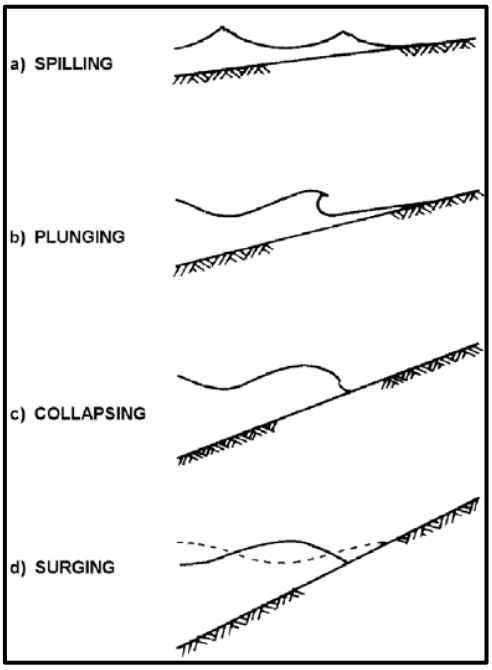

Figure 5: Breaker types (Hedges, 2009)

The surf similarity number (ξ_o), also known as the Iribarren number or the breaker parameter, is used determine the type of breaker.

$$\xi_o = tan\beta \left(\frac{H}{L_o}\right)^{-1/2} \qquad \text{Equation 7}$$

H: Local wave height

L_0: Deepwater wave length

β: The angle of the sea bottom or the structure

For a uniform sloping beach Battjes (1974) estimated the different breaker types for certain surf similarity ranges which are listed in Table 1.

Table 1: Breaker types (Battjes, 1974)

Breaker type	Surf similarity range
Surging	ξo > 5
Collapsing	3.3<ξo < 5
Plunging	0.5 < ξo < 3.3
Spilling	ξo < 0.5

2.2.2.3 Pulsating and impulsive

When a wave reaches a structure it can either be pulsating/non-impulsive, impulsive or near-breaking conditions. Pulsating conditions are found when the waves are small relative to the water depth and therefore have a lower wave steepness and the overtopping waves run reasonably smoothly over the seawall. No wave breaking occurs for pulsating waves.

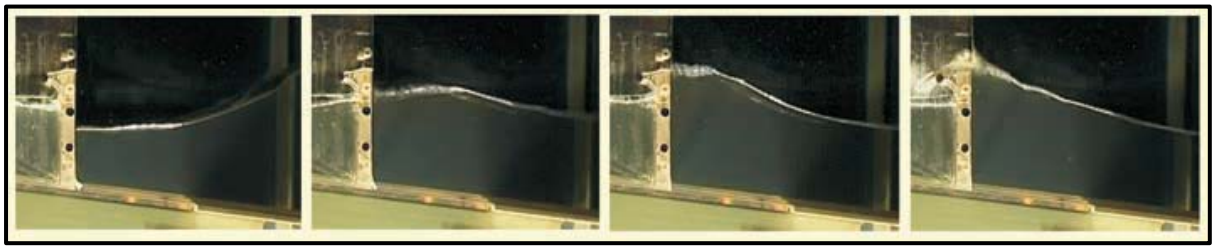

Figure 6: Pulsating/non-impulsive waves (USACE, 2006)

Impulsive conditions occur when waves are large in relation to the water depth and have a higher wave steepness. The waves break against the seawall with forces of up to 40 times larger than pulsating condition. This is due to air being trapped between the seawall and the wave that is breaking. This causes large plumes of water to shoot upwards and over the seawall and result in more overtopping than pulsating waves. Near-breaking conditions behave similarly to impulsive conditions (Pullen et al. 2007).

Figure 7: Impulsive waves (USACE, 2006)

Overtopping equations for vertical walls are separated for pulsating and impulsive conditions in the EuroTop Manual (Pullen et al. 2007). This approach is less accurate according to Goda (2009) since seawalls can experience pulsating, impulsive and near-breaking waves in a single train of random waves.

2.2.3 Wave runup

Wave runup elevation (R) is the extreme water level above the still water level (SWL) reached on a slope of a structure by a wave. Since the waves that reach the structure are irregular, only a few waves will reach the highest levels and the most common design level

used is $R_{2\%}$. This indicates that 2% of the waves in the design condition will reach and exceed the crest level. The origin of the 2% choice in runup is not known and was already used in some of the earliest international papers on runup (Pullen et al. 2007).

The basic equation for runup is (CIRIA; CUR; CETMEF 2007):

$$\frac{R_{2\%}}{H_s} = A.\xi_o + B \qquad \text{Equation 8}$$

A and B are fitting coefficients

ξ_o is the breaker parameter

Equation 12 and Equation 13 improved the runup estimation by compensating for oblique waves, shallow foreshore and bermed slopes by Van der Meer (2002). The equations are valid between $0.5<\gamma_b.\xi_{m-1,0}<10$. The coefficients A, B and C are presented in Table 2. A modified breaker parameter ($\xi_{m-1,0}$) is used by taking spectral wave period ($T_{m-1,0}$) into consideration.

$$\xi_{\mathrm{m-1,0}} = tan\beta \left(\frac{H}{L_{m-1,0}}\right)^{-1/2} \qquad \text{Equation 9}$$

The wavelength is determined with Equation 10.

$$L_{m-1,0} = \frac{\mathrm{g}T_{\mathrm{m-1,0}}^2}{2\pi} \qquad \text{Equation 10}$$

The spectral wave period ($T_{m-1,0}$) is used because it places more weight on the longer wave periods in a wave spectra and can be used for multi-peak wave spectra while the peak period (T_p) is only applicable for single peak wave spectra (Pullen et al. 2007).

$$\mathrm{T}_{\mathrm{m-1,0}} = T_p/1.1 \qquad \text{Equation 11}$$

Valid for: $0.5 \leq \xi_{m-1,0} < 1.75$.

$$\frac{R_{2\%}}{H_o} = A\gamma_b.\gamma_f.\gamma_\beta.\xi_{m-1,0} \qquad \text{Equation 12}$$

Valid for: $\xi_{m-1,0} \geq 1.75$

$$\frac{R_{2\%}}{H_o} = \gamma_f.\gamma_\beta.(B-C)/(\xi_{m-1,0})^{0.5} \qquad \text{Equation 13}$$

γ_b: Berm factor

γ_f: Roughness factor of the slope

γ_β: Oblique wave attack factor

The angle of attack of the wave has an effect on the amount of runup. The largest runup value is found when the waves travel perpendicular to the shore ($\gamma_{\beta=1}$).

Table 2: Runup coefficients(CIRIA; CUR; CETMEF 2007)

Coefficients	Deterministic calculations	Probabilistic calculations
A	1.75	1.65
B	4.3	4.0
C	1.6	1.5

2.3 Ways to reduce overtopping

The amount of overtopping is very dependent on the geographical features of the defensive structure, wave conditions and water level. The guidelines for overtopping will be examined as well as the following structures that are used to reduce the mean rate of overtopping: vertical seawalls, vertical seawalls with the addition of a recurve/parapet structure, flaring-shaped seawall, rubble mound and composite vertical wall.

2.3.1 Guidelines for overtopping

Overtopping can be presented as either mean rate of overtopping (l/s/m) or volume per wave (l/wave). The volume per wave varies greatly form the mean overtopping rate because waves are irregular and only the largest waves should reach the crest of the coastal defence and then overtop the structure. Goda (2010) found that the volume per wave can be between 5-20 times that of the mean overtopping rate. Franco et al. (1995) and Besley (1999) state that it may be unsafe to make use of the mean overtopping rate instead of the volume per wave rate. Figure 8 illustrate the relationship between the maximum overtopping per wave and the mean overtopping rate according to Van der Meer (2002), which shows that the volume per wave can be between 100-500 times that of the mean overtopping rate.

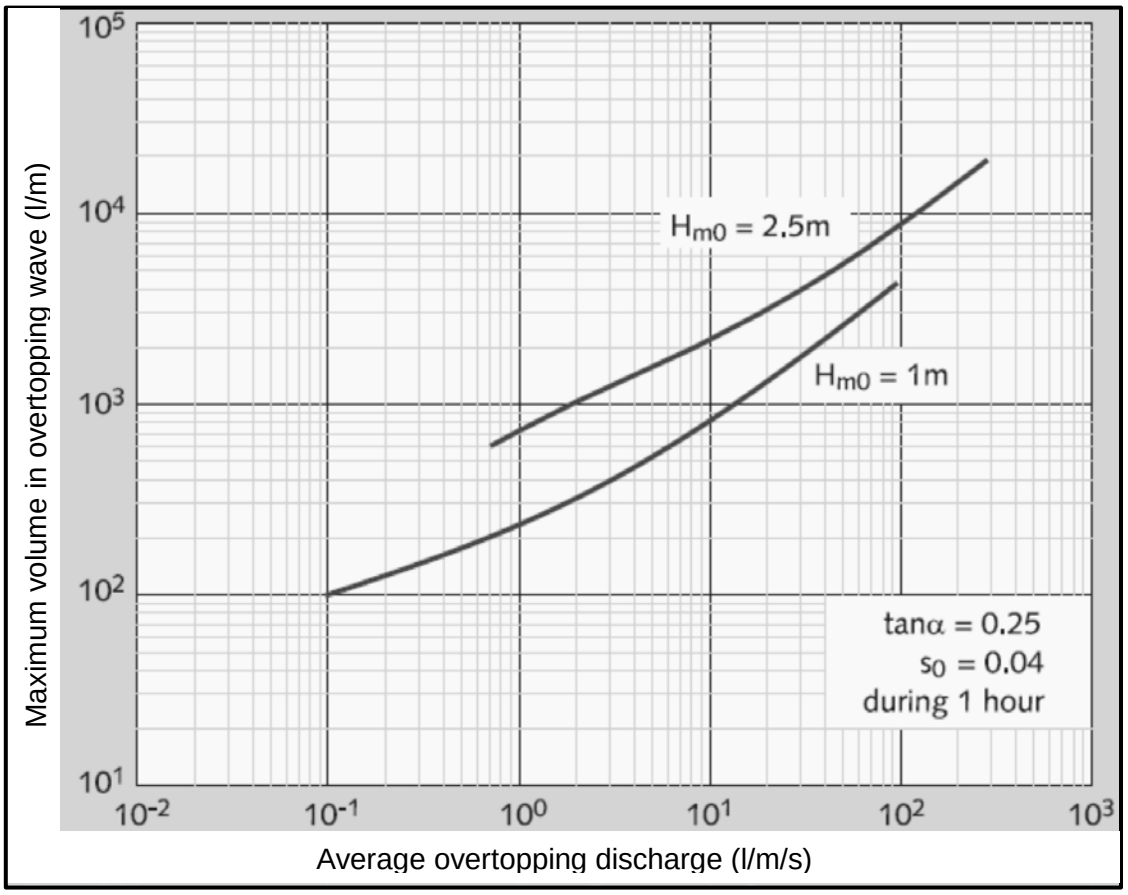

Figure 8: Relationship between maximum volume per wave and mean overtopping rate (Van der Meer, 2002)

The main reason that the mean overtopping rate is still used as the standard guideline is that methods for predicting peak volumes per wave are not well validated and therefore data for these events are still rare (Allsop et al., 2005). It is therefore difficult to specify the safety levels for the peak volumes per wave while the mean overtopping rate guidelines have been well defined.

The guidelines for the allowable mean rate of overtopping are presented in Table 3 from the CIRIA/CUR Rock Manual (CIRIA; CUR; CETMEF, 2007) and are based on work done within the European CLASH project (Allsop et al., 2005).

Table 3: Guideline for overtopping volumes (CIRIA; CUR; CETMEF 2007)

Pedestrians	**Overtopping** rate q (l/s/m)
Unsafe for unaware pedestrians with no clear view of the sea	q>0.03
Unsafe for aware pedestrians with clear view of the sea	q>0.1
Unsafe for trained staff who are well shod and protected	q>1-10
Vehicles	
Unsafe for driving at moderate or high speeds	q>0.01-0.05
Unsafe for driving at low speeds	q>10-50
Marinas	
Sinking of small boats set 5-10 m from wall. Damage to larger yachts	q>10
Significant damage or sinking of larger yachts	q>50
Buildings	
No damage	q<0.001
Minor damage to fittings	0.001<q<0.03
Structural damage	q>0.03
Embankment seawalls	
No damage	q<2
Damage if crest is not protected	2<q<20
Damage if back slope is not protected	20<q<50
Damage even if fully protected	q>50
Revetment seawalls	
No damage	q<50
Damage if promenade is not paved	50<q<200
Damage even if promenade is paved	q<200

2.3.2 Vertical seawall

One of the first estimates of vertical seawall overtopping was determined by Goda & Kishira (1975). They compiled diagrams from data recorded through physical modelling tests using irregular waves and taking wave deformation in the surf zone into account. This made the diagrams easy to use since the only information required is the deepwater wave height (H_o), the water depth at the toe of the seawall (h) and the crest elevation (h_c) relative to the still water level (SWL), which is also known as the freeboard.

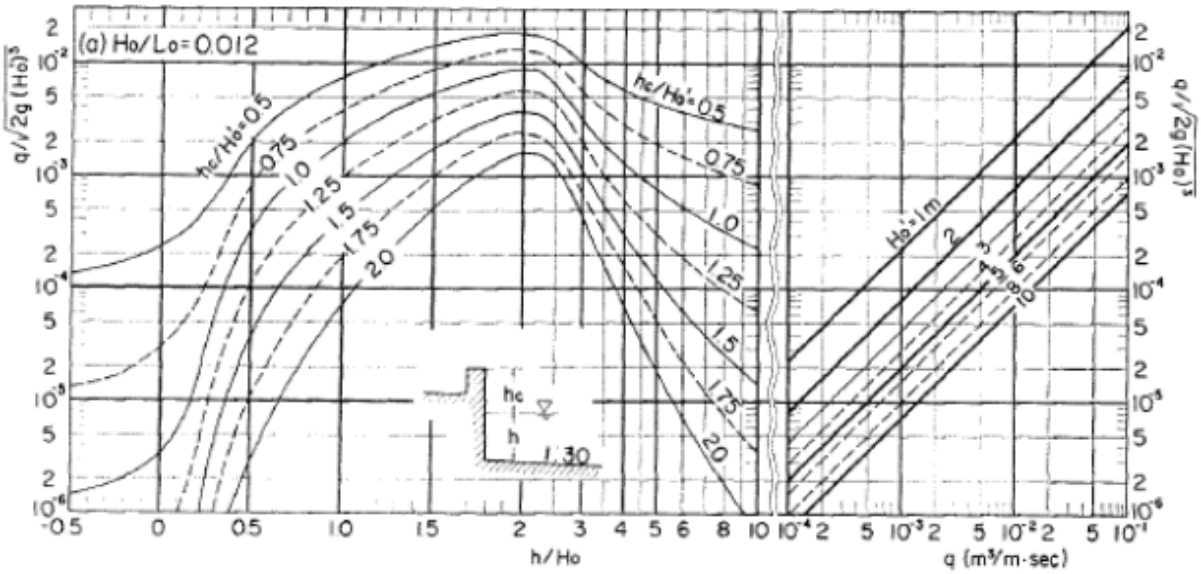

Figure 9: Vertical wall overtopping prediction diagram (Goda et al., 1975)

The EuroTop Manual (Pullen et al. 2007) makes use of overtopping equations instead of diagrams to determine the overtopping for simple vertical seawalls. It also separates formulae for pulsating waves and broken waves conditions which are based on modified formulae from Besley et al. (1998). These equations are slightly more complicated to use than Goda's diagrams since they require the designer to know the spectral significant wave height at the toe of the structure. However, the equations are more accurate since they were calibrated with the CLASH database.

An impulsiveness parameter (h_*) is used to determine which wave condition the seawall will encounter:

$$h_* = 1.35\ \frac{h_s^2 2\pi}{H_{mo} g T_{m-1,0}^2} \qquad \text{Equation 14}$$

For pulsating/non-impulsive conditions (h_*>0.3):

$$\frac{q}{\sqrt{g H_{mo}^3}} = 0.04 \exp\left(-2.6 \frac{h_c}{H_{mo}}\right) \qquad \text{Equation 15}$$

Valid over $0.1 < \frac{h_c}{H_{mo}} < 3.5$

For impulsive conditions (h_*≤0.2):

$$\frac{q}{h_*^2 \sqrt{g h_s^3}} = 1.5 \text{x} 10^{-4} \left(h_* \frac{h_c}{H_{mo}}\right)^{-3.1} \qquad \text{Equation 16}$$

Valid over $0.03 < \frac{h_c}{H_{mo}} < 1$

For broken waves:

$$\frac{q}{h_*^2\sqrt{g h_s^3}} = 2.7\,\mathrm{x}10^{-4}\left(h_* \frac{h_c}{H_{mo}}\right)^{-2.7} \qquad \text{Equation 17}$$

Valid over $h_* < \frac{h_c}{H_{mo}} < 0.02$

H_{mo}: Spectral significant wave height at the toe of the structure. It is equal to four times the standard deviation of the surface elevation ($H_{mo} = 4\sqrt{\mathrm{mo}}$).

h_s: Water depth at the toe of the structure

h_c: Height of the crest freeboard

None of the methods are 100% reliable and it is suggested that the most severe overtopping rate should be used when the methods are in a transitional zone between two overtopping regimes.

2.3.3 Recurve/Parapet

Franco et al. (1995) found that by adding a recurve parapet on top of a vertical wall it is possible to reduce the crest height by 30% for the same mean overtopping rate for relatively small discharges.

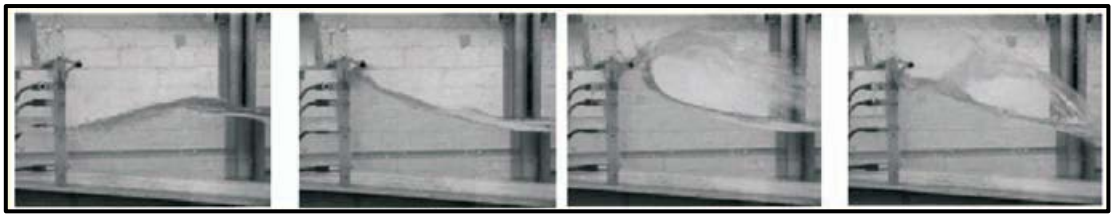

Figure 10: Effect of a parapet on a wave (Pearson et al., 2004)

There was no visible effect on the overtopping rate when the parapet was shifted forwards or backwards and the parapet was only effective in reducing the overtopping when the value of R_c/H_{mo}>0.3. For lower ratios the wave travels over the wall and the geometry of the crest no longer made a difference to the overtopping rate (USACE, 2006).

Kortenhaus et al. (2003) determined that if the mean overtopping rate for a plain vertical wall is known, it is possible to determine the reduction in overtopping rate by multiplying the overtopping rate by a reduction factor (k) by making use of the calculations in Figure 11. The

study was further expanded by Pearson et al. (2004) who determined that the reduction factor was unreliable when k<0.05.

$$k = \frac{q_{with\ recuve}}{q_{without\ recurve}}$$ Equation 18

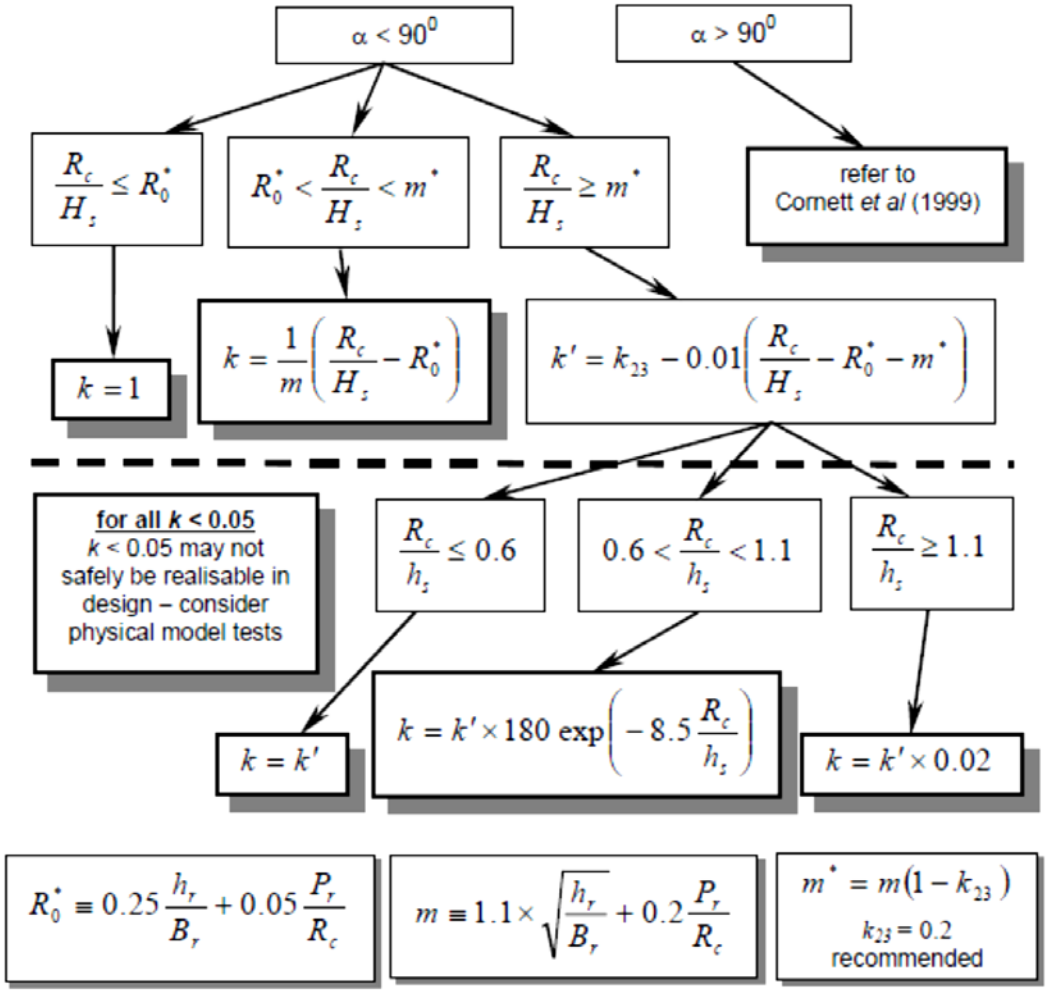

Figure 11: Diagram to determine the reduction factor (k) (Pearson et al., 2004)

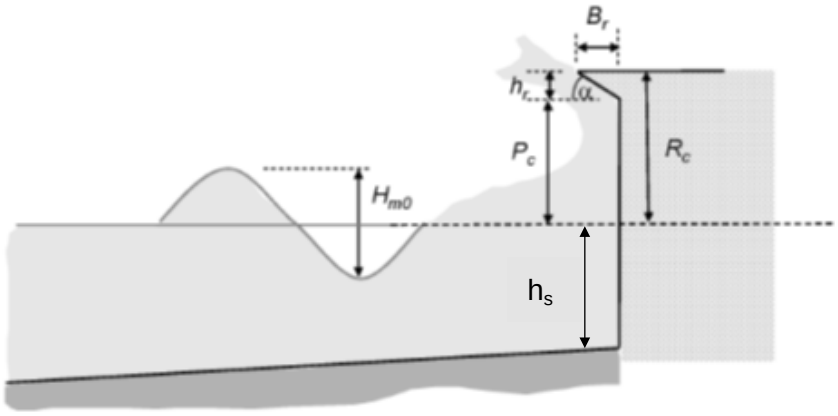

Figure 12: Vertical seawall with parapet (Pullen et al. 2007)

B_r: Horizontal distance of parapet from the wall

H_{mo}: Significant wave height at the toe of the structure

h_r: Height of the parapet

h_s: Water depth at the toe of the structure

P_c: Height of the vertical part of the wall from SWL

R_c: Crest freeboard

α: Angle of the parapet

Within the Neural Network (NN) overtopping prediction software (see section 2.4.3) the effect of the presence of a recurve wall is simplified by increasing the roughness of the structure (Hadewych, 2005). This approximation does give reasonably accurate results but further research was done by Van Doorslaer & De Rouck (2010) on the effect of a vertical wall with a parapet on a smooth dyke. It was determined that by introducing a vertical wall with a parapet the mean overtopping rate was reduced by up to 21 times compared to that of a smooth dyke. They introduced a reduction factor into Van der Meer's overtopping formula for dykes which is found in the TAW (2002) and the EuroTop Manual (Pullen et al. 2007).

2.3.4 Flaring-shaped Seawall

Murakami et al. (1996) studied a relatively new type of seawall design called a Flaring-Shaped Seawall (FSS) which is a non-overtopping seawall. The structure has a large radius which starts on the seabed and the radius increases along with the height of the structure. It was determined that the crest freeboard (h_c) can be approximately half of the offshore wave height while still under non-overtopping conditions.

This design produces a significant wall height if the offshore wave height is large and will therefore not be a practical solution for this study where a minimum wall height is required. Figure 13 shows the design of an FSS and it requires a low armour layer in front of the wall to help dissipate wave energy. This type of coastal protection is more expensive than a conventional composite vertical seawall because of the curved design of the FSS which makes it more difficult to construct.

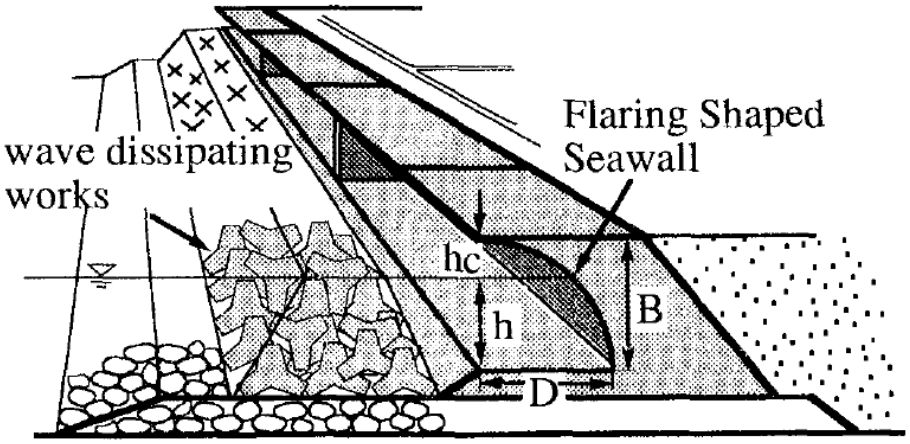

Figure 13: Flaring-shaped seawall (Murakami et al., 1996)

2.3.5 Rubble mound structure

Rubble mound structures are used to break waves and dissipate wave energy which helps to reduce the amount of overtopping. Rubble mound structures are more effective than smooth dykes because of the increase in surface roughness of the structure. Equation 19 is a modified mean overtopping equation for dykes from Pullen et al. (2007).

$$\frac{q}{\sqrt{gH_{mo}^3}} = 0.2\exp\left(-2.3\frac{h_c}{H_{mo}\cdot\gamma_f\cdot\gamma_\beta}\right) \qquad \text{Equation 19}$$

The equation accounts for the surface roughness of the rubble mound (γ_f) and the angle of attack of the wave relative to the shoreline(γ_β).

The length of the crest of the rubble mound has an effect on the amount of overtopping. A rubble mound structure with a crest width (G_c) that is approximately 3 nominal diameters of the stone armour layer wide will reduce the volume of overtopping. If the crest width is equal to the significant wave height at the toe the overtopping value will be reduced by up to 68% (Pullen et al. 2007).

Equation 20 gives the reduction factor (Cr) of overtopping due to the presence of a crest (Pullen et al. 2007).

$$Cr = 3.06 \exp(-\frac{1.5G_c}{H_{mo}}) \quad \text{Equation 20}$$

2.3.6 Composite vertical seawall

Franco et al. (1995) investigated the overtopping of composite and vertical seawalls. They found that composite breakwaters are greatly influenced by the slope, porosity, width and height of the armour crest. If the armour crest is below or at the still water level, the rate of overtopping increases by up to 15% more than a vertical seawall under the same conditions.

There is no standard design formula to determine the overtopping of a composite breakwater with the mound above the SWL for a shallow foreshore. For this scenario the equation for simple rubble mound structures is used and the freeboard level is taken at the height of the seawall or the Neural Network programme can be used (Pullen et al. 2007).

2.3.7 If the mound is below the SWL and the wave conditions are impulsive the equation for a normal vertical wave can be used. When the wave conditions are pulsating, modifications are made to Equation 19 as discussed further in the EuroTop Manual (Pullen et al. 2007). Stability

It is important to determine the stability of armour units used as protection to ensure that the structure is able to survive the duration of a storm and to know what level of damage can be expected. Figure 14 shows two seawalls which have different effects on the stability of the armour of the structure. In Figure a) the stability of the armour is not affected by the crown wall since it is below the crest height of the rubble armour but in Figure b) the vertical wall with the parapet does decrease the stability of the armour. According to the USACE (2006) manual, there is no accepted formula for determining to what extent the stability of such a structure is affected. In such a case revert to physical modelling.

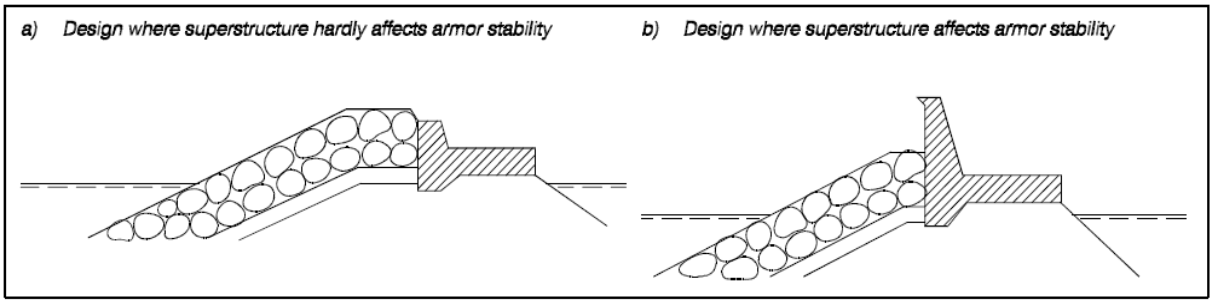

Figure 14: Effect of a vertical wall on armour stability (USACE, 2006)

The two best known stability formulae for rubble mounds are the Hudson formula and the Van der Meer equations (USACE, 2006).

The Hudson formula has several limitations such as: (i) only being applicable in the case of regular waves; (ii) not taking the duration of the storm into account; (iii) no clear definition of the damage level; and (iv) only applicable to non-overtopping and permeable core structures (Allsop, 2009).

The Van der Meer equations are able to include the effects of irregular waves, has a clear definition of the damage level, has a range of core permeabilities and distinguishes between plunging and surging wave conditions (Allsop, 2009). However, the equations are only applicable with regards to deepwater conditions. Further research was done by Van Gent et al. (2005) who modified the equations to include the effects of shallow water.

The following formulae are for rock stability in shallow water from Verhagen & Mertens (2009) which are based on the modified Van der Meer (1988) equations. They can be used to either determine the level of damage or the rock armour size.

$$\xi_{cr} = \left(\frac{c_{pl}}{c_s} P^{0.31} \sqrt{\tan \alpha}\right)^{\frac{1}{P+0.5}} \qquad \text{Equation 21}$$

For plunging conditions: $(\xi_{s-1.0} < \xi_{cr})$

$$\frac{H_{2\%}}{\Delta d_{n50}} = c_{pl} P^{0.18} \left(\frac{D}{\sqrt{N}}\right)^{0.2} (s_{m-1.0})^{0.25} \sqrt{cot \propto} \qquad \text{Equation 22}$$

For surging conditions: $(\xi_{cr} \leq \xi_{s-1.0})$

$$\frac{H_{2\%}}{\Delta d_{n50}} = c_s P^{-0.13} \left(\frac{D}{\sqrt{N}}\right)^{0.2} (s_{m-1.0})^{-0.25} (\xi_{s-1.0})^{P-0.5} \qquad \text{Equation 23}$$

c_{pl}: Plunging coefficient

c_s: Surging coefficient

D: Damage level

d_{n50}: Median rock diameter

$H_{2\%:}$ Wave height exceeded by 2% of waves at the toe of the structure

N: Number of waves in the storm

P: Permeability coefficient

$S_{m-1.0}$: Fictional wave steepness $\quad S_{m-1.0} = 2\pi \, H_{2\%} / (gT_{m-1,0}^2)$

$T_{m-1.0}$: Wave period

α: Angle of slope of the structure

ξ_{cr}: Critical breaker parameter

$\xi_{s-1.0}$: Breaker parameter $\quad \xi_{s-1.0} = tan\alpha / \sqrt{S_{m-1.0}}$

ρ_s: Rock density

ρ_w: Water density

Δ: Relative mass density $\quad \Delta = {(\rho_s - \rho_w)}/{\rho_w}$

2.3.8 Examples of seawalls

Seawalls are used in many locations in South Africa as well as in the rest of the world to protect the coastline and infrastructure from overtopping or direct wave impacts. Figures 15 - 20 show examples of seawalls being used to protect promenades and roads at the back of a beach.

Figure 15: Vertical wall at Port Elizabeth, Eastern Cape (FireflyAfrica, 2012)

Figure 16: Seawall with parapet at Cape Town, Western Cape (Cape Town Collectables, 2012)

Figure 17: Sloped seawall at Durban, KwaZulu-Natal (Steel, 2011)

Figure 18: Flaring seawall at Kunigami, Okinawa (Kobelco, 2012)

Figure 19: Rock revetment and seawall at Galveston, Texas (Marine Insight, 2012)

Figure 20: Sloped seawall with recurve, Nice, Provence-Alpes-Côte d'Azur (Patrick, 2005)

Figure 21: Vertical seawall at Weston-super-Mare, Somerset (The Telegraph, 2012)

Figure 22: Vertical wall at Teignmouth, Devon (Gayton, 2010)

In Japan flaring seawalls are used to protect several highways against typhoon waves. England and France both use a variety of different seawalls and have large tidal variations. The United States of America regularly experiences hurricanes and also makes use of a wide variety of coastal protection schemes in order to protect its coastline. These conditions are not experienced by South Africa which does not have a large tidal variance, and does not experience frequent hurricanes, but occasionally has to bear the brunt of severe storms.

2.4 Overtopping prediction tools

There are several free software sources available to the public in order to predict overtopping. Three programmes that will be discussed are the CRESS tool, the PC-overtopping software and the CLASH database.

2.4.1 CRESS Tool

Coastal and River Engineering Support System (CRESS) is the name of the Dutch online software that has a variety of calculations for coastal hydraulic problems. It was created by The Netherlands' Ministry of Infrastructure and Environment, Delft University of Technology and UNESCO-IHE. The software contains many components including overtopping calculations for rubble mound structure based on Franco et al. (1995) and vertical seawalls based on Van der Waal (1992).

2.4.2 PC-overtopping software

The PC-overtopping software was created from the TAW 2002 Technical Report on Wave Runup and Wave Overtopping at Dykes (Van der Meer 2002).

The software is useful in predicting the overtopping values of sloped structures and takes roughness and permeability into account. The following output is given by the software: 2% runup level, mean overtopping discharge and percentage of overtopping waves.

The software's drawbacks are that it can only be used with sloped structures and that the roughness and permeability of the crest of the structure is ignored (Pullen et al. 2007).

2.4.3 CLASH database

The CLASH programme is an acronym for 'Crest Level Assessment of Coastal Structures by full-scale monitoring, Neural Network prediction and Hazard analysis on permissible wave overtopping'. It was created in 2002 in order to solve the problem of the model/scale effect that was identified by the EC OPTICREST project which found an underestimation of wave overtopping in small-scaled models compared to the prototypes. The CLASH project also had to produce a generic prediction method to assist with crest height design or assessment (De Rouck et al. 2009).

Field measurements were conducted on prototypes at three sites in Europe and the prototypes were then modelled in scale physical models. This gave insight into the

scale/model effect which was later used in the EuroTop Manual (Pullen et al. 2007) to calibrate specific overtopping formulas and reduce the scaling errors.

A large database of more than 10 000 model tests was collected from previous tests that had been conducted over the past 30 years. It was required to fill in missing data in the database known as 'white spots' in order to cover a wide range of test scenarios. From this database a Neural Network programme ("intelligent system") was created to estimate the mean overtopping rate for a wide variety of structures which include vertical and composite seawall structures (Van der Meer et al. 2009). This Neural Network has 14 neurons as an input layer for the parameters used to describe the geometry of the structure and wave characteristics. Then there are 20 neurons in a hidden layer followed by a signal neuron as an output layer which returns the mean overtopping in $m^3/s/m$. Only tests with non-zero overtopping values are returned which poses a problem if there is uncertainty or if there is any overtopping for a certain design condition.

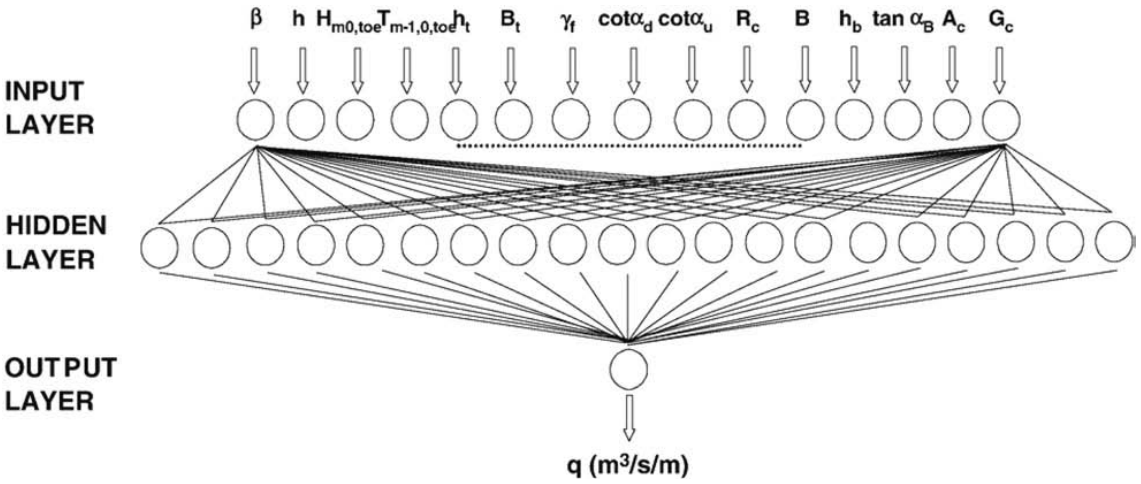

Figure 23: Neural Network layers (De Rouck et al., 2009)

There was a great deal of difficulty in choosing the right parameters for describing overtopping tests due to the complexity of structure. By making use of the CLASH database, it is possible to determine the expected amount of overtopping for a structure if a similar structure had been tested under similar wave conditions. The Neural Network can be used to determine first estimates of overtopping. It determines the type of structure from the input parameters and interpolates between the results in the CLASH database to determine the mean overtopping rate.

2.5 Other factors that influence overtopping

2.5.1 Storm Surge

Storm surge is an increase in water level and can be caused by wind set-up, reduced atmospheric pressure, rotation of the earth, coastline topography and storm motion (British Standards Institution, 2000). To determine the height of a storm surge the predicted tidal levels are subtracted from the measured tidal levels. For the design conditions of coastal structures it is often required that both the storm surge and significant wave height of the same return period should be used. This can lead to an over-conservative answer if the events are dependent and not interdependent (British Standards Institution, 2000). It is often difficult to statistically determine if events are interdependent and faced with the uncertainties of sea level rise, the conservative approach will be used in this study.

2.5.2 Wind

Apart from the contribution to storm surge, wind has three other major effects on the overtopping process (Kim, 2009):

1. It can change the shape of the incident wave resulting in different breaking conditions on a structure (pulsating or impulsive).
2. Splashing water can be carried over the crest of a structure and significantly increase the rate of overtopping in cases of low mean overtopping rates.
3. The physical parameters of the overtopping water can be changed such as the velocity, water distribution and overtopping loads.

According to Pullen et al. (2007), wind has little effect on the rate of overtopping of green water but can increase the volume of overtopping by up to 4 times in cases of water spray where the rate of overtopping is below 1 l/s/m. However, the effect of wind is very difficult to reproduce and is mostly ignored in physical modelling.

2.5.3 Sea level rise

Sea level rise (SLR) poses a serious problem for all low-lying areas near the coast. It increases the risk of flooding and increases the water depth allowing larger waves to reach the shore. The cause of sea level rise is largely due to thermal expansion of the oceans and the loss of land-based ice. Each process contributes roughly 50% to the total sea level rise. The average sea level rise for the 20th century was 1.7 mm/year but the global sea level is

projected to rise much more during the 21st century than during the previous century (Metz et al. 2007).

Even small changes in the sea level can cause significant changes in wave energy because it is sensitive to water depth. An increase in wave energy will lead to increased damage to the shoreline from the wave forces and wave runup (Kim, 2009). It is important to take sea level rise into account when determining the water levels as well as the associated wave height for the different water depths when conducting physical modelling.

The United States Army Corps of Engineers has specified in USACE (2009) that all new activities have to take sea level rise into account. They suggest that the three modified National Research Council (NRC, 1987) scenarios or the six climate change scenarios from the International Panel on Climate Change (IPCC, 2007) could be used.

The A1FI scenario for carbon emissions is the worst of the six case scenarios from the IPCC. It estimates that the global temperature will increase with 4 °C by 2099 from 1999. The A1FI scenario predicts that the world population will grow rapidly and will continue to rely heavily on fossil fuels for energy. This is estimated to cause the global sea level to rise by 0.26 m - 0.59 m. Both new and existing coastal defence structures will have to deal with this increase in sea level (Metz et al. 2007).

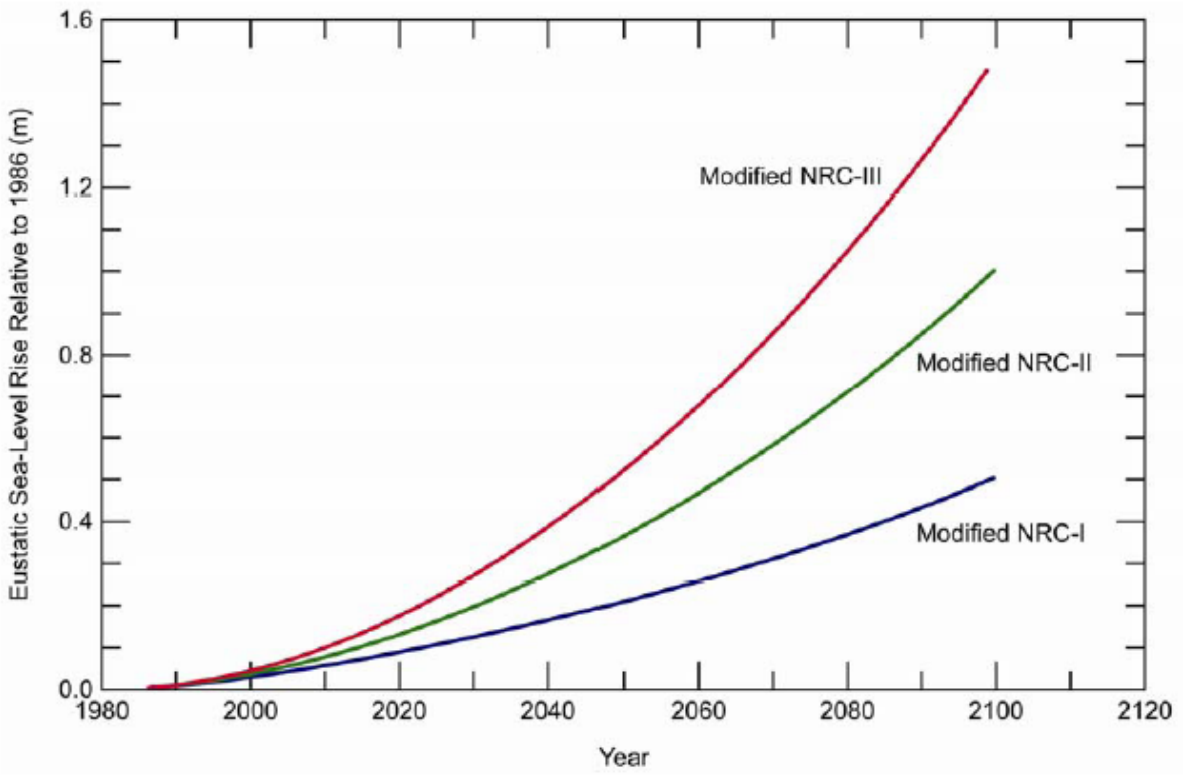

Figure 24: Modified NRC sea level rise scenario (USACE, 2009)

The USACE (2009) report suggests that the lowest estimate could be used as the minimum for a design but the decision is up to the designer and the client. This creates confusion since the lowest estimate of the IPCC scenarios is B1 and is between 0.18 – 0.38 m and the upper estimate of the modified NRC scenarios is 1.5 m for the year 2100.

Headland (2012) suggests that faced with the uncertainties in SLR one should rather design for shorter periods such as 20 year and then re-evaluate the SLR rate. The designs would then be adapted for the new design conditions and could then incorporate a new SLR scenario without increasing the cost to the design. He compared the cost between building once-off to building over a period of time and found that is considerably cheaper to build over time. This method is more flexible and is better suited for the uncertainties that exist in the different SLR scenarios although the method is only applicable in certain cases.

2.6 Extreme value analysis

When designing a coastal structure a return period is selected and then the significant wave height and water level associated with that return period is determined from the extreme value series using a distribution function. This can be done using an extreme value analysis model which determines the risks of extreme events by fitting a theoretical probability distribution to observed extreme events.

According to Goda (2010), the definition of a return period is the average duration of time during which the extreme events exceeding a certain threshold value would occur once. The return period is derived from a distribution function.

There are two methods used to select the data that is used in the extreme value analysis. The first is the total sample method and makes use of regular intervals of wave data that is collected in order to determine the extreme series. This method should be avoided when a large wave data observation records or hindcast wave data is used since the method does not have statistical independence between data. This method is only used when the length of the data series is in months and not in years (Edge, 1988).

The second method is the peak value method which identifies the peak wave height of individual storms by using a time lag between the data to determine the extreme value series. There are two different types of peak methods which are used: Annual maximum series (AMS) method which uses the largest wave height per year and the partial duration method which uses all the wave heights that exceed a threshold value (Goda, 2010).

There are many distributions that can be used for plotting the extreme value series such as the exponential, generalised Pareto, Gumbel, generalised extreme value, Weibull, Frechét, gamma, Pearson Type III, Log-Pearson Type III and lognormal (DHI 2009). When selecting the distribution to fit to an extreme value series, any of the four methods can be used to determine the most appropriate distribution function (Edge, 1988):

- Graphical method
- Least square method
- Method of moments
- Maximum likelihood method

The graphical method is used for an initial estimate but is subjective while the method of moments requires only a few calculations but is unable to handle the extreme series from the peaks over threshold method. The maximum likelihood method and least square method are generally used by statisticians.

The cumulative probability function F(x) and the probability density function f(x) of the selected distribution is used to determine the return period (T) of the extreme events. The extreme value series is defined as the variable X. The cumulative distribution function is the probability (p) that X is less than or equal to x (Abarbanel et al. 1992).

$$F(x) = P(X \leq x) \qquad \text{Equation 24}$$

$$p = 1 - F(x) = 1 - \int_{-\infty}^{x} f(y)dy \qquad \text{Equation 25}$$

The probability density function is the derivative of the cumulative probability function for a continuous random variable.

$$f(x) = \frac{dF(x)}{dx} \qquad \text{Equation 26}$$

The return period is defined as

$$T(x) = \frac{1}{1-F(x)} \qquad \text{Equation 27}$$

2.7 Wave modelling

Delft3D Suite is a process based model and makes use of the SWAN (Simulating WAves Nearshore) model to solve wave propagation. It is the prescribed model for TU Delft for coastal protection studies and nearshore modelling. SWAN accounts for wave generation and growth by wind, wave dissipation through whitecapping, bottom friction, depth-induced

wave breaking and non-linear wave-wave interactions. The model requires bathymetric detail, water level and wind field as an input (Deltares, 2011).

An energy density spectrum derived by Pierson & Moskowitz (1964) is used to describe the wave-generation process of how a turbulent wind field could interact with a sea surface. It was based upon measurements taken in the North Sea and is used to describe a fully developed sea state. The Joint North Sea Wave Project (JONSWAP), based on an extensive data set, found that the Pierson-Moskowitz spectrum did not have the correct peakedness. The JONSWAP data revealed that the observed spectrum was not fully developed and that the spectrum continued to develop with wave-wave interactions. They modified the Pierson-Moskowitz spectrum to form the JONSWAP spectrum which included a peakedness factor and a spectral width parameter (USACE, 2006).

SWAN describes waves with an action density spectrum (N) rather than an energy density spectrum (E) since the energy density is not conserved in the presence of currents. The action density spectrum is equal to the energy spectrum divided by the frequency. SWAN can use either the JONSWAP spectrum or a Pierson-Moskowitz spectrum to determine the action density spectrum. The independent variables are the frequency (σ) and the direction (θ) (Booij et al., 1999).

$$\mathrm{N}(\sigma, \theta) = \mathrm{E}(\sigma, \theta)/\sigma \qquad \text{Equation 28}$$

The evolution of the wave spectrum in the position (x,y) and time (t) is described by the spectral action balance equation which is shown for the Cartesian coordinates by Equation 29.

$$\frac{\partial}{\partial t}N + \frac{\partial}{\partial t}C_x N + \frac{\partial}{\partial t}C_y N + \frac{\partial}{\partial \sigma}C_\sigma N + \frac{\partial}{\partial \theta}C_\theta N = \frac{S}{\sigma} \qquad \text{Equation 29}$$

Starting on the left-hand side, the first term in Equation 24 represents the rate of change of action density in time. The next two terms represent the propagation of action in geographical space with propagation velocities C_x in the x space and C_y in the y space. The fourth term accounts for the shift in frequencies due to changes in depth. The fifth term accounts for the refraction and propagation in directional space. The last term is the source term (S) and represents the effects of wave generation, wave dissipation and non-linear wave-wave interactions(Booij et al., 1999).

2.8 Physical modelling

Coastal structures can often have complex geometry and physical modelling is still the best means of optimising the design (Hadewych, 2005). In large projects physical modelling is often combined with numerical modelling. The results of physical modelling are then frequently used to validate or calibrate the results of the numerical modelling.

Assessing overtopping can be done by either measuring the volume per overtopping wave or the mean overtopping rate. The distribution of overtopping from waves is uneven because ocean waves are irregular. This is the main reason for favouring the mean overtopping rate assessment. The results of the overtopping tests were found to be reproducible over an interval of 1000 waves or more. Intervals of a shorter period should be avoided because there is a greater variability in results when repeating tests (Hadewych, 2005).

According to Hughes (1993) the definition of a physical model is “a physical system reproduced so that the major dominant forces acting on the system are represented in the model in the correct proportion to the actual physical system.”

A physical model should ideally be designed to behave in all aspects in the same way as the prototype. This should include the mass, velocity, acceleration and resultant forces. Similitude is achieved when all the major influencing factors are in proportion between the model and the prototype. The factors that do not dominate in the model and which are not in proportion in the model must be insignificant in order not to influence the modelling process. The requirements of similitude depend on the degree of accuracy that is desired in achieving the same behaviour as the prototype.

Models can be geometrically, kinematically and dynamically similar to the prototype (Hughes, 1993). A model is geometrically similar to a prototype when all the geometric dimensions of the model are to scale when compared to the prototype. This can include small details of the prototype such as surface roughness which is more difficult to model accurately. Kinematic similarity is achieved when the ratio of motion between particles in the prototype and the model are correct. Dynamic similarity is achieved when all the forces on the model are in the correct scale to the prototype.

2.8.1 Hydraulic criteria

Achieving perfect similitude is not possible and most models can be simplified into the interplay of two major forces. This enabled the development of similitude criteria where the focus in each criterion is on the two major forces while accepting that the other forces are

small enough to be ignored. This can result in scaling errors when the smaller forces start having an effect on the model (Hughes, 1993).

- The Froude criterion is a parameter that expresses the influence of inertial and gravity forces.
- The Reynolds criterion is where inertial and viscosity forces dominate.
- The Weber criterion is where inertia and surface tension forces dominate.
- The Cauchy criterion is where inertial and elastic forces are most important.
- The Euler criterion is where pressure forces are the dominate force on the flow. Here the two forces are pressure and inertia forces.

For modelling overtopping and stability the Froude criterion will be used since the inertial and gravitational forces are dominant.

2.8.2 Scale ratios

A scale ratio is the ratio of a parameter of the prototype to the value of the same parameter of the model.

The equation for the length ratio is given by Equation 30:

$$N_L = \frac{Length_{\ prototype}}{Length_{\ model}} \qquad \text{Equation 30}$$

Table 4 gives the ratios of similitude of Froude and Reynolds and is used to determine the scaling equations for geometric, kinematic and dynamic similitude.

Table 4: Similitude ratios of Froude and Reynolds (Hughes, 1993)

Characteristic	Dimension	Froude	Reynolds
Geometric			
Length	$[L]$	N_L	N_L
Area	$[L^2]$	$N_L{}^2$	$N_L{}^2$
Volume	$[L^3]$	$N_L{}^3$	N_L^3
Kinematic			
Time	$[T]$	$N_L^{1/2}N_\rho^{1/2}N_\gamma^{-1/2}$	$N_L^2 N_\rho N_\mu^{-1}$
Velocity	$[LT^{-1}]$	$N_L^{1/2}N_\rho^{-1/2}N_\gamma^{1/2}$	$N_L^{-1}N_\rho^{-1}N_\mu$
Acceleration	$[LT^{-2}]$	$N_\gamma N_\rho^{-1}$	$N_L^{-3}N_\rho^{-2}N_\mu^2$
Discharge	$[L^3T^{-1}]$	$N_L^{5/2}N_\rho^{-1/2}N_\gamma^{1/2}$	$N_L N_\rho^{-1} N_\mu$
Kinematic Viscosity	$[L^2T^{-1}]$	$N_L^{3/2}N_\rho^{-1/2}N_\gamma^{1/2}$	$N_\rho^{-1}N_\mu$
Dynamic			
Mass	$[M]$	$N_L^3 N_\rho$	$N_L^3 N_\rho$
Force	$[MLT^{-2}]$	$N_L^3 N_\gamma$	$N_\rho^{-1}N_\mu^2$
Mass Density	$[ML^{-3}]$	N_ρ	N_ρ
Specific Weight	$[ML^{-2}T^{-2}]$	N_γ	$N_L^{-3}N_\rho^{-1}N_\mu^2$
Dynamic Viscosity	$[ML^{-1}T^{-1}]$	$N_L^{3/2}N_\rho^{1/2}N_\gamma^{1/2}$	N_μ
Surface Tension	$[MT^{-2}]$	$N_L^2 N_\gamma$	$N_L^{-1}N_\rho^{-1}N_\mu^2$
Volume Elasticity	$[ML^{-1}T^{-2}]$	$N_L N_\gamma$	$N_L^{-2}N_\rho^{-1}N_\mu^2$
Pressure and Stress	$[ML^{-1}T^{-2}]$	$N_L N_\gamma$	$N_L^{-2}N_\rho^{-1}N_\mu^2$
Momentum, Impulse	$[MLT^{-1}]$	$N_L^{7/2}N_\rho^{1/2}N_\gamma^{1/2}$	$N_L^2 N_\mu$
Energy, Work	$[ML^2T^{-2}]$	$N_L^4 N_\gamma$	$N_L N_\rho^{-1} N_\mu^2$
Power	$[ML^2T^{-3}]$	$N_L^{7/2}N_\rho^{-1/2}N_\gamma^{3/2}$	$N_L^{-1}N_\rho^{-2}N_\mu^3$

2.8.3 Model Bed Set-up

There are two types of physical models in coastal engineering: fixed bed and movable-bed models. In a fixed bed model the hydrodynamic forces cannot modify the bed and are used to study waves and currents. Movable-bed models allow the hydrodynamic forces to modify the bed which is made from loose material. This often creates scaling problems and is occasionally used to study sedimentary problems (Hughes, 1993).

3 Strand site conditions

3.1 Location

The Strand is located on False Bay. Parts of the bay provide natural shelter from the offshore wave conditions and the majority of the waves that reach the Strand propagate from a south-westerly direction. On the southern and eastern side, the Strand is shielded by the Hottentots-Holland mountain range which influences the local wind climate.

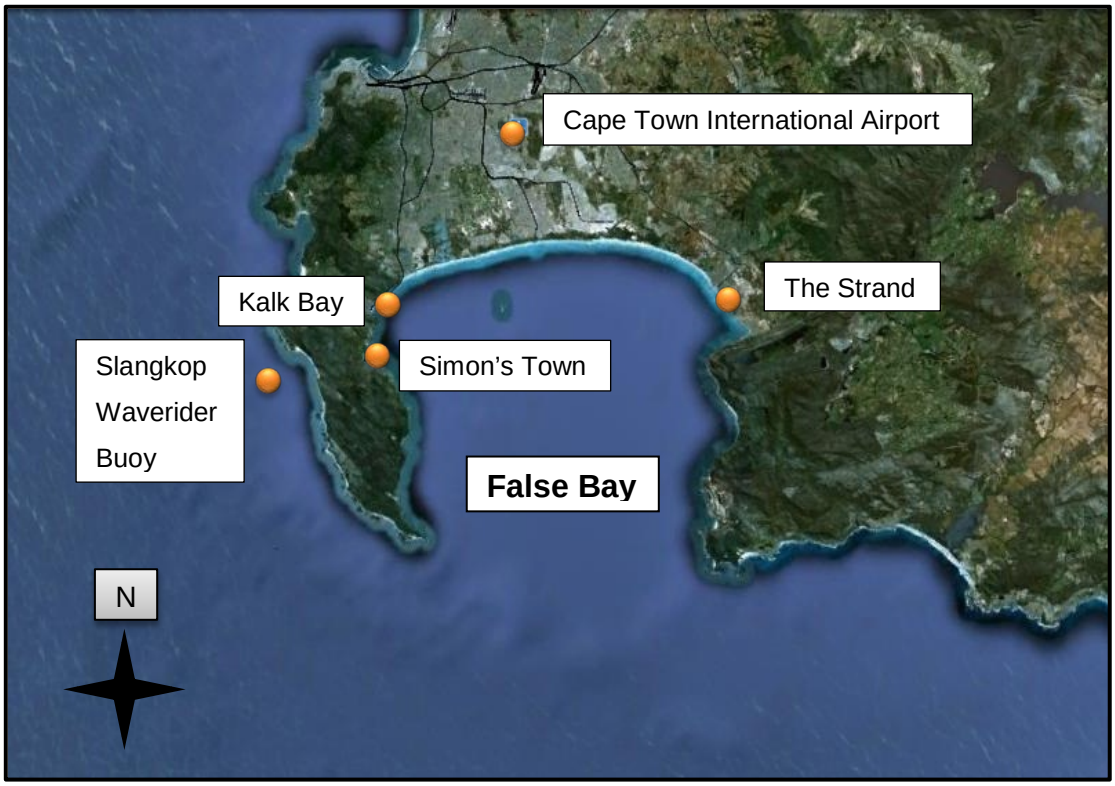

Figure 25: False Bay

Simon's Town is also located on False Bay and has a harbour which is used by the South African Navy. The harbour has a tidal gauge and data was made available for this study. The South African Navy has completed several surveys of the water depth inside the False Bay area and this data was also kindly provided for this thesis (SANHO, 2011).

Information about the wind direction and speed is recorded at Cape Town International Airport as well as at the Strand and this data was provided by the South African Weather Service for this study (SAWS, 2011).

Figure 26 shows the area of interest at the Strand which is located between the Lourens River and Greenways. The area contains a public road which is situated directly behind the beach and spans the entire length between the Lourens River and the beginning of Greenways. This area needs to be protected from overtopping, while trying to minimise the impact that the proposed coastal defences may be cause to the current visibility of the ocean for the public driving along the road, as well as developments situated along the road and pedestrians.

Figure 26: Area of interest in the Strand

3.2 Current defences

The current coastal defences along the coast at the Strand consist of various different solutions applied along the beach. The primary defences consist of natural sand dunes, vertical walls, recurve walls and composite vertical walls.

The vertical wall was constructed in the 1940s and the recurve wall was built between the Strand Pavilion and a large parking area in the 1960s. The vertical wall and recurve structures along the coast have reached the end of their design lifespan

and require urgent upgrading. The walls are made of concrete and many of them contain a number of cracks. In several locations large sections of the wall are broken.

The composite vertical structure was built in 2008 at location I shown in Figure 27 and spans 165m along the beach. The structure was built by simply adding a rubble mound structure in front of the existing vertical wall. This has proved to be successful in protecting the seawall from wave action and significantly decreased overtopping in the area but decreased the available beach area (at low tide).

Figure 27 and Table 5 give a description of the type of protection that is currently used at different locations along the Strand. The height provided in Table 5 was taken on top of the seawall and varies along the beach from locations A to I.

Figure 27: Locations of frequent overtopping

The yellow lines in Figure 27 indicate areas of concern that were identified by the local municipality's stormwater maintenance team. Locations E and H both have a seawall height of approximately 2 m above Land Levelling Datum (LLD) which is the lowest along the beach front and as a result these areas more frequently experience overtopping events during storms than other locations (Roelou Malan, personal communication, 5 August 2012).

Locations H to I have the lowest beach level in front of the seawall with the lowest point being only 0.8 m above LLD. This results in waves reaching the back of the beach at water levels of MHWS or above.

Location E has a moderately high beach level and narrow beach width. The seawall encounters no waves but occasionally experiences wave runup reaching the back of the beach. During times when the sand builds up to the top of the seawall at Location E, the wave runup is able to pass right over the wall and cause flooding.

Table 5: Varying seawall heights and types of protection

Location	Wall height above LLD (m)	Beach height in front of seawall above LLD (m)	Type of defence
A	4.0	3.8	Vertical wall and sand dune
B	3.2	2.2	Vertical wall
C	3.0	2.2	Vertical wall
D	2.8	2.6	Vertical wall
E	2.0	2.0	Vertical wall
F	4.0	2.0	Recurve wall
G	2.5	1.7	Vertical wall and sand dune
H	2.1	1.2	Vertical wall
I	2.6	0.8	Composite vertical wall

3.2.1 Sand dunes

Sand dunes offer a soft solution for preventing overtopping where beach width is sufficient to allow their formation. However, at the Strand, human interference has diminished their effectiveness in reducing overtopping and trapping windblown sand. In location A to B the sand dunes still provide the road with very good protection from the sea. In locations C, G and H the sand dunes provide limited protection. At all other locations there are no significant sand dune formations due to the narrowness

and low height of the beach. In Figure 28, near location G, an access road to the beach is shown. The road has been built in an area which had established sand dunes and has caused damage to them. The municipality also mechanically remove sand from the area to allow stormwater to flow towards the sea. These actions prohibit the dunes from further development.

In Figure 29 a stormwater outlet can be seen located next to a sand dune. This has caused erosion to the dune and exposed the vertical wall to wave action during high tide. The public also causes damage by walking on the vegetation of the dunes which destabilises them and leads to greater dune erosion over time.

Figure 28: Access road to the beach passing through a sand dune, near location G (05/09/2012)

Figure 29: Sand dune in front of a vertical wall, near location H (05/09/2012)

3.2.2 Vertical wall

Vertical walls at the Strand contain very little steel and are thin. This makes them weak as a defensive structure. The primary reason for the construction of the vertical wall was to keep sand from moving freely onto the pavement and not to prevent overtopping.

It has been found that the sand is occasionally blown or washed up to the top of the wall which can be seen in Figure 30. On high tides waves no longer reach the back of the beach but wave runup is able to and continues over the wall onto the road behind it. The maintenance teams try to limit the sand build up against the wall by manually removing it and taking the sand to the lower beach.

Figure 30: Vertical wall with sand built up to the top of the wall at location E (05/09/2012)

Figure 31: Vertical wall with stormwater outlet near location H (05/09/2012)

3.2.3 Recurve wall

A recurve wall was built between the Strand Pavilion and Location F to protect a slipway as well as a large parking area which is used by vendors. The wall consists of small precast concrete units that were added to the edge of the parking area. Figures 32 and 33 shows the condition of the wall and the vendors' stalls located directly behind it. The concrete has become brittle and shows significant damage as a result of reaching the end of its design life.

Figure 32: Recurve wall along the parking area at location F (05/09/2012)

Figure 33: Damaged recurve wall at location F (05/09/2012)

3.2.4 Composite vertical wall

A composite vertical wall has been built in the Strand at Location I which was part of emergency protection measures after the existing wall was knocked down by wave impact and the area suffered high volumes of overtopping during the storm in August 2008. The design was based on WSP (2008).

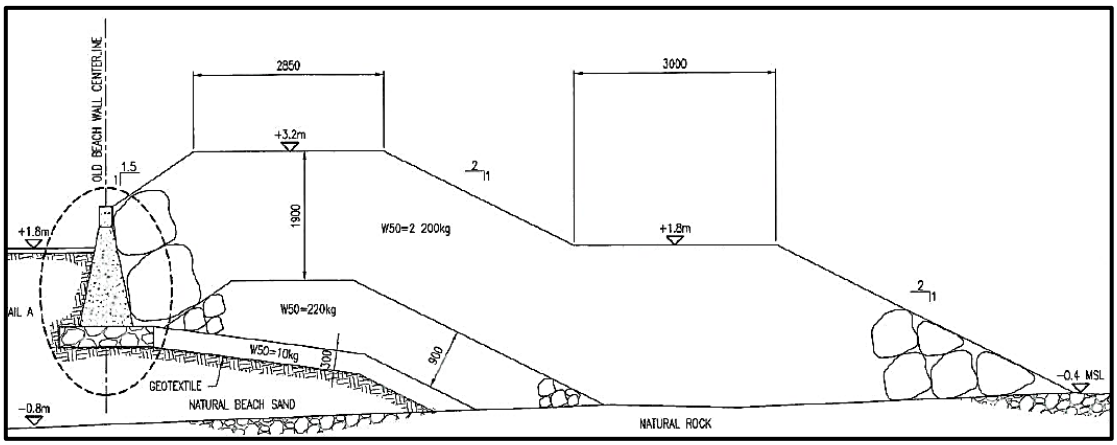

Figure 34: Composite vertical wall (WSP 2008)

Physical model tests were done by the University of Stellenbosch for PD Naidoo & Associates in 2011 as part of an Environmental Impact Assessment and re-assessment of the structure (IWEE, 2011). The structure was able to reduce overtopping considerably and modelled overtopping was only excessive with a 1:100 year water level. The failing condition was when the overtopping was measured

above 1 l/s/m. It was found that the overtopping associated with the 1:100 water level became acceptable when the crest level of the vertical wall behind the rubble mound was increased by only 0.6 m to LLD +3.2 m. This showed that overtopping is very sensitive to changes in the freeboard level of a composite vertical wall, especially when the rock structure is very permeable as in the case of the Strand. The results of the tests are shown in Table 6.

Table 6: Modelled overtopping for existing composite vertical wall (Institute of Water and Environmental Engineering, 2011)

Test	4	5	6	10	11
Seawall crest (m above LLD)	2.60	2.60	2.60	3.20	3.20
Water level (2010)	1:1 year	1:20 years	1:100 years	1:20 years	1:100 years
Water level (m above LLD)	1.43	1.67	1.79	1.67	1.79
H_s (m) (generated at -10 m CD)	1.20	1.70	1.88	1.69	1.88
Overtopping (l/s/ m)	0	0.486	2.333	0.036	0.189

The composite vertical wall is a good solution for the prevention of overtopping but it considerably decreases the width of the beach which at certain sections along the Strand is already less than 20 m wide. This solution can only be used in a small section along the Strand that is not commonly used by the public for recreational activities such as swimming or sunbathing. Figure 35 and Figure 36 show the composite vertical wall located at the Strand taken during low tide. During high tide the entire beach in front of the rock revetment is covered by water, exposing only part of the revetment above the water level.

Figure 35: Composite vertical wall at location I, looking west (19/07/2012)

Figure 36: Composite vertical wall at location I, looking east (19/07/2012)

3.2.5 Beach maintenance

The Roads and Stormwater Department of the local municipality is responsible for the maintenance of drainage outlets and roads in the area. This includes the defensive structures that protect the road.

The drainage outlets are scattered along the beach at regular intervals and with no standardised elevation. The outlets experience problems due to stand blockage and aging infrastructure. Many of the outlet mouths are located inside the wall while others have pipes that extend to the MLWS. When the drainage outlets are blocked during large rainfall events, certain low-lying streets behind Beach Road occasionally

experience localised flooding. The extent of this flooding can be exacerbated when combined with overtopping. The seawall then acts as a dam wall by retaining the water and not allowing it to flow back towards the ocean.

Sand is periodically removed from the seaward side of the wall to prevent the stormwater outlets becoming blocked. An attempt is made to maintain a freeboard of 1.2 m in front of the seawall where the stormwater outlets are located. At the sections without any stormwater pipes the sand is allowed to build up to a minimum freeboard of 0.3 m before the sand is removed and the freeboard is then adjusted to 1.2 m. The sand that is removed is dumped at the water's edge during low tide which is then redistributed by the waves during high tide.

The back of the beach is regularly cleaned and any plant, organic or inorganic material is removed from the top 0.2 m of sand. This hampers the growth of the vegetation which is essential in stabilising the sand dunes.

3.2.6 Proposed upgrades to coastal defences

The improvements which have been planned for the coastal protection along the Strand consist of an expansion of the existing composite vertical wall and the construction of a new recurve wall which is to replace the existing vertical and recurve walls.

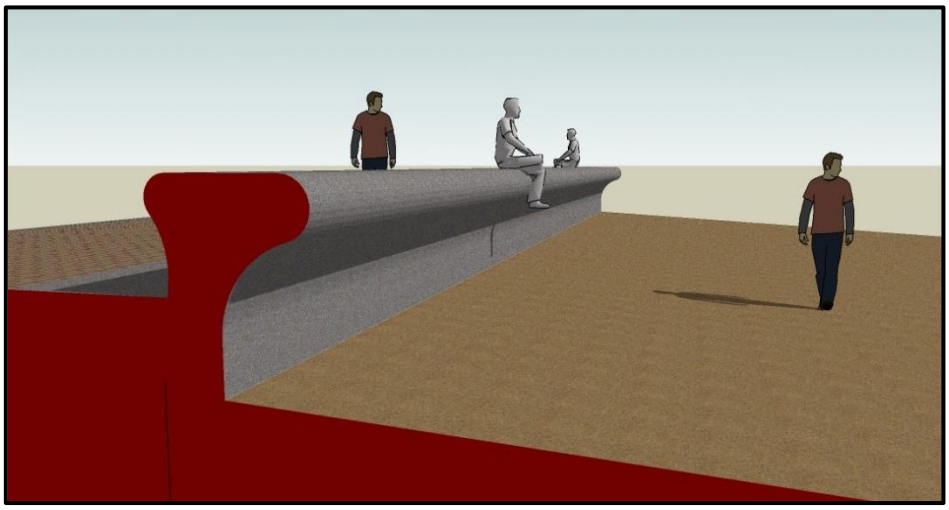

Figure 37: Artist's impression of the proposed recurve wall along the Strand (WML Coast, 2011)

The design of the recurve wall was also tested by the University of Stellenbosch on behalf of PD Naidoo & Associates and formed part of a series of tests which included recurve composite walls (IWEE, 2011).

3.3 Tidal levels

The only location inside False Bay which measures tidal level systematically is located inside the harbour at Simon's Town. The tidal levels can also be accurately predicted long in advance by making use of tidal equations. The predicted tidal levels are derived from the astronomical cycles of the moon, sun and other planets.

The measured tidal levels for Simon's Town were provided by the South African Navy Hydrographic Office and are listed in Table 7. The tidal levels are frequently adjusted based on latest measurements. The values listed in Table 7 were published in 2012 and are valid until 2014.

The datum that is used is in this study is Land Levelling Datum (LLD) since it is the standard datum used by the Chief Director, Surveys and Mapping for the Precise Levelling of the Republic of South Africa (SANHO, 2012). Land surveyors commonly refer to the Land Levelling Datum as Mean Sea Level which can cause confusion with Mean Level.

Table 7: Tidal levels for Simon's Town (SANHO, 2012)

Tidal Characteristics	Chart Datum (m)	Land Levelling Datum (m)
HAT – Highest Astronomical Tide	2.09	1.25
MHWS – Mean High Water Spring	1.79	0.95
MHWN – Mean High Water Neap	1.29	0.45
ML – Mean Level	1.00	0.16
MLWN – Mean Low Water Neap	0.73	-0.11
MLWS – Mean Low Water Spring	0.24	-0.60
LAT – Lowest Astronomical Tide	0.00	-0.84

The HAT and LAT are predicted to occur about every 19 years. The other tides are averaged over this same period. The LAT is also referred to as Chart Datum and is used for navigational charts of South Africa as well as Namibia. Storm surge and other meteorological conditions can cause higher and lower values than predicted by the table. The ML is situated at 0.16m above LLD (MSL) and is the average level of MHWS, MHWN, MLWS and MLWN.

3.4 Offshore to nearshore wave transformation

The nearshore wave climate at 10 points inside False Bay along the -10 m contour was provided from a previous study by Stellenbosch University (US, 2011). The wave data was determined by using a SWAN model to transform 11 years of NCEP (US National Center for Environmental Prediction) hindcast wave data from deepwater to the nearshore area. The offshore NCEP point is located south of False Bay at 35.0° S and 18.75° E as the input for the wave conditions for the SWAN model. Figure 38 shows the location of the wave data points and the Waverider buoy. In Figure 39 a plot of the bathymetry that was used in the SWAN model is shown. The coordinate system that was used is in this study is the Hartebeesthoek94/Lo19.

The wave climate at the -10 m contour located opposite the Strand was used in this study to determine wave roses and an Extreme Value Analysis (EVA) was conducted on the dataset. Further numerical modelling was done in this study based on the provided data at the -10m contour to determine the wave height at the back of the beach.

Figure 38: Location of wave data points

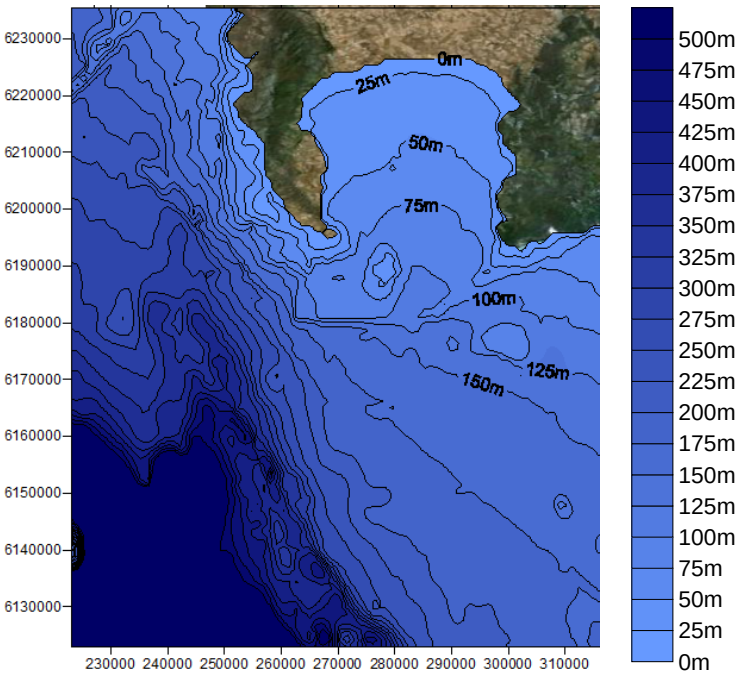

Figure 39: Bathymetry plot of the SWAN run for False Bay

The NCEP wave data was used because there are no wave measurement buoys located inside False Bay and the closest wave buoy is a directional Waverider buoy located at Slangkop which is near Cape Point. It provides a fair representation of the deepwater conditions approaching Table Bay (Smith & Luger, 2003) but is perhaps not suitable for False Bay. The NCEP hindcast wave data was established using a third generation wind wave model (WAVEWATCH III) (Chawla et al. 2011). The model makes use of the recorded wind and atmospheric conditions of a region to determine the wave conditions of that area.

3.4.1 Wave direction and wave height

The wave data from both the offshore NCEP and the Strand point were arranged into directional bins with a width of 22.5°. Wave roses and exceedance tables were then created to determine the directional distribution of the waves for both of the points. From the wave roses and tables of the two points it is possible to see that the majority of waves travel from a south-westerly direction (225°). At the offshore point and at the Strand, 54% and 88% of the waves respectively came from 225° direction. The vast majority of waves at the Strand are found to come from the southwest and the south.

Table 8: Exceedance table of the Strand

Hmo (m)		Nautical Direction (deg)							Total	Exceedance (%)
>=	<	157.5	180	202.5	225	247.5	270	292.5	0.00	100.00
0.0	1.0		1.50	10.12	85.28	0.04	0.01		96.95	3.05
1.0	2.0			0.01	3.04				3.05	0.00
2.0	3.0								0.00	0.00
		0.00	1.50	10.13	88.32	0.04	0.01	0.00		
		Percentage occurrence (%)								

Table 9: Exceedance table of offshore

Hmo (m)		Nautical Direction (deg)															Total	% Exceedance
>=	<	0	22.5	45	67.5	90	112.5	135	157.5	180	202.5	225	247.5	270	292.5	315	337.5	0.00	100.00
0.0	1.0								0.00	0.01	0.01	0.00	0.01					0.03	99.97
1.0	2.0					0.12	0.95	0.38	0.33	0.33	1.23	4.92	1.70	0.13	0.08	0.06		10.23	89.74
2.0	3.0	0.01				0.66	3.68	1.12	0.87	0.91	5.37	25.71	7.25	0.34	0.35	0.26	0.02	46.55	43.19
3.0	4.0	0.00			0.00	0.63	1.61	0.33	0.35	0.58	3.53	14.88	4.54	0.44	0.28	0.13	0.01	27.31	15.88
4.0	5.0					0.04	0.09	0.04	0.06	0.24	1.18	5.83	2.58	0.26	0.09	0.05	0.00	10.48	5.40
5.0	6.0					0.02	0.01		0.02	0.08	0.48	1.94	1.06	0.19	0.02	0.01		3.82	1.58
6.0	7.0									0.02	0.18	0.49	0.35	0.05	0.01			1.09	0.48
7.0	8.0										0.02	0.16	0.13	0.00				0.32	0.17
8.0	9.0											0.10	0.02	0.01				0.13	0.04
9.0	10.0											0.01						0.01	0.03
10.0	11.0											0.01	0.01					0.03	0.00
		0.01	0.00	0.00	0.00	1.47	6.34	1.87	1.63	2.15	12.01	54.06	17.66	1.42	0.83	0.51	0.04		
		Percentage occurance (%)																	

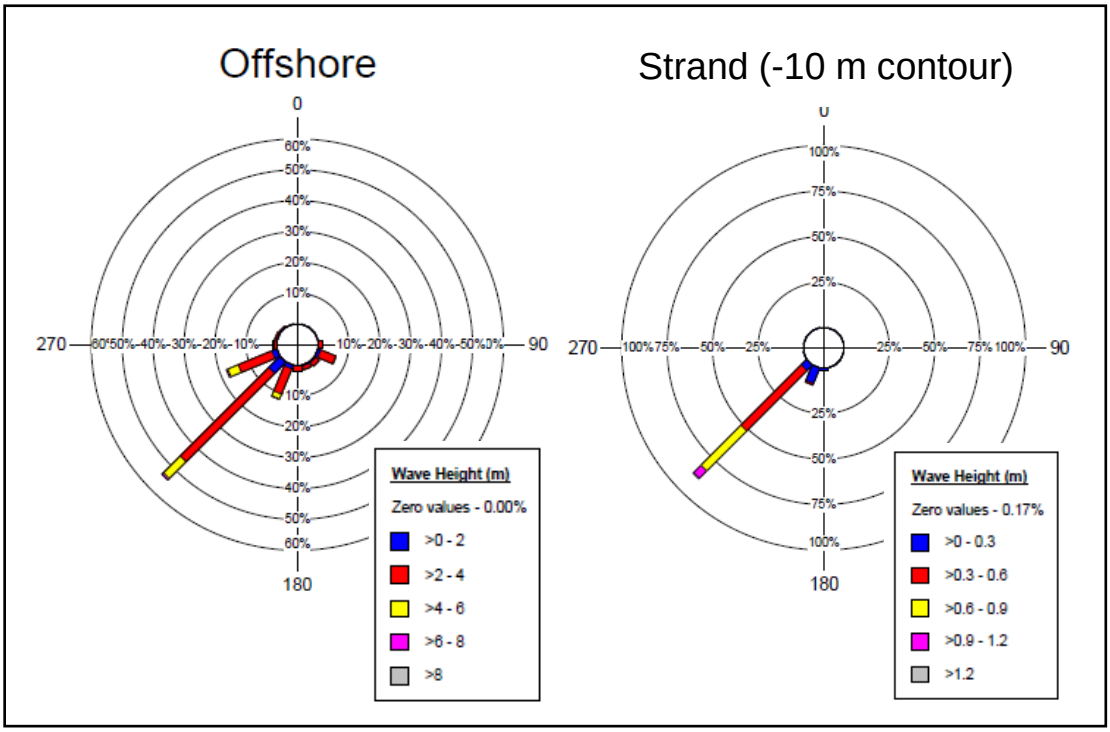

Figure 40: Wave rose of the NCEP offshore point and nearshore Strand point

43% of the significant wave heights offshore exceed 2 m and as the waves propagate towards the Strand, 97% of the significant wave heights are below 1 m. This clearly shows the sheltering effect that the bay has on the wave climate of the Strand.

3.4.2 Extreme Value analysis

An extreme value analysis (EVA) was conducted using MikeEVA software on the wave conditions that are available at CD -10 m. A PDS (Partial Duration Series) model was used with the 10 largest events per year selected to form the time series. To ensure independences between events in the PDS, an inter-event time of 24 hours was used. This ensures that the events do not all come from the same storm system. The model also uses a Monte Carlo simulation to determine the uncertainty of the estimated return periods by generating 10 000 random samples which have the same characteristics as observed samples (DHI, 2009).

The following four types of probability distributions were used along with the Method of Moments to estimate their parameters:

- Weibull
- Generalised Pareto

- Gamma/Pearson Type III
- Exponential

Two goodness-of-fit tests were done on the data set to determine which of the distributions best represent the data series.

- *SLSC*: Standardised Least Squares Criterion
- *PPCC I*: Probability Plot Correlation Coefficient based on the correlation between the ordered observations and the corresponding order statistics

The results of the EVA and the goodness-of-fit tests are shown in Table 10. There is very little difference between the different wave heights of the same return period for the different types of distributions. The goodness-of-fit test was also very similar, showing no real distinction between the distributions. This indicates that any of the distributions could be used for the EVA.

Table 10: EVA results for the wave heights

		Wave height (m)			
	Return Period [years]	**Weibull**	**Generalised Pareto**	**Gamma/ Pearson Type III**	**Exponential**
Estimated value	2	1.39	1.39	1.39	1.39
	5	1.53	1.53	1.53	1.54
	10	1.62	1.62	1.62	1.64
	20	1.71	1.71	1.71	1.73
	50	1.83	1.82	1.83	1.85
	100	1.91	1.90	1.92	1.94
Standard deviation	2	0.04	0.03	0.04	0.03
	5	0.06	0.06	0.06	0.05
	10	0.08	0.08	0.07	0.06
	20	0.10	0.11	0.09	0.06
	50	0.12	0.15	0.11	0.08
	100	0.14	0.19	0.13	0.08
Goodness of fit	SLSC	0.028	0.027	0.028	0.028
	PPCC1	0.992	0.993	0.992	0.992

To further distinguish between the distributions, the time series and the different distributions were plotted on a semi-logarithmic graph with their return period. It was possible to see that the Weibull distribution provided the best fit for the time series

and was therefore chosen as the distribution for the EVA. Figure 41 shows the extreme wave heights plotted for the Strand using a Weibull distribution.

The cumulative distribution function and the probability density function for the Weibull distribution that was used is(DHI, 2009):

Valid range: $\alpha > 0, \kappa > 0, \xi < x < \infty$

ξ: Location parameter

α: Scale parameter

κ: Shape parameter

Cumulative distribution function F(x):

$$F(x) = 1 - \exp\left[-\left(\frac{x-\xi}{\alpha}\right)^{\kappa}\right] \qquad \text{Equation 31}$$

Probability density function f(x):

$$f(x) = \frac{\kappa}{\alpha}\left(\frac{x-\xi}{\alpha}\right)^{\kappa-1} \exp\left[-\left(\frac{x-\xi}{\alpha}\right)^{\kappa}\right] \qquad \text{Equation 32}$$

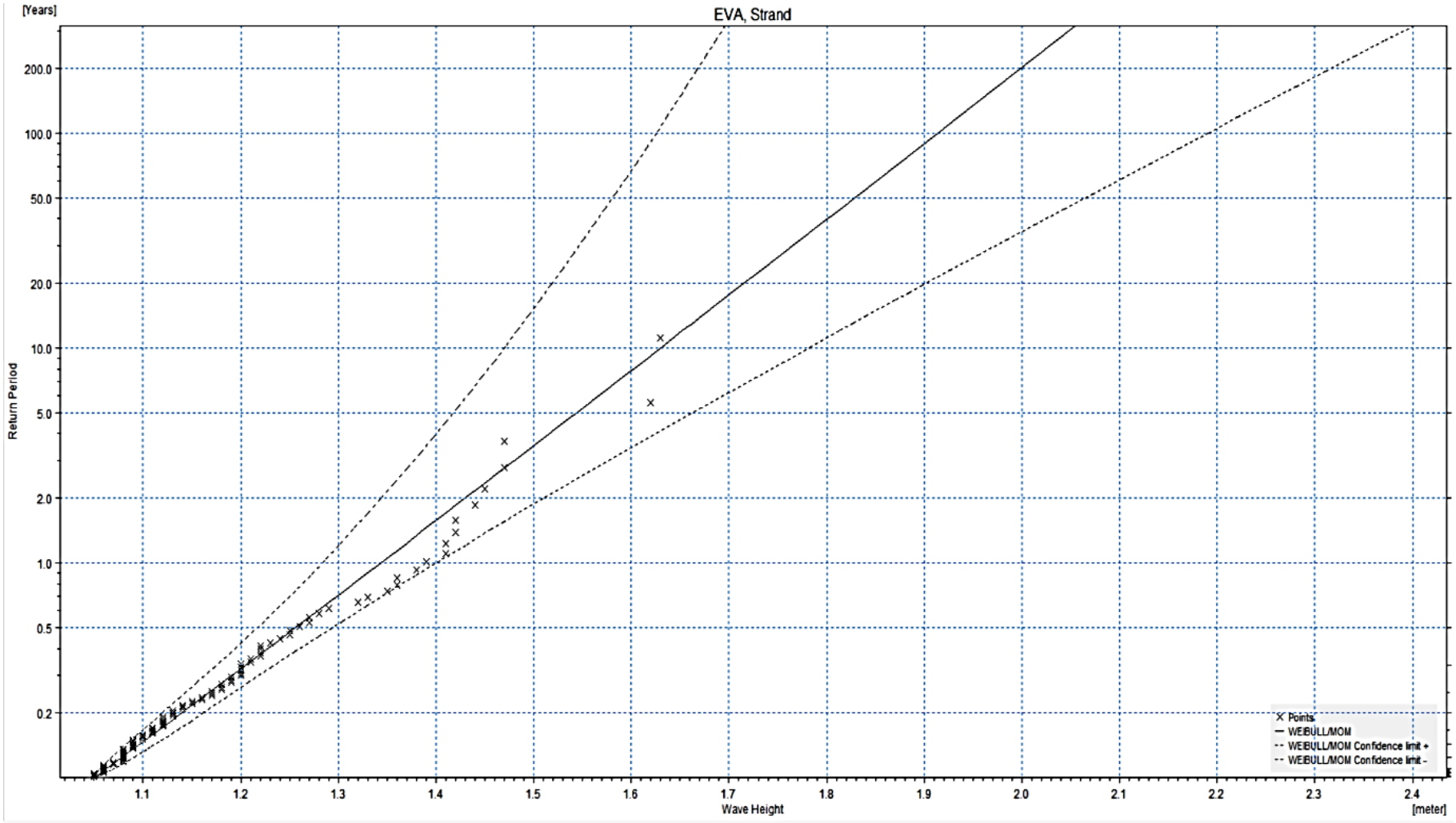

Figure 41: EVA plot of H_{mo} for the Strand (-10m CD) using a Weibull distribution

3.5 Period

The offshore NCEP wave data was used to create occurrence tables for T_p and H_{mo}. Table 11 shows that the 60% of the waves at the offshore location have a period ranging between 10 to 13 seconds. The most frequently occurring period is around 11 seconds.

Table 11: Exceedance table of the offshore point

Hmo (m)		Tp (s)																Total %	Exceedance (%)
>=	<	3 to 4	4 to 5	5 to 6	6 to 7	7 to 8	8 to 9	9 to 10	10 to 11	11 to 12	12 to 13	13 to 14	14 to 15	15 to 16	16 to 17	17 to 18	18 to 19		
0.0	1.0		0.02	0.01														0.03	99.97
1.0	2.0	0.00	0.18	0.38	0.39	0.74	1.41	3.33	2.47	0.90	0.25	0.12	0.04	0.00	0.00	0.01		10.23	89.74
2.0	3.0		0.08	1.62	2.38	1.71	2.56	6.67	12.44	11.08	5.37	2.03	0.44	0.11	0.04	0.01	0.01	46.55	43.19
3.0	4.0			0.06	1.35	1.36	1.04	1.96	4.11	7.24	6.26	2.98	0.75	0.14	0.05	0.02		27.31	15.88
4.0	5.0				0.03	0.16	0.27	0.58	1.43	2.66	2.78	1.91	0.52	0.12	0.02	0.01		10.48	5.40
5.0	6.0					0.01	0.03	0.11	0.30	0.89	1.00	1.01	0.36	0.10	0.01			3.82	1.58
6.0	7.0							0.01	0.04	0.18	0.39	0.29	0.12	0.06				1.09	0.48
7.0	8.0									0.02	0.06	0.14	0.06	0.02	0.01			0.32	0.17
8.0	9.0										0.01	0.06	0.05					0.13	0.04
9.0	10.0											0.00	0.00	0.01				0.01	0.03
10.0	11.0											0.01	0.01	0.01				0.03	0.00
		0.00	0.28	2.06	4.15	3.98	5.30	12.66	20.79	22.98	16.12	8.55	2.36	0.56	0.13	0.05	0.01		
		Percentage occurrence (%)																	

At the Council for Scientific and Industrial Research (CSIR) it was found that the NCEP predictions of periods in the area are slightly underestimated (Marius Rossouw, personal communication, 8 August 2012). Figure 42 is a comparison of 11 years' NCEP data of predicted peak periods for Slangkop and the measured peak periods at the Slangkop directional Waverider buoy. The shorter periods are mostly overpredicted while the longer periods are underpredicted by the NCEP data for our region. It is therefore more appropriate to estimate that 12 seconds is the predominant wave period for the False Bay region.

Strand site conditions

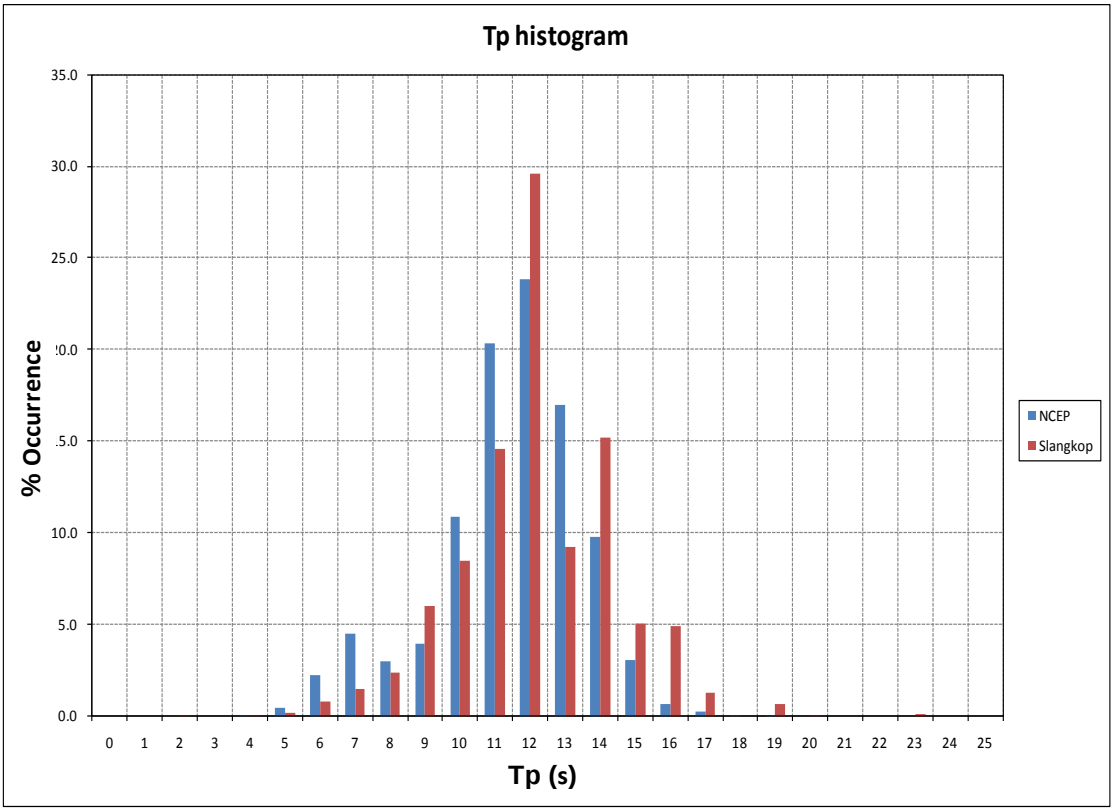

Figure 42: Underestimation of T_p by NCEP data, provided by the CSIR

A scatter graph was created for both the nearshore and offshore locations. It is used to estimate the wave period expected with the extreme wave heights. This is important because a 1:100 year wave height could have a different period associated with it compared to a 1:1 wave condition.

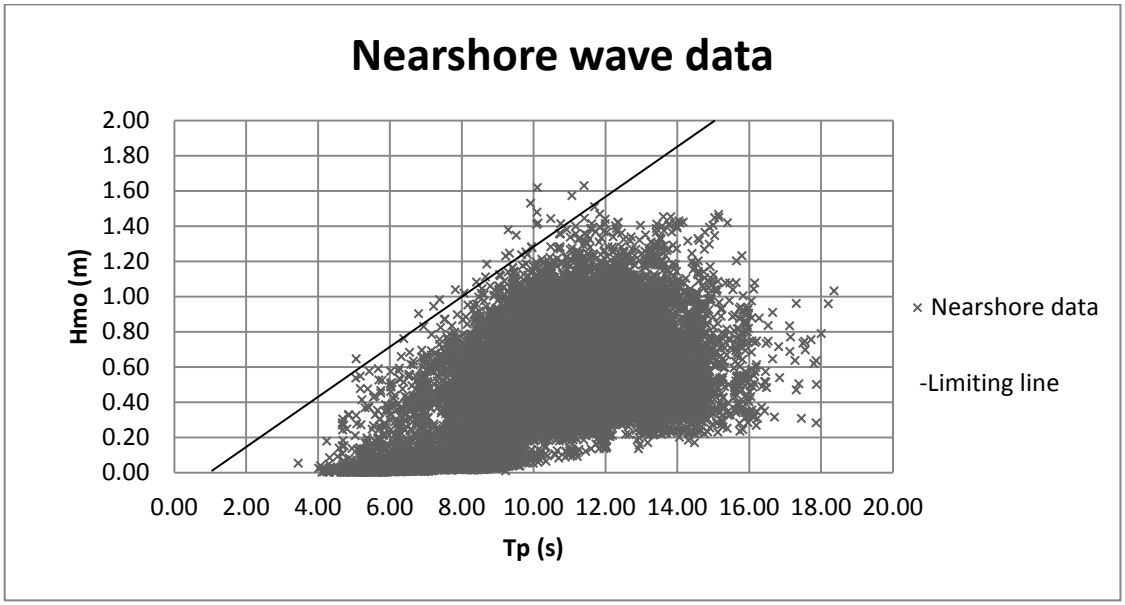

Figure 43: Nearshore period and wave height scatter graph

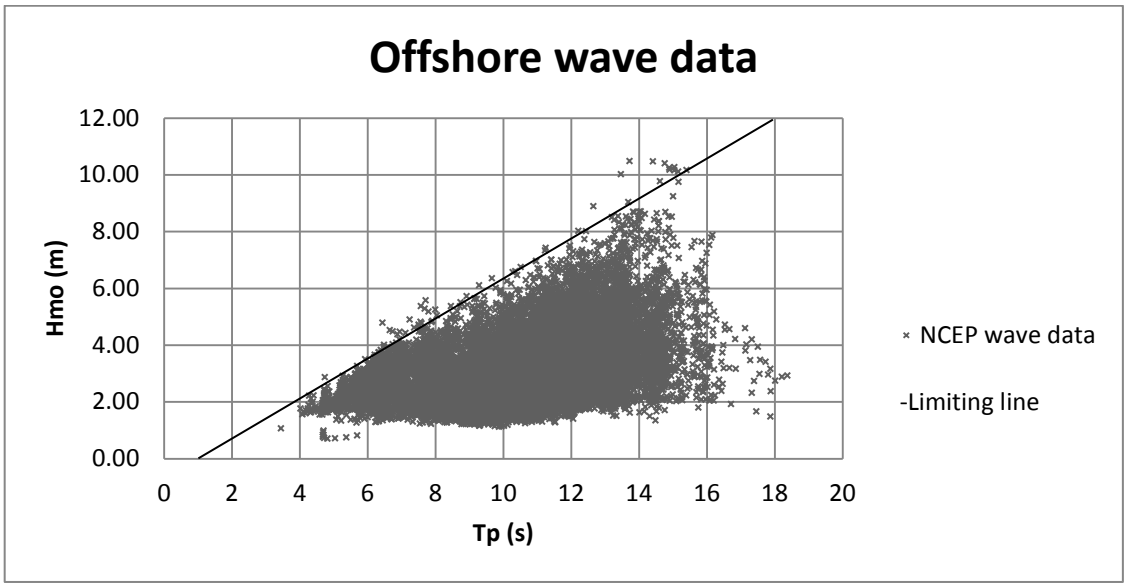

Figure 44: Offshore wave height and period scatter graph

Figure 43 and Figure 44 show how the wave height is related to the period and that the largest wave heights are not found at the longest period. The limiting lines in the figures has been adjusted by 1 second to the right to compensate for the underprediction of the period from the NCEP data.

The figures also show that the largest waves at the offshore point do not coincide with the largest wave at the nearshore point. The offshore point has a longer period associated with the largest wave height than the nearshore point. This may be due to longer period waves refracting more than shorter period waves. This results in some of the longer period waves being refracted away from the Strand or that the longer period waves break before they reach the Strand since longer period waves also experience more shoaling.

The 1:100 year significant wave height for the Strand (-10m CD) is 1.91 m and has a peak period of around 14 seconds. The 1:100 year significant wave height for the offshore point is approximately 12 m (IWEE, 2011) and has a peak period of around 18 seconds.

3.6 Wind

False Bay has a complex wind pattern with variable surface friction and wind stress caused by the interference in the wind flow by the surrounding topography. This can result in the formation of cyclonic curvature around False Bay (Jury, 1984). This

makes it very difficult to schematise these wind conditions in a numerical wave model.

Hourly wind data was made available by the South African Weather Service for the Strand and Cape Town International Airport from January 2001 until July 2011 (SAWS, 2011). The data was sorted and wind roses were created to show the direction, occurrence and speed for the different locations. Wind roses were created for the different seasons over the ten-year period as well as for the entire period.

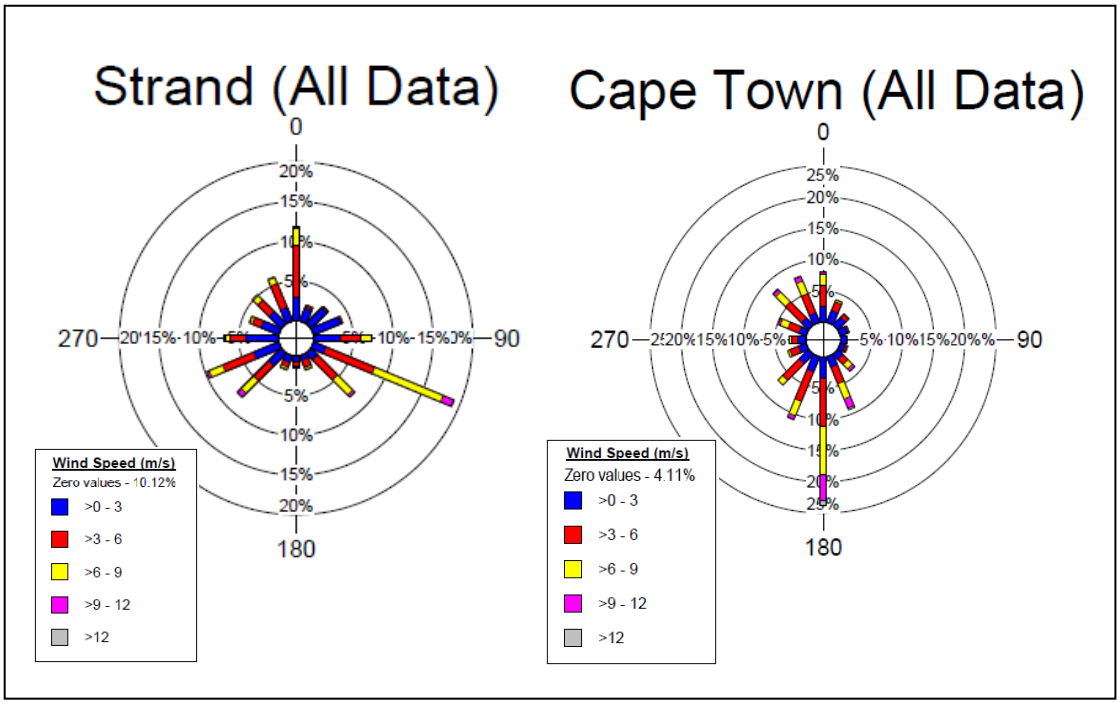

Figure 45: Wind roses for the Strand and Cape Town International Airport

The two main wind directions that dominate at the Strand are a northerly wind during winter and a south-easterly wind during the rest of the year. The northerly wind would decrease the overtopping rate because the wind is directed offshore while the south-easterly wind would have little effect on the overtopping rate since it is directed in the longshore direction.

The landscape around Cape Town International Airport is flat and therefore the wind direction and speed differ from the Strand which is sheltered by a large mountain range. The mountain range starts north of the Strand, stretching along the eastern side of False Bay. The airport is largely dominated by southerly wind conditions throughout the year except for during winter when a northerly wind mostly occurs. The seasonal wind roses can be found in Figure A1-2 in the Appendix for both Cape Town and the Strand.

The maximum hourly wind speed that was recorded during the 11 years of data for the Strand was 16.5 m/s and the average wind speed was 4 m/s while at the airport the maximum wind speed was 17.3 m/s and the average wind speed was 5 m/s.

The wind roses show that, although the two areas are located in False Bay and are within 50 km from each other, they had very different wind directions. This is in agreement with the study of Jury, (1984) which showed that the wind direction between wind stations around False Bay does not correlate well.

The effect of the wind was not modelled with physical modelling because the wind conditions at the Strand would not increase the overtopping rate. Wind sensitivity tests using numerical modelling on the waves were done to determine the influences it may have on the wave period and wave height.

3.7 Sensitivity of the wave height and period to wind

There was a measure of uncertainty concerning the wave height and period at the Strand because the wave data was determined with a SWAN model without taking into account the effect that wind has on waves as they advance from offshore to nearshore.

It was therefore necessary to do a sensitivity analysis on the original NCEP wave data using the same SWAN model set-up but including different wind conditions. The SWAN input files that were used to determine the wave heights for the Strand was provided by a PhD student (James Joubert) who modelled False Bay for the Civil Engineering Department of Stellenbosch University (US, 2011).

The model used the NCEP wave data that was coupled with different JONSWAP gamma values for each wave height and direction. The gamma values are the peakedness factor of the energy density spectrum. The gamma values were determined from the Slangkop directional buoy that was associated with the same direction and wave height. The breaker index and bottom friction values were set to the default values of SWAN (US, 2011).

The sensitivity tests were done with a wave condition that is frequently found. H_s was set to 3.3 m and T_p to 12 seconds travelling from the SW. The wind directions that were tested were from the SW, S, SE and N with the average wind speed of the airport of 5 m/s. Each wind condition was applied over the entire model as a worst case scenario. In the Appendix are the results for the wave height directional

sensitivity for the average wind condition for the directions mentioned. There is no visible difference in the wave period or the wave height distribution for the different wave directions for the average wind speed along False Bay.

It was found that when the wind speed was increased to 10 m/s for the same offshore wave conditions, the significant wave height distribution along False Bay changes considerably but the period remained constant. The wave heights increased inside the bay when the wind came from the south but decreased only slightly when it came from the north. This indicates that only strong wind conditions blowing onshore have an effect on the wave height.

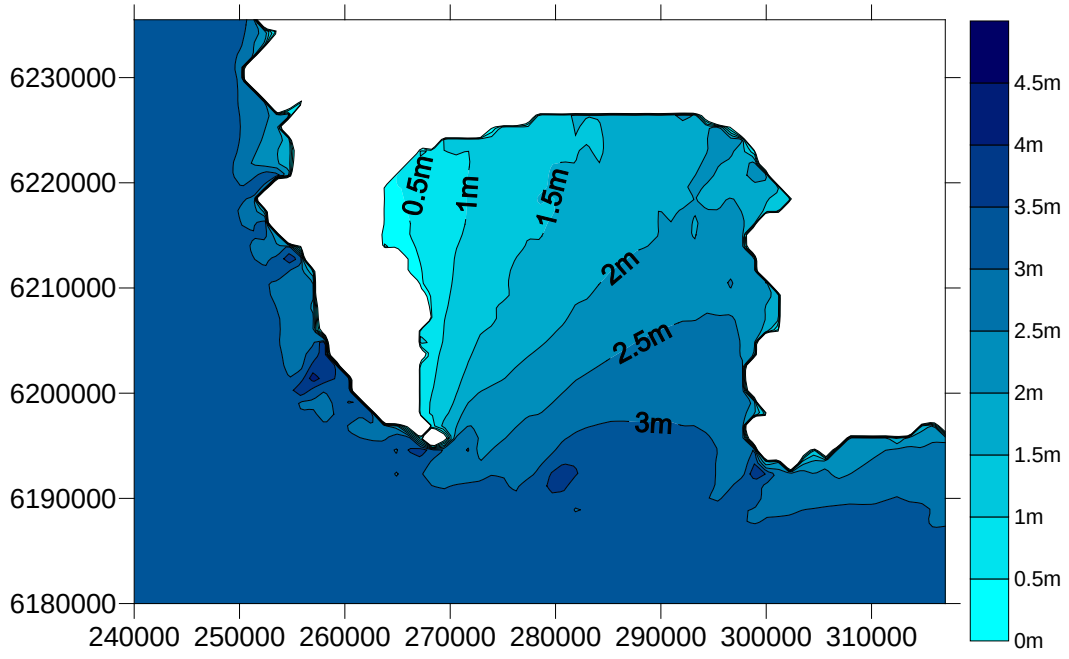

Figure 46: H_{mo} distribution without wind

Figure 47 shows the wave height distribution inside False Bay with a 10 m/s wind from the north which is very similar to the wave distribution without wind.

Strand site conditions

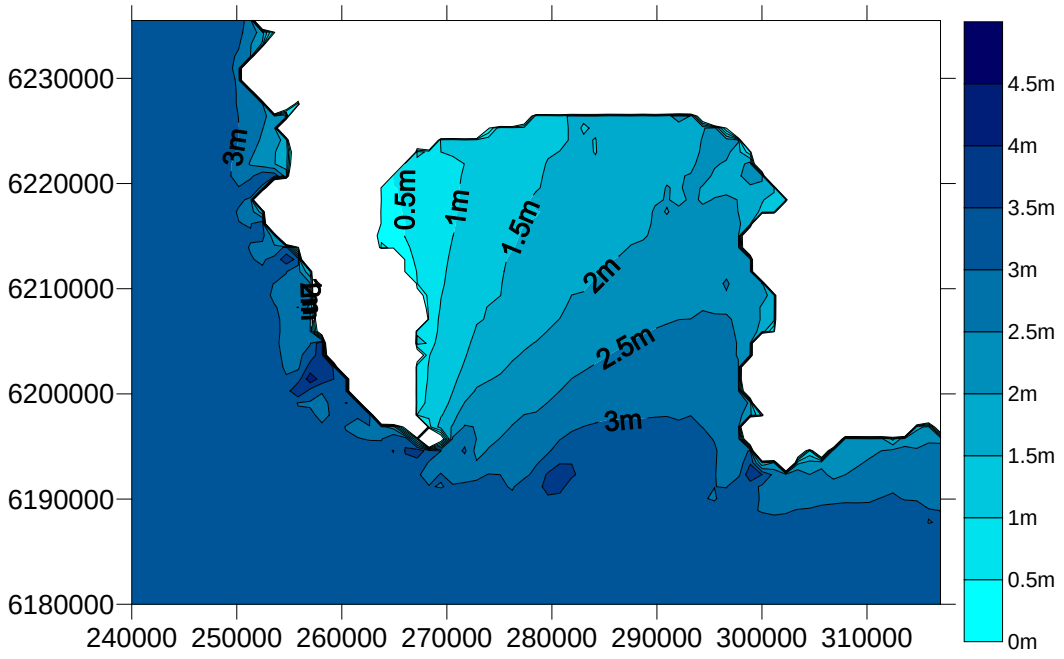

Figure 47: Hs distribution with a 10 m/s northerly wind

Figure 48 shows the wave height distribution with a 10 m/s southerly wind with increased H_{mo} inside False Bay by approximately 0.5 m.

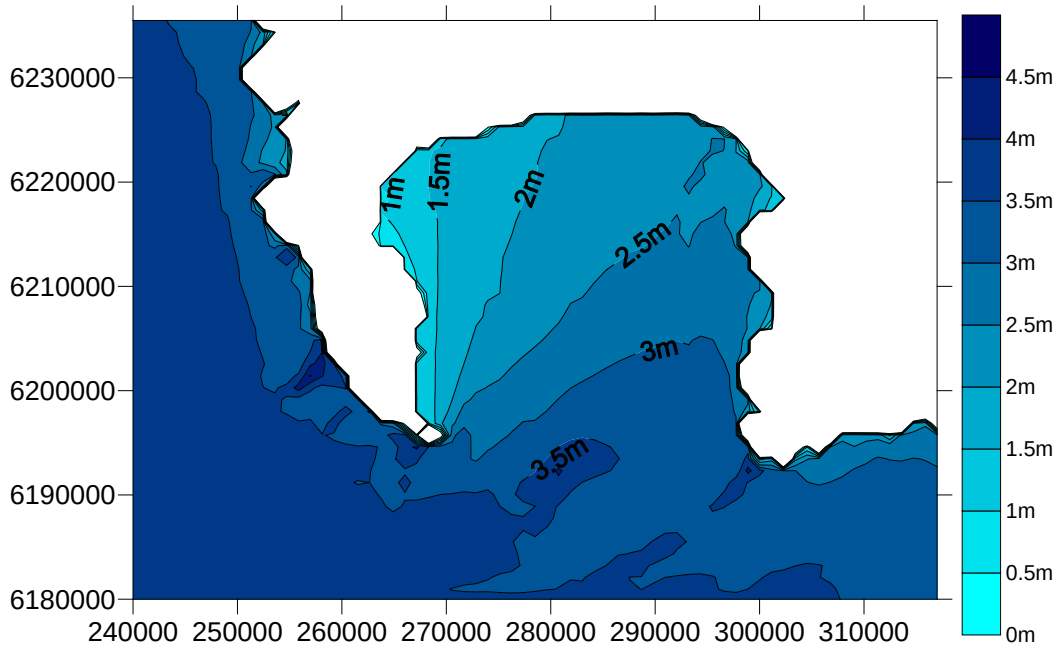

Figure 48: H_{mo} distribution with a 10 m/s southerly wind

By not applying wind to the offshore wave conditions when running the SWAN model was accurate in obtaining for the wave conditions for False Bay since there is no difference between the no wind condition and the average wind condition because of the low average wind speed. It would be unrealistic to apply a larger than average wind condition in determining the wave climate over a long period but it should be

taken into consideration that large southerly winds are able to increase the significant wave height inside False Bay. This can become important if the nearshore wave height is not depth dependent and will cause design conditions to occur more often. The sensitivity of wave height at the back of the beach to changes in wave height at the -10m contour at the Strand will be modelled using Delft3D

3.8 Storm Surge

The storm surge for False Bay was determined by using the residual tidal level of Simon's Town. The predicted tidal levels were subtracted from the measured tidal levels to give the residual tide.

Simon's Town is located on the opposite side of False Bay and is also surrounded by a mountain range on the western side which could cause the wind direction to differ from the Strand. It could be possible that the onshore wind set-up conditions for Simon's Town could at the same time create an offshore wind set-down condition at the Strand or not influence the Strand water level at all. However, in the absence of other tidal information it was assumed that the storm surge of Simon's Town was the same as the Strand (IWEE, 2011). Figure 49 shows the onshore wind direction for Simon's Town and the Strand.

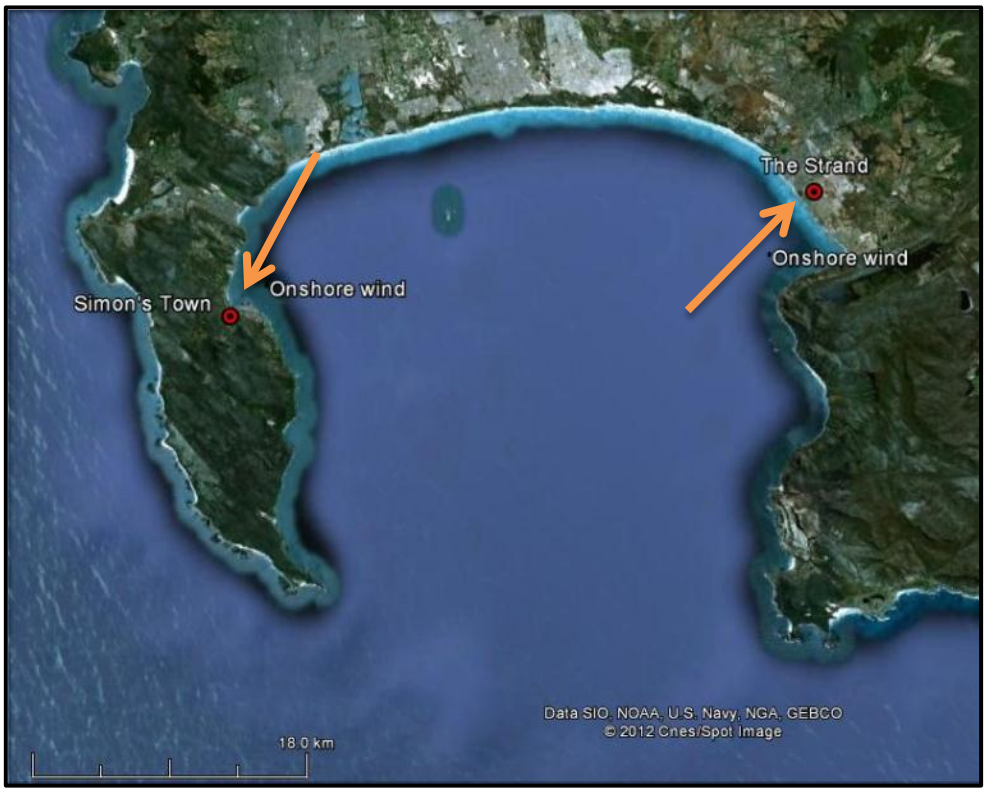

Figure 49: Onshore wind direction for Simon's Town and the Strand

Seven years of recorded data was used to determine the residual tide. There were several gaps in the data which was caused by the occasional breakdown of the tidal gauge and maintenance work done on it.

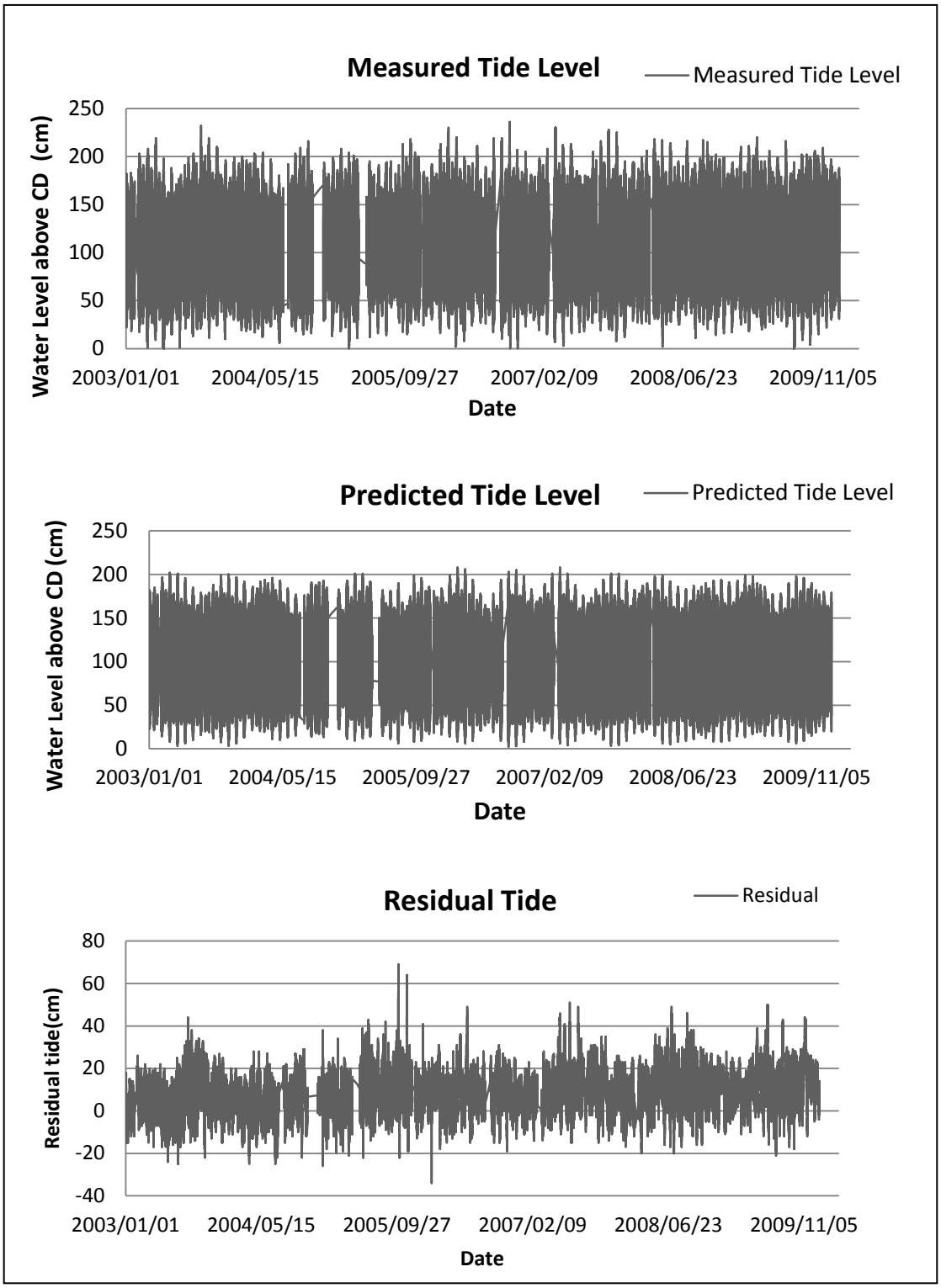

Figure 50: Measured, predicted and residual tide

3.8.1 Extreme value analysis

An EVA analysis was conducted on the residual data to determine the associated return period for the different storm surge events. The same process was completed for the residual tide as it was for the extreme wave height. Again no clear indication could be found in results of the EVA simulation to determine which distribution best represented the time series. The results of the distributions that were tested in the EVA can be seen in Table 12. Therefore the distributions were again plotted on a semi-logarithmic graph. From the different distribution graphs it was possible to see that the Gamma/Pearson Type III distribution provided the best fit for the residual tide time series. Figure 51 shows the Gamma/Pearson Type III distribution applied to the time series. Confidence limits shown in the figure are 95%.

Table 12: Results of EVA for storm surge

		Storm surge (cm)			
	Return Period [years]	**Weibull**	**Generalised Pareto**	**Gamma/ Pearson Type III**	**Exponential**
Estimated values	2	51.22	50.89	51.31	50.50
	5	60.51	60.39	60.47	58.78
	10	66.77	67.06	66.57	64.26
	20	72.85	73.75	72.44	69.52
	50	80.79	82.88	80.06	76.32
	100	86.80	90.07	85.79	81.42
Standard deviation	2	2.98	2.77	3.04	2.43
	5	5.07	5.06	4.97	3.46
	10	6.72	7.31	6.35	4.15
	20	8.46	10.11	7.72	4.80
	50	10.92	14.80	9.55	5.65
	100	12.90	19.23	10.96	6.28
Goodness-of-fit statistics	SLSC	0.035	0.033	0.034	0.046
	PPCC1	0.994	0.995	0.994	0.993

The cumulative distribution function and probability density function for the Gamma/Pearson Type III distribution is(DHI, 2009):

$$\text{Range: } \kappa > 0, \xi \leq x < \infty \text{ for } \alpha > 0, -\infty < x \leq \xi \text{ for } \alpha < 0$$

Cumulative distribution function F(x).

Strand site conditions

$$F(x) = \begin{cases} G\left(\kappa, \frac{x-\xi}{\alpha}\right) & , \alpha > 0 \\ 1 - G\left(\kappa, \frac{x-\xi}{\alpha}\right) & , \alpha < 0 \end{cases}$$ Equation 33

Probability density function f(x):

$$f(x) = \frac{1}{|\alpha|\Gamma(\kappa)}\left(\frac{x-\xi}{\alpha}\right)^{\kappa-1} \exp -\left(\frac{x-\xi}{\alpha}\right)$$ Equation 34

Γ(.) is the gamma function

G(.,.) is the incomplete gamma integral

ξ: Location parameter

α: Scale parameter

κ: Shape parameter

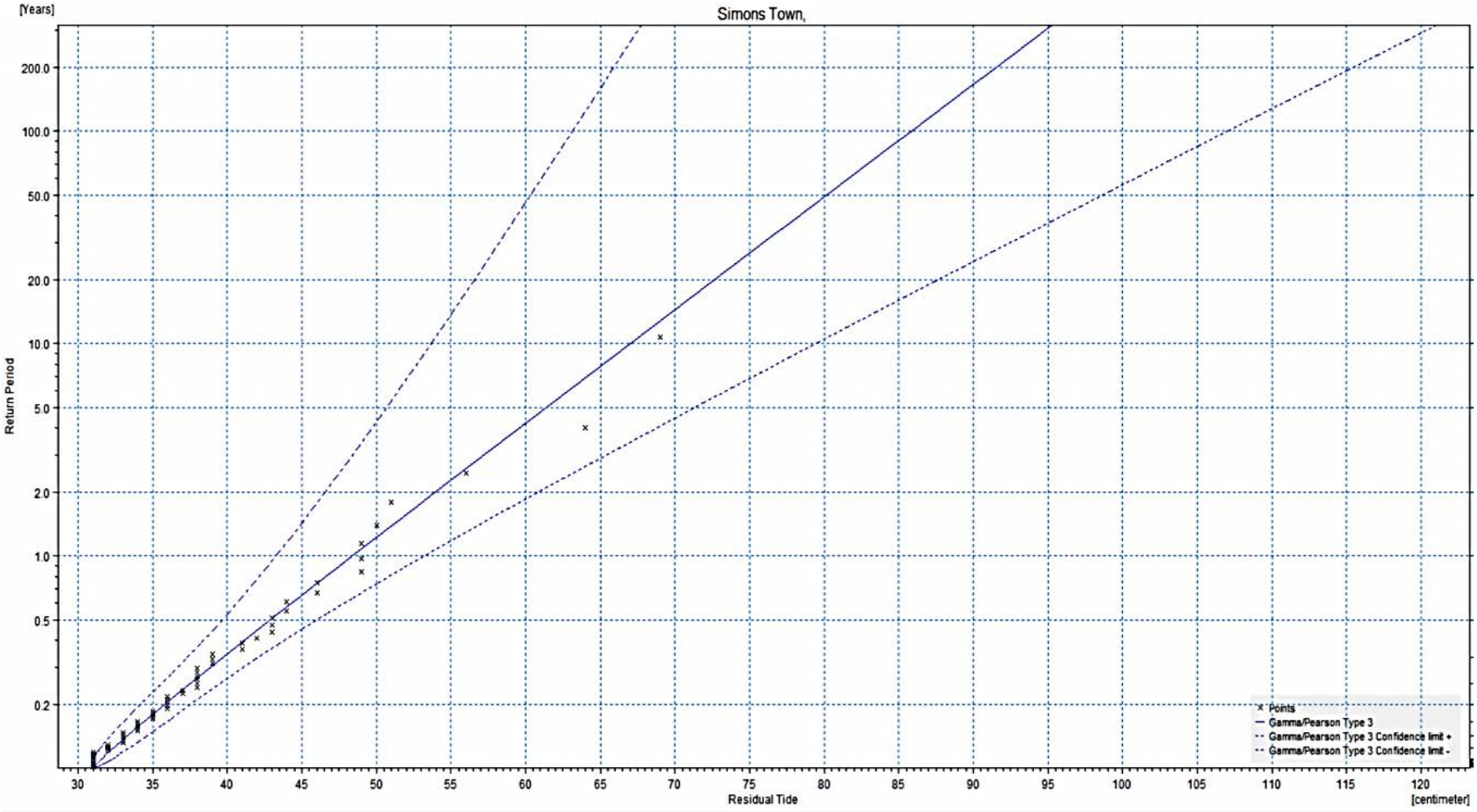

Figure 51: EVA plot of residual tide for False Bay using a Gamma/Pearson Type III distribution

3.9 Extreme water level

The extreme water level is a combination of the storm surge, rise in sea level and tidal level. A study was done by PRDW (2010) on the effect of global climate change on the design conditions of Table Bay. It was recommended that the storm surge in 100 years' time may be increased by 21%. This was based on an expected increase in offshore wind speeds of up to 10% for the year 2115 which was reported by the Department for Environment, Food and Rural Affairs of the UK Government (DEFRA, 2006).

The increase in wind speed is directly proportional to the atmospheric pressure component in storm surge and the wind set-up component is proportional to the square of the wind speed (PRDW, 2010).

Table 13 shows the increase in storm surge as a result of the increase in wind speed caused by climate change.

Table 13: Increase in storm surge due to increase in wind speed

	Return period of storm surge (cm)					
Year	1	10	20	50	100	**Increase (%)**
2012	48	67	72	80	86	0.0
2022	49	67	73	81	87	1.2
2032	50	69	75	83	89	3.4
2062	53	73	80	88	94	10.0
2112	58	81	88	97	104	21.0

Table 14 shows the extreme water level that was determined by taking the MHWS tide and adding the storm surge and sea level rise of the same return period to it.

Table 14: Extreme water level

Extreme water level above LLD (cm)							
Year	**SLR (cm)**	**MHWS (cm)**	**Return period**				
			1	**10**	**20**	**50**	**100**
2012	0	95	143	162	167	175	181
2022	6	95	150	168	174	182	188
2032	12	95	157	176	182	190	196
2062	30	95	178	198	205	213	219
2112	80	95	233	256	263	272	279

Sea level rise was taken as 0.8 m which is the average of the Copenhagen Diagnosis of 2009 (Allison et al. 2009) which stated that the sea level rise would be double that of the IPCC projections of 2007 (IPCC, 2007) which ranged from the lower estimate of the B1 scenario (0.18 m) and the upper estimate of the A1F1 scenario (0.59 m).

4 Nearshore wave modelling

The wave height and wave period at the back of the beach are important parameters used in overtopping calculations and generic overtopping software, and are required for physical modelling. In order to determine the H_{mo} at the toe of the structure, a numerical model needs to be used. The model that was used is Delft3D-Wave which is a 3rd generation process-based model which utilises SWAN.

Numerical tests were done on the current MHWS level and the current beach level. Various beach levels and extreme water levels with their associated extreme wave heights were tested for the return period of: 1:1, 1:10, 1:20, 1:50 and 1:100 years. Sensitivity analyses were done on the change in period, JONSWAP gamma coefficient and depth-induced breaker index.

4.1 Delft3D-Wave Set-up

The Delft3D-Wave programme requires a computational grid to be created and a depth file to give information about the bathymetry to the grid. Output location files can be given for the computational grid which then returns tabulated information about each location point. Information such as H_{mo}, water depth, directional spreading and T_p is recorded in the output table.

Output location data was requested at 54 locations along the back of the beach which gave a good representation of the entire length of the beach. The output locations are shown in Figure 52.

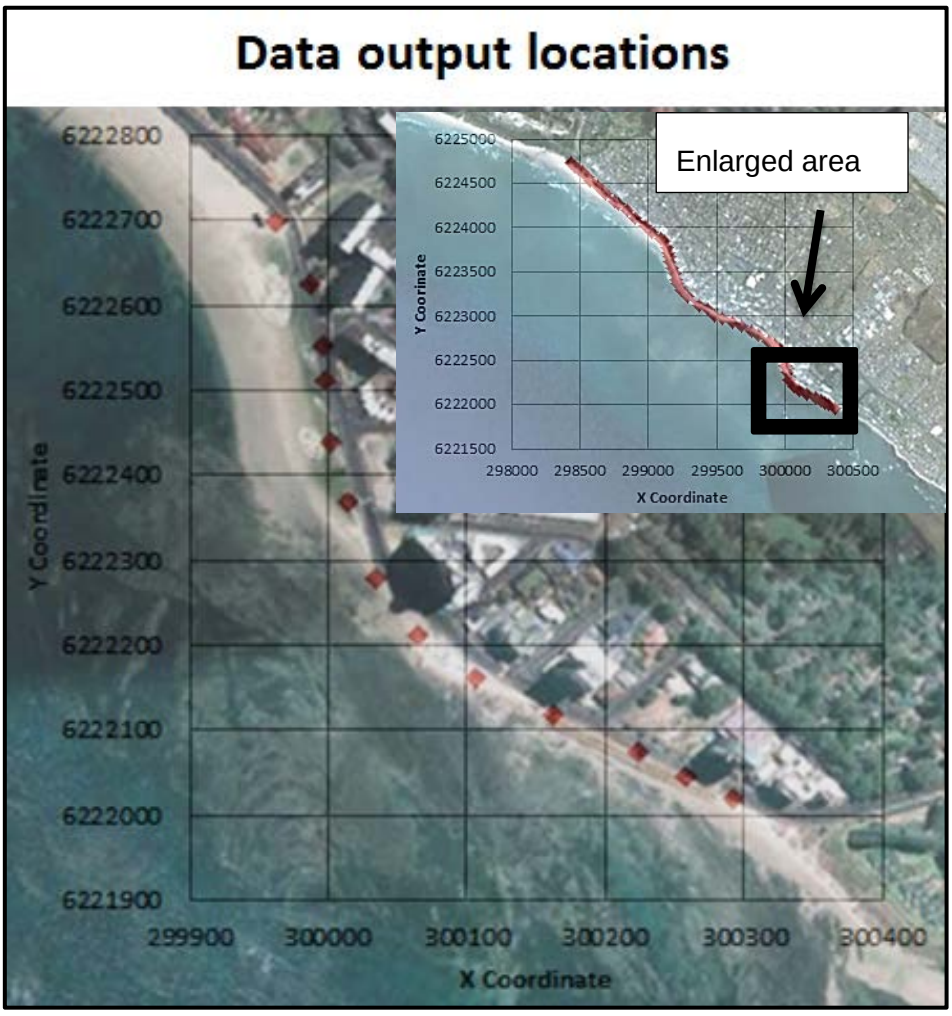

Figure 52: Data output locations at the back of the beach along the Strand

4.1.1 Computational grid and bathymetry

The SA Naval survey data (SANHO, 2011) provided information regarding the bottom profile only at and below depths of approximately 2.8 m below Land Levelling Datum (LLD). The land survey data of the beach was done by (WJM, 2011) between Greenways and the Lourens River, from 1 m below LLD up to the back of the beach.

To supplement the previous surveys, in 2012 photos were taken to provide further information about those reefs that were visible during low tide. The photos were taken at low tide on 19/07/2012 when the tidal level was at LLD -0.6 m. These photos were then used in conjunction with satellite images of the area in order to provide information regarding some of the unsurveyed sections between the limits of the land survey data and the naval survey data.

Figure 53: Reefs visible at the Strand during low tide at -0.6m LLD (19/07/2011)

This was only able to provide a best estimate of the elevations of the visible reefs and still left out sections for which there are no survey data. It was not possible to make any further improvements to the survey data due to time constraints. Delft3d makes use of triangular interpolation to derive the missing values. This creates a degree of uncertainty in the shallow regions between LLD -2.8 m and LLD -1 m. To improve the reliability of numerical modelling of the Strand area in future studies, more detailed survey data will be needed for these shallow rocky areas.

Two computational grids were used in order to decrease the computational time that is needed to run the model. The first is a large grid which is coarser than the inner grid. Each grid cell of the coarser grid has a dimension of approximately 30 x 30 metres. The coarser grid starts at a depth of 11 m below LLD and extends to the back of the beach. The input boundary conditions were given to the model for the coarser grid on the south-westerly boundary while leaving the other boundaries open. This allows energy to enter the modelling area from one direction and to leave the modelled area by the open boundaries on the sides.

In order to avoid having the modelled area influenced by the loss of energy from the open side boundaries, the length of the modelled area was extended on either side of the area of interest so that the area was unaffected. The width of the grid is 7.3 km while the width of the area of interest is only 3.4 km.

The second grid is a nested grid that was placed inside the first grid. It has a starting depth of approximately 6 m below LLD and extends to the back of the beach. The

nested grid cell dimensions are 10 x 10 metres and the grid only covers the width of the area of interest, from Greenways to the Lourens River. The nested grid receives input information for its boundaries from the coarser grid cells that are closest to the boundary of the nested grid. The nested grid is then able to provide more detail regarding the wave height at the back of the beach.

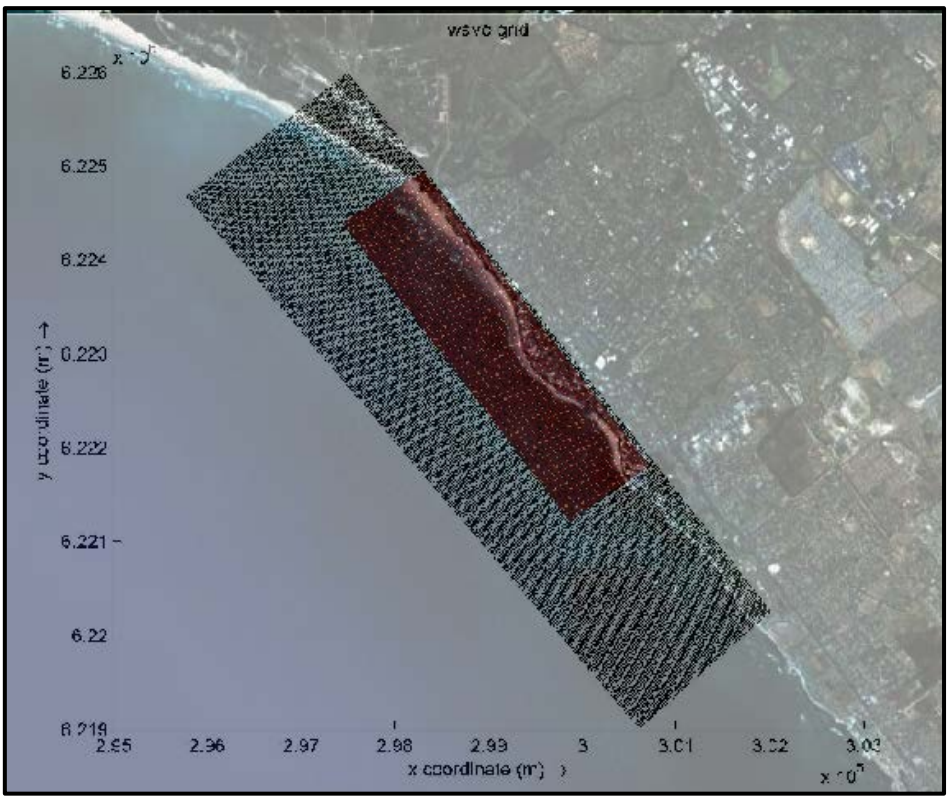

Figure 54: Location of the two computational grids

The bathymetric data for the two grids was created by combining the navigational chart of False Bay, South African Navy survey data of False Bay, land survey data of the Strand beach and visual observations of emerged rocks at known low water tide levels. This data was used to create a sample data file which contained coordinate and depth information from the 11 m below LLD contour, where the wave climate data was available, towards the back of the beach.

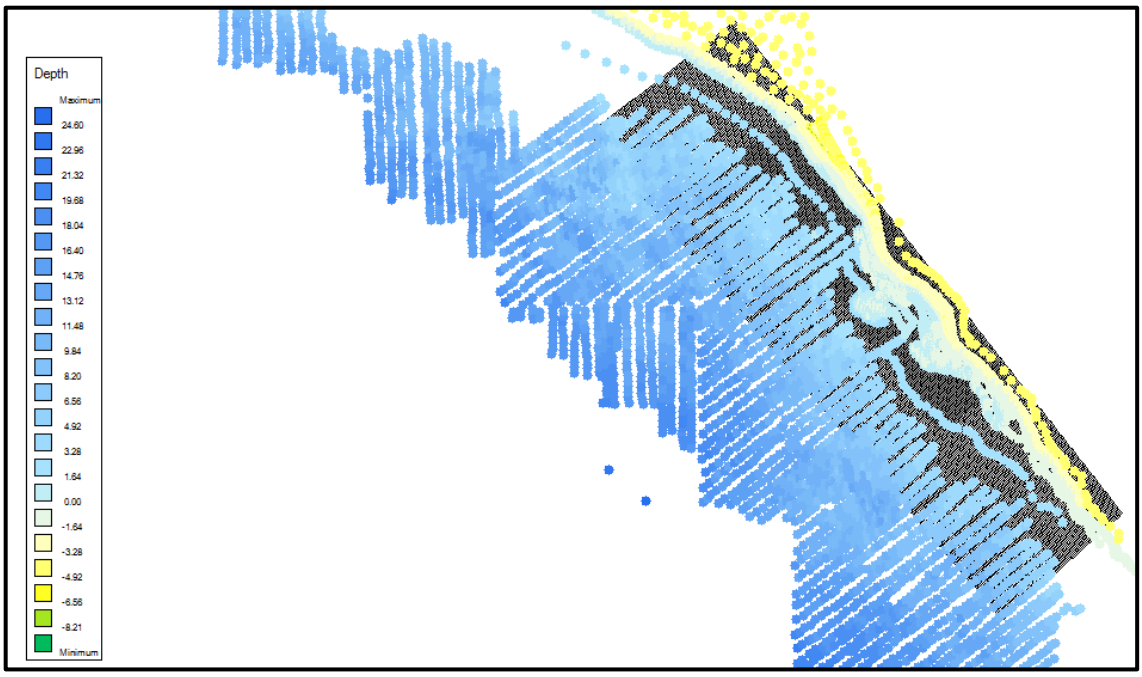

Figure 55: Large grid with depth samples

The depth files for the grids were created by making use of grid cell averaging and triangular interpolation. This provided grid cells without information about the depth inside the cells with the depth information of surrounding cells. Figure 56 shows the depth file that was used by the computations grid derived from the depth samples shown in Figure 55.

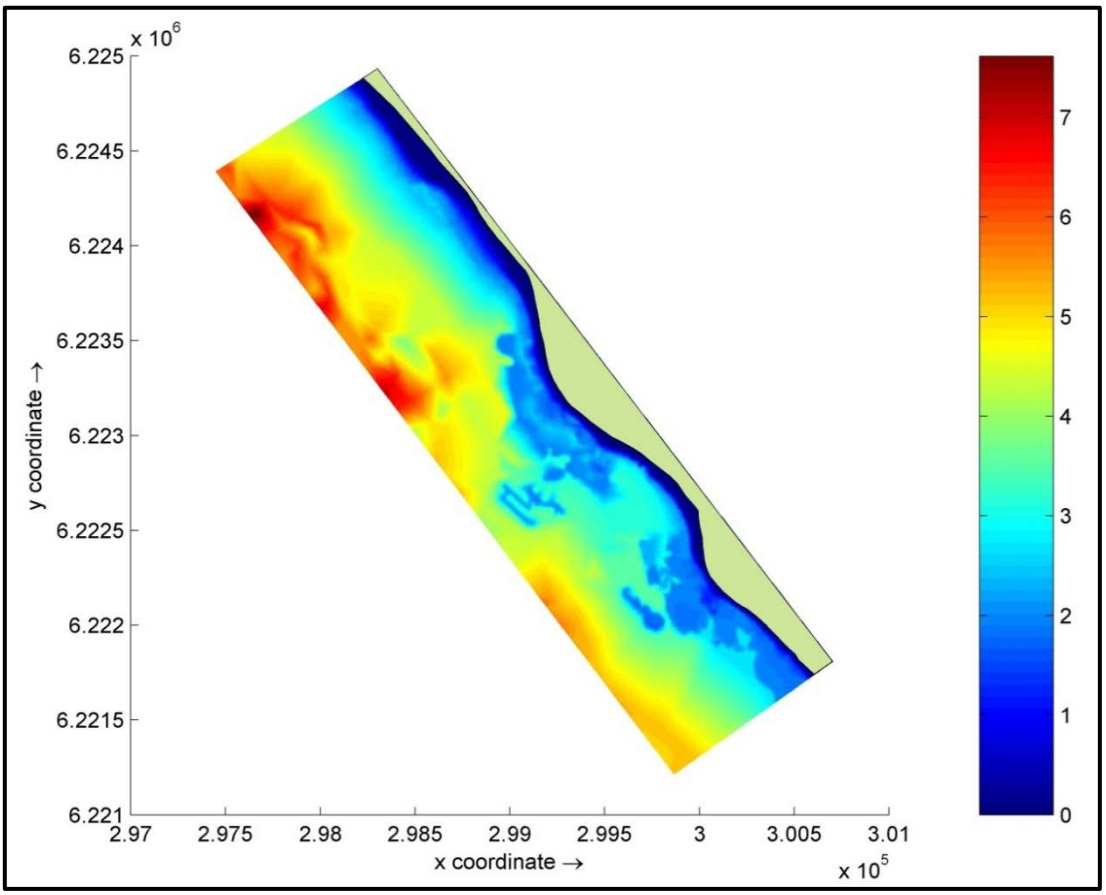

Figure 56: Depth file used by the nested computational grid (depth in m below CD)

4.1.2 Input variables

The wave direction was taken as 225 nautical degrees since the analysis of the wave direction showed that 88% (based on NCEP data) of the waves at the Strand arrive from that direction. The wave peak period was taken as 12 seconds which is the most frequently occurring period in False Bay. An analysis on the sensitivity of the period on the wave height at the back of the beach was completed.

Wave set-up was activated for all the tests, (the residual tide that is measured at Simon's Town does not incorporate wave set-up in the measurements since the measuring gauge is located inside the harbour.)

Sensitivity runs were also done on the gamma value for the JONSWAP spectrum for values of 2.4, 2.7, 3 and 3.3. No visible differences were found in the wave period or wave height at the back of the beach. The default value of 3.3 was used.

The directional spreading was determined from the results of the SWAN analysis of False Bay. The input value for Delft3D-Wave model was 12.4 degrees which was

taken from the output directional spreading value at the Strand from the SWAN model.

There is no information available about the bottom friction of the area. Certain sections along the beach consist only of sand while others contain rock embankments. It was decided to make use of the recommended JONSWAP frictional value of 0.067 m^2/s^3 which is based on a study done by Bouws & Komen (1983) for swell conditions in shallow water. The value was derived from the analysis of a storm in the North Sea with a peak wave period of 11.6 seconds which is very similar to the peak wave period used for this study.

The depth-induced breaker index is unknown for False Bay. Battjes & Stive (1985) found that there is no significant variation in the breaker coefficient due to variation of beach slope or surf similarity parameter. They found that the breaker index is dependent on deepwater wave steepness. It was found that the average breaker index was 0.73 which is within the range of the literature review. A sensitivity run was done and it was found that an increase in the breaker index had an influence on the overall wave height at the back of the beach. It was found that increasing the value from the default Delft3D-Wave value of 0.73 by 0.1 resulted in an overall increase of H_{mo} by 0.08 m at the back of the beach with a 1:20 year water level. Decreasing the breaker index to 0.63 for the same water level resulted in an average decrease of H_{mo} by 0.08 m at the back of the beach. This shows that wave height is somewhat sensitive to the breaker index. The default value of 0.73 was used for the model but this deserves further attention in further studies of this shallow area.

4.2 Numerical modelling results

4.2.1 Design wave height at the back of the beach

The design wave height at the back of the beach was determined by testing different water levels and different wave heights, and the results at the back of the beach were then compared. The input wave heights were selected from the EVA analysis.

4.2.1.1 Current beach level at MHWS

The beach level that was surveyed was tested with MHWS water level and H_{mo} with 1:1 year return period wave height. It was found that the only location that experienced wave action at the back of the beach was between Location H and

Location I as indicated in Figure 27. The other location did not encounter wave action because the water level is below the beach level at the back of the beach.

The result of the test can be seen in Figure 57 which shows the wave height along the Strand. The areas which were found not to encounter wave action at the back of the beach are the areas with the widest beach and highest beach level. The area which did encounter wave action corresponds to the area known for wave action and overtopping as indicated by the Municipality and shown in Figure 27. The average H_{mo} at the back of the beach between Location H and Location I was 0.5 m for 1:1 year return period wave height.

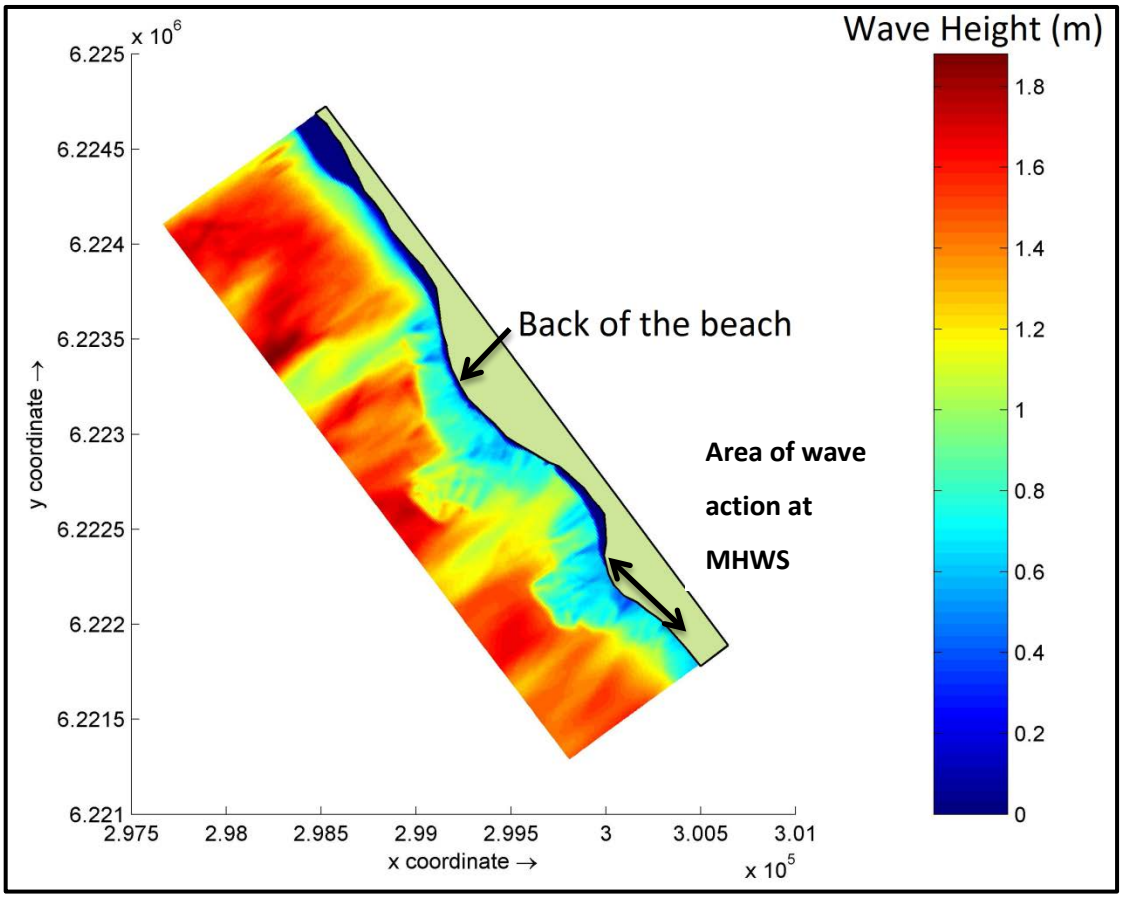

Figure 57: Wave height along the Strand for MHWS and 1:1 year wave condition

When the extreme 1:1 year water level was tested with the 1:1 year wave condition it was found that the same area still experienced wave action and that the H_{mo} at the back of the beach increased to an average height of 0.82 m. This is as a result of the increase in water depth which allows larger waves to reach the back of the beach.

4.2.1.2 Fixed beach level and varied H_{mo}

Due to the variability of the beach level along the Strand, tests were done to determine what the effect of maintaining the beach level at a certain fixed level would have on the wave height at the back of the beach. The slope of the beach was changed by maintaining the original plan width of the beach and then setting the beach level at the back of the beach to the desired level. Triangular interpolation was then used to determine the slope of the beach.

A wave height variability test was done by varying the input extreme wave condition while using a constant beach level at the back of the beach of LLD +1 m. The water level was kept constant at LLD +1.67 m (1:20 year water level in 2012).

Using different wave heights associated with the return period of 1:1, 1:20, 1:50 and 1:100 as an input wave condition resulted in the same average significant wave height along the back of the beach. As expected, the wave height at the back of the beach is depth dependent. Results are shown in Table 15.

Table 15: Average H_{mo} along the back of the beach for different extreme wave heights

Return Period	1:1	1:20	1:50	1:100
H_{mo} Input (m)	1.35	1.71	1.83	1.91
H_{mo} at toe (m)	0.62	0.62	0.62	0.62

Wave action was encountered all along the beach when the beach level was maintained at LLD +1 m. The largest wave conditions were still experienced at Location H to Location I and decreased towards Location A. This could be as a result of the beach width being the narrowest resulting in a steeper beach slope and having the deepest water depth in front of the beach between Location H to Location I. This allows larger waves to reach the back of the beach since less energy could be dissipated by the waves breaking along the shorter width of the beach. The wave height distribution is shown in Figure 58 for a 1:20 year water level along the Strand with the beach level maintained at LLD +1 m. The wave heights shown were all rounded up to the highest digit.

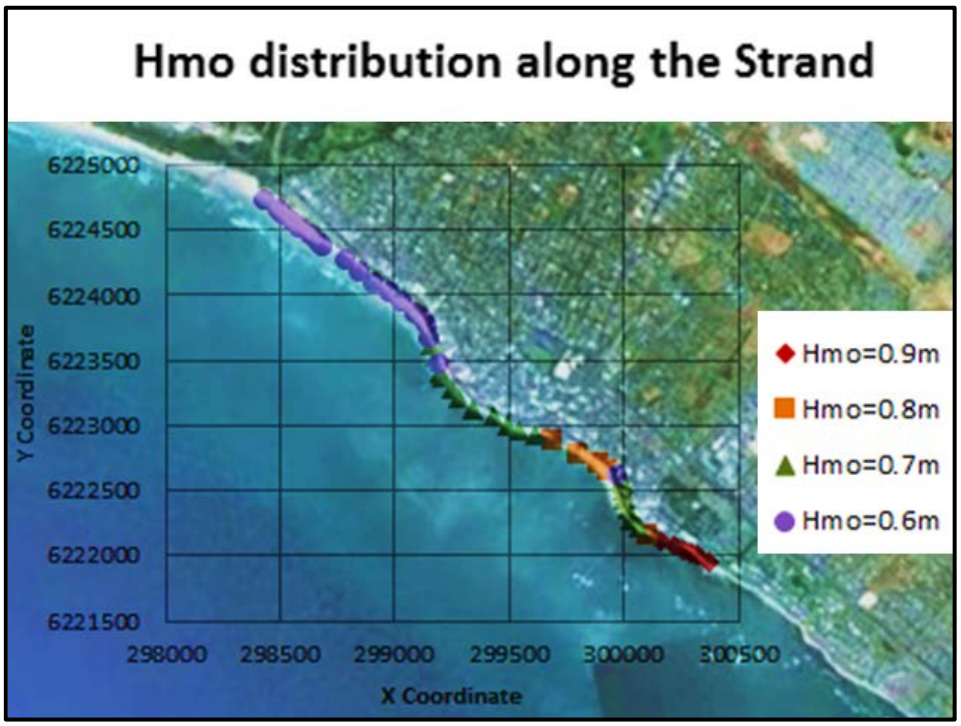

Figure 58: H_{mo} distribution along the Strand for beach level of LLD+1m (1:20 year water level)

4.2.1.3 Average H_{mo} for varied water level and beach level

Tests were then done to determine what the effect of varying the beach level and water level would have on the average H_{mo} at the back of the beach. The input wave condition was shown not to have an effect on the wave height at the back of the beach and therefore the 1:100 year wave height was used as the input wave condition for all the tests. The beach levels were tested at LLD, LLD +0.5 m, LLD +1 m and LLD +1.5 m. The results of the tests are shown in Figure 59.

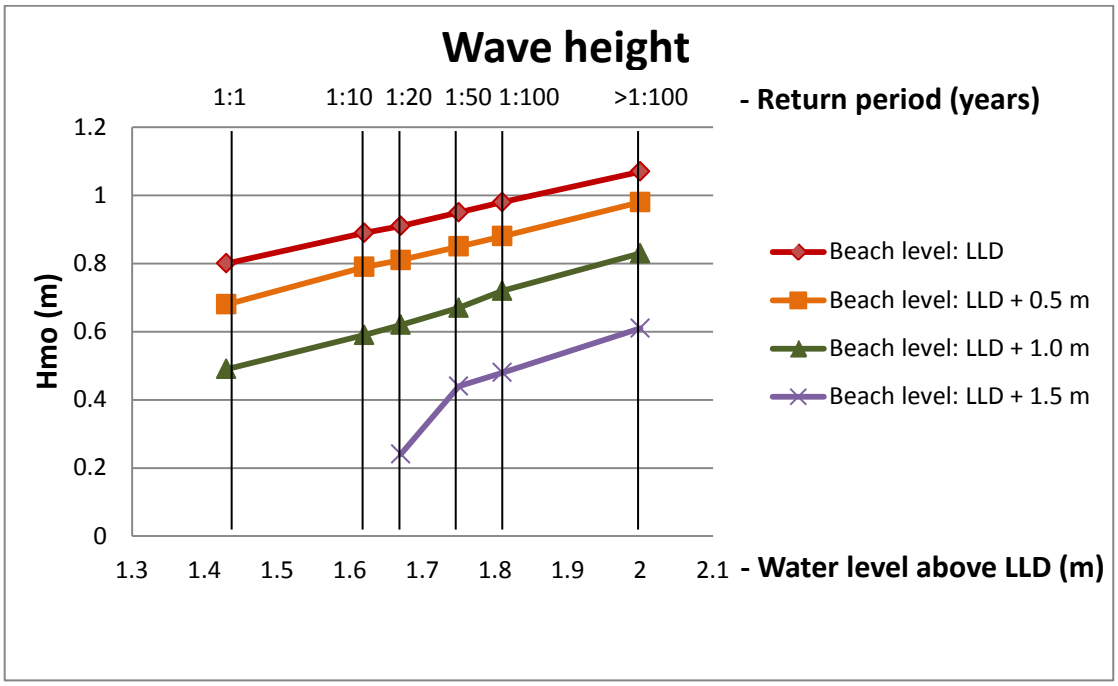

Figure 59: Average H_{mo} at different beach levels for the back of the beach

All the tests showed that the wave height increases with water depth and that the largest waves were found at the lowest beach levels and highest water level. At a beach level of LLD +1.5 m waves could only be measured starting at the 1:20 year water level. The same wave height at a beach level of LLD +1.5 m and at an extreme water level of LLD +2 m (>1:100 year) was found at a water level of LLD+1.67m (1:20 year) and a beach level of LLD +1 m.

As expected the wave height at the back of the beach is dependent on the water depth from high water levels as well as low beach levels.

5 Calculated overtopping

Overtopping calculations were done for the vertical wall using empirical calculations based on the EuroTop Manual (Pullen et al. 2007). The reduction factor for the recurve wall was also determined so that it could be used by multiplying the factor to the overtopping rate of the vertical wall to provide a first estimate of the overtopping for the recurve wall.

5.1 Vertical Wall

The expected overtopping rate for the vertical wall sections at the Strand could be determined by making use of Equations 15, 16 and 17. From the equations it is possible to test which variables have a large influence on the overtopping rate and whether trends in the results can be identified.

The effect of freeboard, period, wave height and water depth was tested. For all the tests a constant water level of LLD +2 m was used to limit the variables. The equations were used according to their valid ranges as indicated in the literature study.

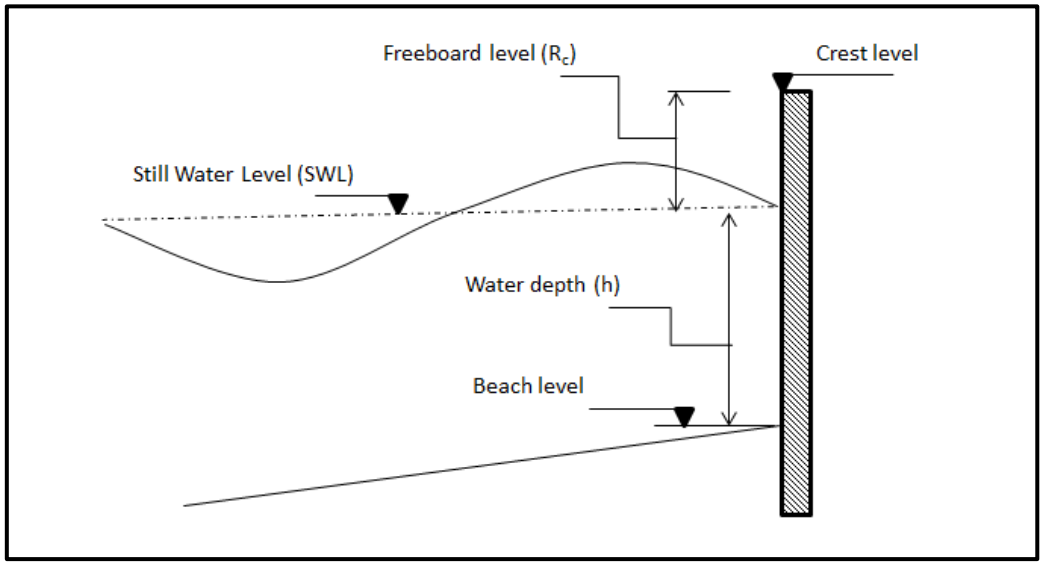

Figure 60: Vertical seawall parameters

5.1.1 Varied freeboard

The effect of varying the freeboard was tested on a fixed beach level of LLD +1 m, T_p of 12 seconds and H_{mo} of 0.6 m. The important variables that were used are listed in Table 16.

Calculated overtopping

Table 16: Results of freeboard on overtopping rate

Crest level (m above LLD)	2.80	3.10	3.40	3.70	4.00	4.50
h*	0.012	0.012	0.012	0.012	0.012	0.012
$h^*.R_c/H_{mo}$	0.016	0.022	0.028	0.034	0.040	0.050
R_c (m)	0.80	1.10	1.40	1.70	2.00	2.50
Overtopping (l/s/m)	8.54	3.62	1.89	1.12	0.72	0.39

Equation 17 was found to be valid for the selected variables. The results show that overtopping is very sensitive to changes in freeboard level. It is therefore very important to build the seawall at the correct crest level to reduce overtopping. Figure 61 shows the results of Equation 17 plotted on a logarithmic graph. As expected, the greatest increase to the overtopping was found at the lowest crest level.

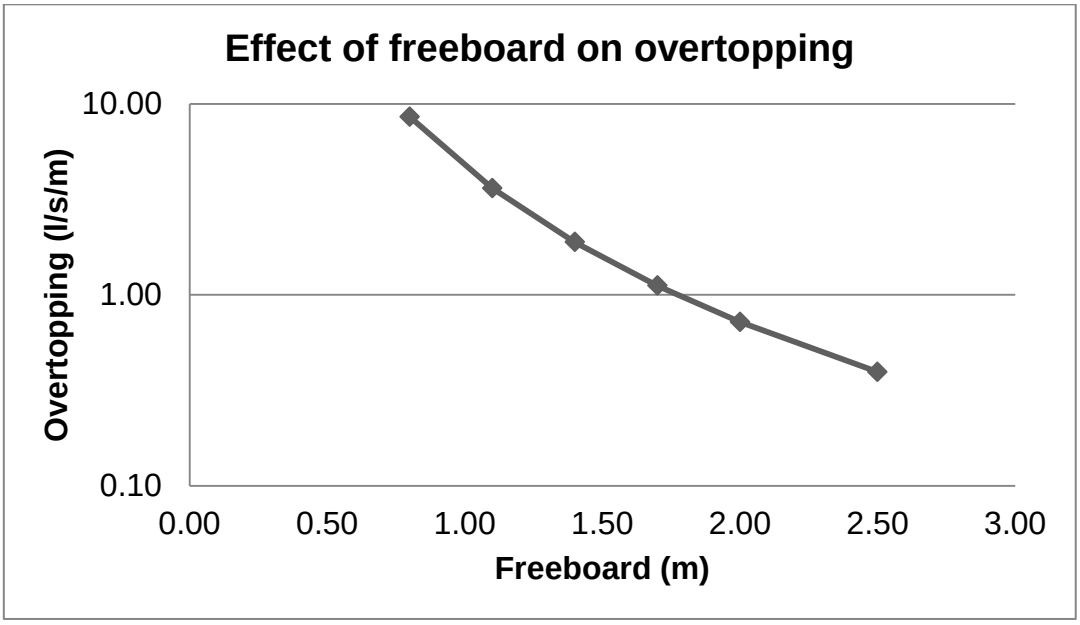

Figure 61: Calculated effect of freeboard on overtopping rate

5.1.2 Varied peak period

The sensitivity of the overtopping rate to changes in the wave peak period was tested. All other variables were kept constant. A beach level of LLD +1 m, H_{mo} of 0.6 m and freeboard of 1.7 m was used. Table 17 contains the results of the overtopping rate using Equation 17 to determine the overtopping.

Calculated overtopping

Table 17: Results of T_p on overtopping rate

T_p (seconds)	8	9	10	11	12	13	14	15	16
h*	0.027	0.022	0.017	0.014	0.012	0.010	0.009	0.008	0.007
$h^*.R_c/H_{mo}$	0.077	0.061	0.049	0.041	0.034	0.029	0.025	0.022	0.019
Overtopping (l/s/m)	0.63	0.75	0.86	0.99	1.12	1.25	1.39	1.53	1.67

Figure 62 shows the results of the sensitivity that a change of period has on the overtopping rate. The overtopping is shown to increase gradually as the period increases. The increase in period from 8 to 16 seconds causes 165% increase in overtopping.

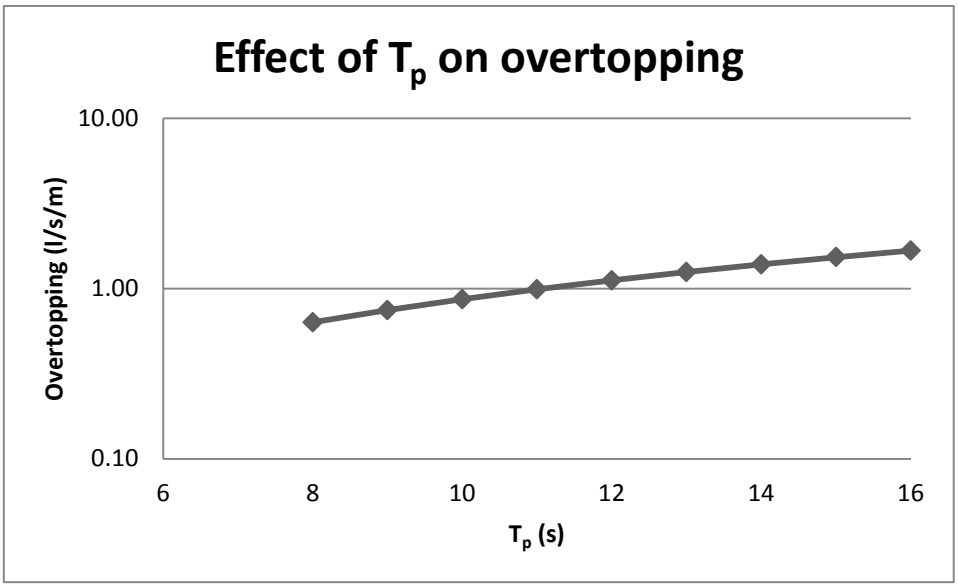

Figure 62: Calculated effect of T_p on overtopping rate

5.1.3 Varied wave height

The effect of increasing the wave height was tested. The following variables were kept constant: beach level of LLD +1 m, water level of LLD +2 m, peak period of 12 seconds and freeboard of 1.7 m. The results are shown in Table 18 using Equation 17.

Table 18: Results of H_{mo} effect on overtopping rate

H_{mo} (m)	0.4	0.5	0.6	0.7	0.8
h*	0.018	0.015	0.012	0.010	0.009
$h^*.R_c/H_{mo}$	0.077	0.049	0.034	0.025	0.019
Overtopping (l/s/m)	0.281	0.601	1.116	1.886	2.969

Calculated overtopping

Figure 63 shows the results of Table 18. The overtopping rate increased significantly as the wave height was increased. This shows that as expected, overtopping is highly sensitive to variability in wave height at the toe of the structure.

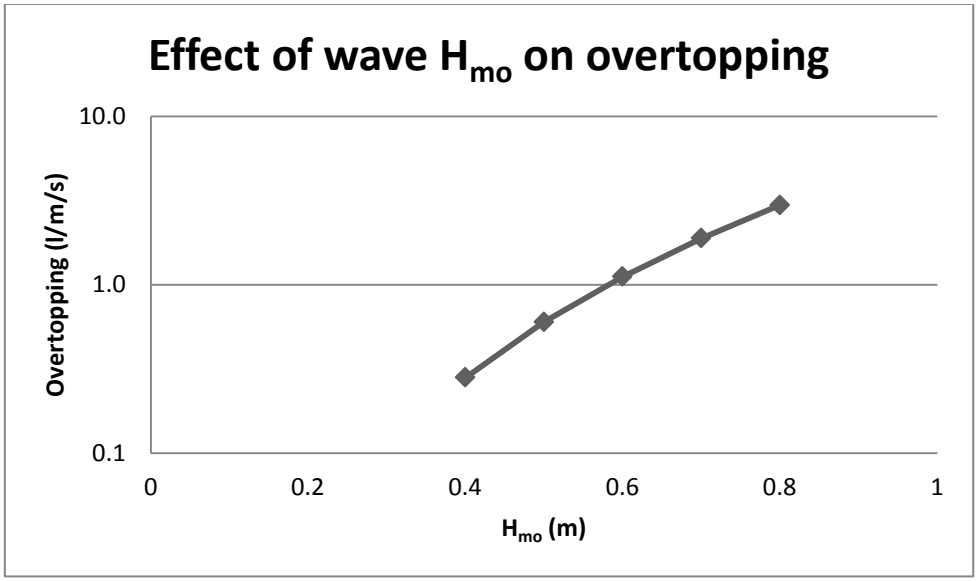

Figure 63: Calculated effect of H_{mo} on overtopping

5.1.4 Varied water depth

The effect of varying the water depth at the toe of the vertical wall on the overtopping rate was tested. A peak period of 12 seconds and H_{mo} of 0.6 m was used. The water depth was increased from 1 m to 3 m. The results of the tests can be found in Table 19 and are shown in Figure 64.

Table 19: Results of varied water depth on overtopping

	h (m)	3.0	2.5	2.0	1.5	1.0
	h*	0.109	0.076	0.048	0.027	0.012
	h*.R_c/H_{mo}	0.254	0.177	0.113	0.064	0.028
q (l/s/m)	**Equ15**	0.135	0.135	0.135	0.135	0.135
	Equ16	2.022	2.297	2.686	3.285	4.363
	Equ17	2.105	2.067	2.021	1.964	1.886
	Valid Equ	Equ16	Equ17	Equ17	Equ17	Equ17

Figure 64 shows that there are no real differences in the overtopping rate at different water depths provided that the wave height is kept constant. The overtopping increased very slightly when the water depth was increased but then decreased as Equation 17 was no longer valid and Equation 16 became valid. The water depth at

the toe of the structure can be varied by changing the beach level. Physical model tests can be done to determine if changes in beach level can be used to decrease the overtopping rate.

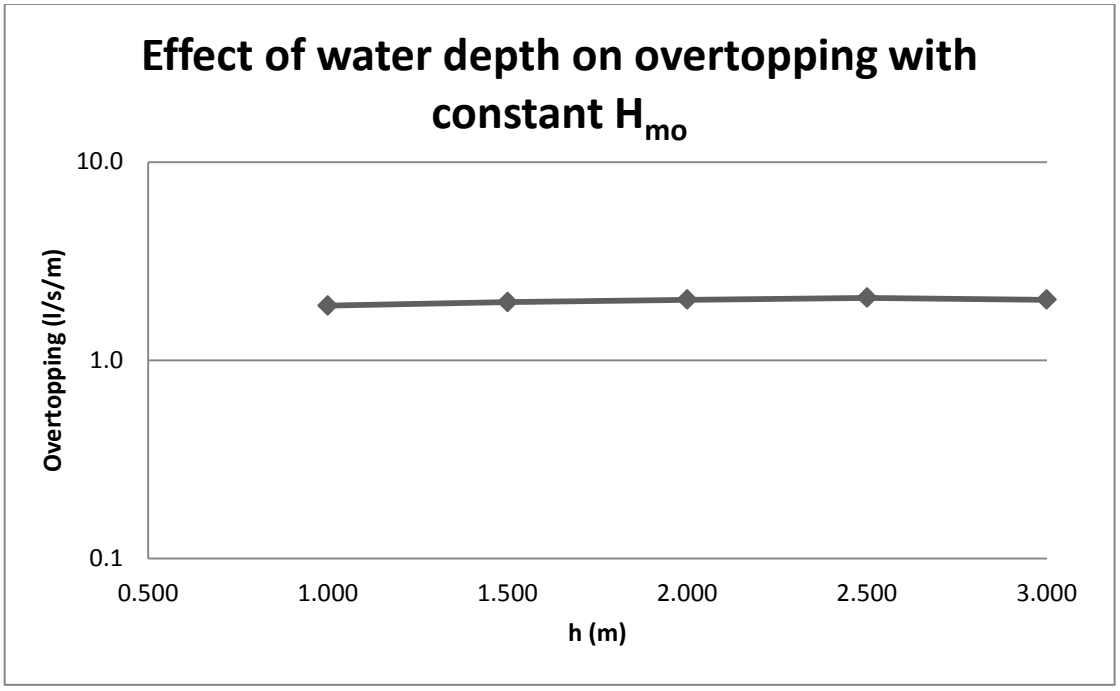

Figure 64: Effect of water depth on overtopping with constant H_{mo}

In reality increasing the water depth would increase the depth limited wave height which would result more overtopping. Equation 16 and 17 do not take this into consideration since they require the H_{mo} at the toe of the structure to be provided.

5.2 Recurve wall

The expected overtopping for a recurve wall could be estimated by making use of a reduction factor (k).The factor was determined with Figure 11 but the k values were all found to be smaller than 0.05. This made the k values unreliable since there was significant scatter found in the results of Kortenhaus et al. (2003) when k<0.05 and it is recommended that physical modelling should rather be used to determine the overtopping rate. Table 20 shows the parameters that were used to determine the reduction factor theoretically.

Table 20: Parameters to determine the recurve reduction factor

R_c (m)	0.8	1.1	1.4	1.7	2.0
P_c (m)	0.2	0.5	0.8	1.1	1.4
Br (m)	0.5	0.5	0.5	0.5	0.5
hr (m)	0.6	0.6	0.6	0.6	0.6
k'	0.199	0.194	0.188	0.183	0.178
m	1.255	1.296	1.319	1.334	1.345
m*	1.004	1.037	1.055	1.068	1.076
R_o*	0.313	0.323	0.329	0.332	0.335
h_c/H_{mo}	1.43	1.90	2.41	2.83	3.33
k	0.040	0.004	0.004	0.004	0.004

Physical modelling was done to determine the actual reduction factor and then be compared to the calculated reduction factor. The actual reduction value can then be applied to empirical calculations to estimate the optimum crest level for a recurve wall.

5.3 Trends from calculations

The empirical formulae give good insight into the major factors that influence the overtopping rate for a vertical wall. The major factors influencing overtopping were found to be the wave height at the toe of the wall and the freeboard height. The overtopping was found to increase gradually with longer wave periods and changes in water depth were seen to cause no visible changes to the overtopping.

6 Physical modelling

6.1 Previous physical modelling

The proposed defences for the Strand have been designed by the consultancy firm PD Naidoo & Associates in 2011 and tested by Stellenbosch (IWEE, 2011). These tests consisted of several recurve walls and composite recurve walls and the results were made available for this study.

The tests were done at various water levels, wave heights and crest levels, making it difficult to determine the main influences in the reduction of the overtopping. No comparisons were done between the recurve wall and a vertical wall therefore the effectiveness of the recurve wall in reducing overtopping is unknown. The results of the tests from the previous study (IWEE, 2011) are compared to the tests of this study to determine whether trends between the test scenarios are similar.

6.2 Physical modelling for this study

The physical modelling for this study is a continuation of previous tests but will focus on the effectiveness of the recurve wall in reducing the overtopping rate compared to a vertical wall. The influence of the beach level and beach slope on the overtopping rate was also investigated in order to determine if maintenance to the beach would help to reduce the required height of the seawall. Overtopping sensitivity tests were also done using wave period. The accuracy of the tests was examined and comparative tests were done with the previous physical modelling tests.

In order to make the test results comparable with each other, the factors which could influence the outcome of the results were limited. A constant scale, wave height, duration of tests and water level were used. The period was kept constant for all the tests except when the sensitivity of the variance of period on the overtopping rate was investigated.

6.2.1 Model Set-up

The tests were completed in a glass flume at the Stellenbosch University's Hydraulic Laboratory. The flume is 1 m wide and 40 m long and is equipped with a wave generator. The wave generator is capable of wave absorption which removes the reflected waves once they reach the wave generator.

The wall sections that were tested were inserted into the flume 27.5 m away from the wave generator and the length of the wall sections were 980 mm. The significant wave height was measured using three electrical resistance probes which measure the electrical resistance of the water to determine the wave height.

The probes were calibrated regularly because they are sensitive to changes in water temperature and other water properties. The probes were placed along the middle of the flume and were not able to be placed at the toe of the wall because the water depth was too shallow for measurements to be taken. The wave height measured in the middle of the flume would not be the same as the wave height at the toe of the structure because the waves undergo shoaling as the water depth decreases. This results in an increase in wave height. This is a limitation in the physical modelling as performed.

An overtopping tray was constructed and placed directly behind the wall section. A catchment plate was used to funnel the water into the overtopping tray. The overtopping water was collected and measured using a scale with an accuracy of less than 10 grams.

All tests were run for a duration of 1000 waves so that the test results could be repeatable. Repeat tests were also conducted to determine the variability in the results.

The bottom profile of the flume that was used is not made as an accurate representation of the Strand since no survey data is available between the water depth of LLD-2.8m and the beach. More accurate survey data is required for the profile to be accurately modelled. The average slope of the flume is 0.012. This is reasonably close to the average nearshore slope of the Strand seabed which is 0.01. Figure 65 shows the layout of the flume and the bottom profile that was used for the majority of the tests. Minor modifications were made to the last few metres of the bottom profile in front of the wall sections when the influence of different beach slopes was being tested.

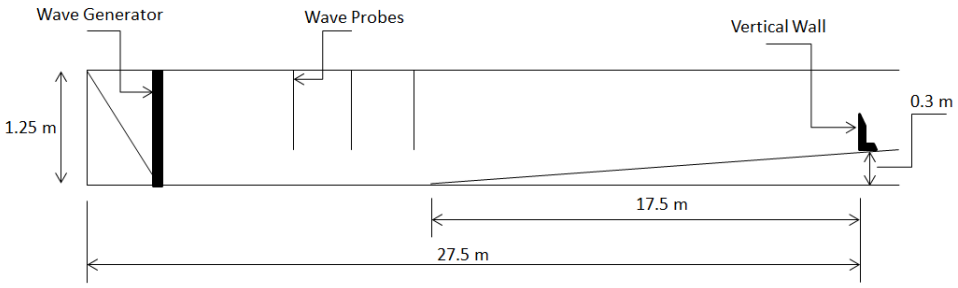

Figure 65: Flume layout

The wall sections were constructed out of Perspex and bolted onto a base plate which was attached to the concrete bottom profile. Figure 66 shows the dimensions of the recurve wall section that was constructed. The wall was made with slots at the bottom so that modular strips could be added to the bottom of the wall sections to increase the height of the crest. The dimensions of the recurve wall are based on the design of a proposed recurve wall for the Strand by WML Coast (2011).

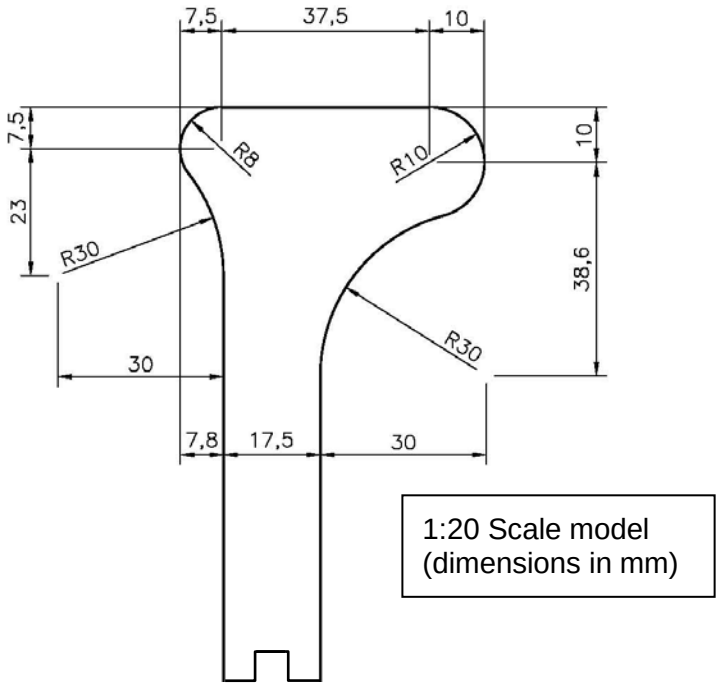

Figure 66: Side view of the recurve wall (WML Coast, 2011)

Figure 67 shows a side view of the recurve wall with the modular sections inserted below the wall. Behind the wall the catchment plate can be seen funnelling the overtopped water into the overtopping tray.

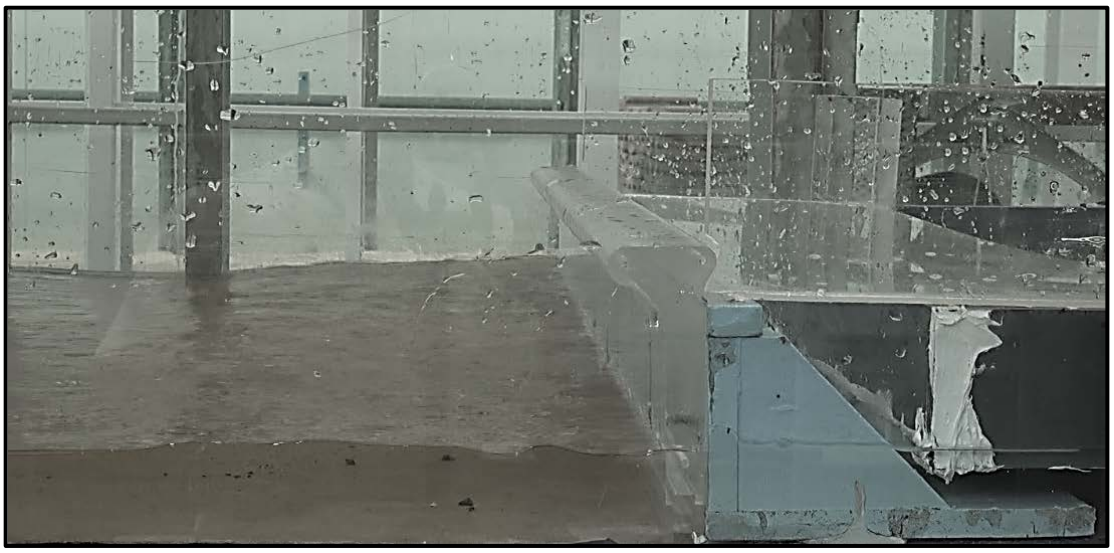

Figure 67: Side view of recurve wall in the flume with a low beach level

6.2.2 Wave height and water depth

To limit the variables of the physical modelling only one water level and wave height was used. The beach level at the back of the beach at the Strand varies between LLD +1.5 m and LLD +1 m. It was decided to make use of an extreme water level of LLD +2 m in order to test the overtopping conditions for several different beach levels while waves were still able to reach the back of the beach.

The H_{mo} was selected as 0.6 m which is associated with two beach level conditions: an extreme water level of LLD +2 m, a beach level of LLD +1.5 m and a 1:20 year water level of LLD +1.67m at a beach level of LLD +1 m.

6.2.3 Scaled Parameters

A length scale (L_{Scale}) of 1:20 was chosen. Table 21 shows the scaling equations for the main parameters which were used.

Table 21: Scaled parameters

Parameter	Equation	Prototype	Model
Period	$T_{model} = T_{prototype}/\sqrt{L_{Scale}}$	12 s	2.683 s
Wave height	$H_{model} = H_{prototype}/L_{Scale}$	0.6 m	0.03 m
Water depth	$h_{model} = h_{prototype}/L_{Scale}$	LLD +2 m	0.1 m
Overtopping	$q_{model} = q_{prototype}/L_{scale}^{\frac{3}{2}}$		

H: Wave height

h: Water depth at toe

$L_{Scale:}$ Length scale

q: Overtopping rate

T: Period

6.2.4 Model tests

6.2.4.1 Recurve vs. vertical wall

The effect of adding a recurve profile on a vertical seawall was tested by comparing results of the two types of wall section at the same crest level. Ten tests were completed with one test for each of the wall sections at a specified crest level. The crest levels were varied from LLD +2.8 m to LLD +4 m at 300 mm increments. A T_p of 12 seconds, H_{mo} of 0.6 m, water level of LLD +2 m and beach slope of 1:50 were used.

6.2.4.2 Slope of the beach profile

The effect of different beach slopes for the Strand beach area was tested. The following slopes were tested: 1/50, 1/30, 1/20, 1/10. The Strand has a shallow rock bank which is located at approximately LLD – 0.2 m and stretches from below the seawall at the back of the beach towards the sea. The slope of the beach was tested with a constant beach level of LLD +1 m at the toe of the recurve wall. Figure 68 shows the different slopes, beach levels and the rock layer.

Four different freeboard tests were completed per beach slope by varying the wall height. The period, wave height and water level were kept constant during these tests.

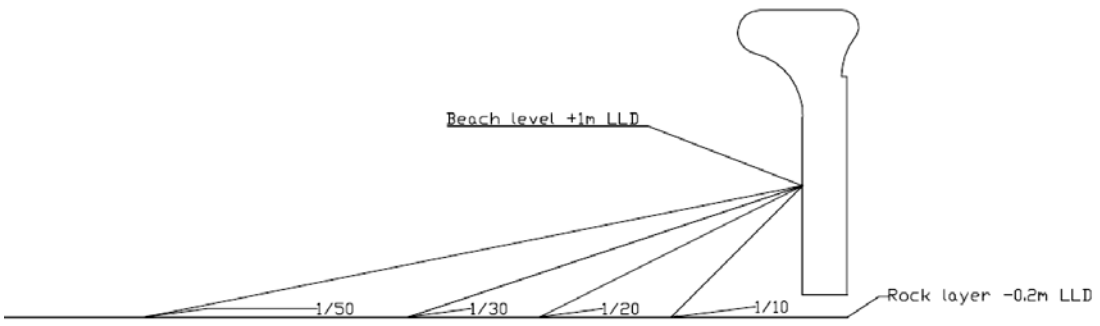

Figure 68: Beach slope

A T_p of 12 seconds, H_{mo} of 0.6 m and water level of LLD +2 m were used. The beach width was changed as the slope was adjusted to ensure that the beach level was maintained as +1 m LLD for all the tests. Table 22 shows the width of the beach for the different beach slopes.

Table 22: Beach width

Slope	Beach width (m)
1/10	12
1/20	24
1/30	36
1/50	60

6.2.4.3 Sensitivity

6.2.4.3.1 Period

The sensitivity of overtopping to period was tested. T_p was increased from 8 second to 16 seconds in increments of 2 seconds. The water level was at LLD +2 m, beach level was at LLD +1 m, crest level was at LLD +3.4 m and the slope was at 1:50.

6.2.4.3.2 Beach level

The sensitivity of overtopping to changes in beach levels was tested. The beach levels of LLD, LLD +0.5 m, LLD +1 m and LLD +1.5 m were tested. The beach slope was kept constant at 1:50, the water level was at LLD +2 m, the crest level was at LLD +3.4 m and an H_{mo} of 0.6 m was used.

6.2.4.4 Comparative and accuracy tests

Four test scenarios were repeated to determine if the tests could be accurately repeated and what the variability in the test results are. Each of the four scenarios was repeated 3 times.

The first two scenarios that were chosen to be investigated was a recurve wall with a high crest level of LLD +3.7 m which would produce low overtopping results (Test 12) and a low crest level of LLD +2.8 m which would result in higher overtopping (Test 9). A T_p of 12 seconds, H_{mo} of 0.6 m and water level of LLD +2 m were used.

PD Naidoo & Associates Consulting Engineering has made the results of their physical modelling tests of overtopping at the Strand available for this (IWEE, 2011). Two scenarios were chosen from their set of tests to determine the accuracy of this study's results compared to the set of tests from the previous study. The two test scenarios that were chosen are Test US19 and Test US20. A T_p of 12 seconds, H_{mo} of 1.7 m and water level of LLD +1.67 m were used.

6.3 Results

6.3.1 Effectiveness of a recurve seawall

The recurve wall was found to be effective in reducing the overtopping at each of the freeboard heights that were tested. The results are shown in Figure 69. It is noticeable that the effectiveness of a recurve wall increases as the freeboard height increases.

The overtopping limit for trained staff to be able to walk safely next to the wall and vehicles to drive slowly on a road is 1 l/s/m. This limit was reached with the recurve wall at a freeboard of 1.2 m while the vertical wall only managed to achieve this limit with a freeboard of 1.6 m. The recurve wall clearly has an advantage by offering the same level of protection as a vertical wall at a 25% lower freeboard level.

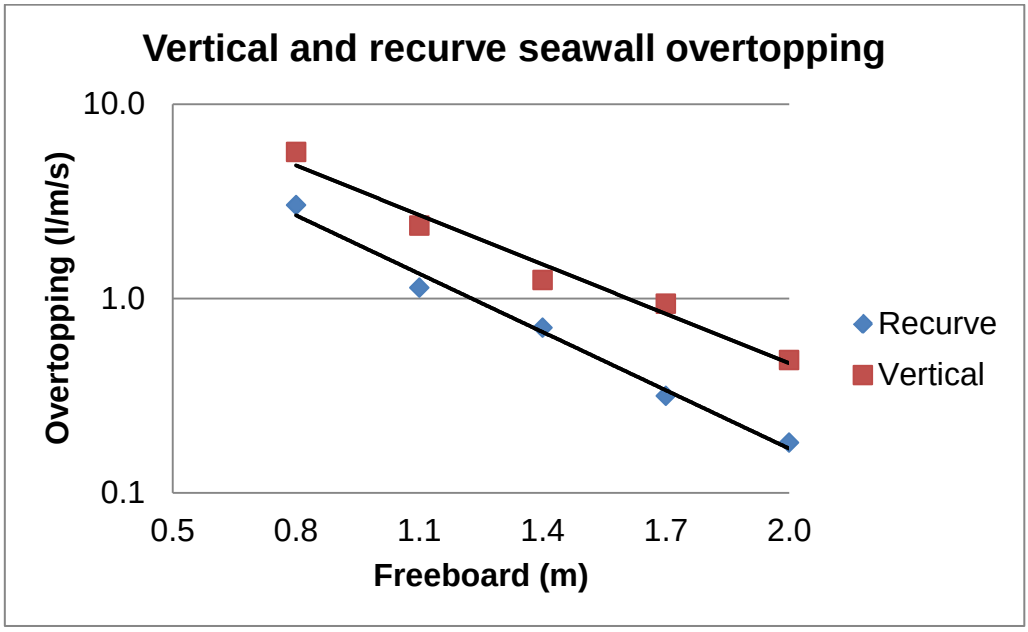

Figure 69: Effectiveness of the recurve wall

Additional information regarding the tests shown in Figure 69 can be found in Table 23.

Table 23: Effectiveness of recurve wall results

			Prototype		
***Test**	**Date**	**Wall Type**	**Rc (m)**	**H_{mo} measured (m)**	**q (l/s/m)**
13	11/04/2012	Recurve	0.8	0.56	3.016
14	03/04/2012	Recurve	1.1	0.58	1.133
15	03/04/2012	Recurve	1.4	0.58	0.704
16	03/04/2012	Recurve	1.7	0.60	0.314
17	03/04/2012	Recurve	2.0	0.60	0.181
22	04/04/2012	Vertical	0.8	0.56	5.67
18	04/04/2012	Vertical	1.1	0.58	2.368
19	04/04/2012	Vertical	1.4	0.58	1.242
20	04/04/2012	Vertical	1.7	0.60	0.936
21	11/04/2012	Vertical	2.0	0.60	0.481

Constants	
Slope	1/50
T_p (s)	12
Water level above LLD (m)	2

*Tests are grouped by wall type and arranged according to increasing freeboard.

6.3.2 Slope of the beach profile

The tests for the beach profile show that there was an increase in the overtopping rate when the beach slope became gentler and the beach width increased. The lowest overtopping rates were found to be at the steepest beach slope of 1:10 which had the narrowest beach width. The highest overtopping was found where the beach profile had a slope of 1:30 and a relatively wide beach.

Figure 70 shows that the slope and thereby the width of the beach have an influence on the rate of overtopping but not at low freeboard levels. For a freeboard height of 0.8 m there was found to be no significant difference in the overtopping rate. This could be because the overtopping rate was high since the recurve wall was less effective in preventing overtopping. The influence of the beach width and slope becomes more apparent as the freeboard level increases.

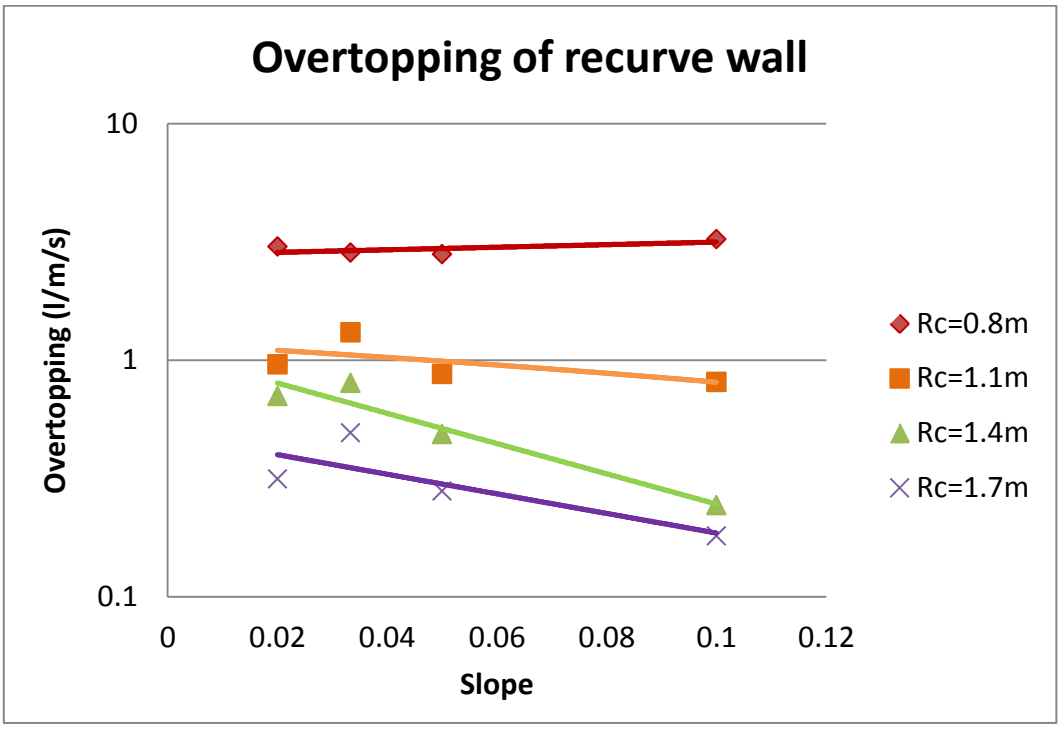

Figure 70: Effect of beach slope on overtopping for pulsating waves

The waves that reached the recurve wall were all pulsating. The reason why a lower overtopping rate is found at the steepest beach slope could be as a result of the waves propagating over a much shorter distance (beach width is reduced as beach steepness increases) along the decreasing water depth which results in less shoaling. A gentler sloped wider beach which would experience an increase in wave height earlier from shoaling since the water depth decreases further away from the seawall. More details about the results can be found in Table 24.

Separate tests should be done to distinguish between the effect that the beach slope and the beach width has on the overtopping rate. The tests should be done for both pulsating and impulsive wave conditions to determine if there are differences between the different wave conditions.

Table 24: Beach slope test results

			Prototype		
Test	**Date**	**Slope**	**R_c (m)**	**H_{mo} measured (m)**	**q (l/s/m)**
13	03/04/2012	1/50	0.8	0.56	3.016
14	03/04/2012	1/50	1.1	0.58	1.133
15	03/04/2012	1/50	1.4	0.58	0.704
16	03/04/2012	1/50	1.7	0.6	0.314
5	27/03/2012	1/30	0.8	0.56	2.847
6	28/03/2012	1/30	1.1	0.56	1.312
7	27/03/2012	1/30	1.4	0.56	0.801
8	28/03/2012	1/30	1.7	0.58	0.493
1	26/03/2012	1/20	0.8	0.56	2.806
2	26/03/2012	1/20	1.1	0.56	0.874
3	26/03/2012	1/20	1.4	0.56	0.487
4	26/03/2012	1/20	1.7	0.56	0.279
9	30/03/2012	1/10	0.8	0.58	3.24
10	30/03/2012	1/10	1.1	0.58	0.809
11	30/03/2012	1/10	1.4	0.6	0.244
12	30/03/2012	1/10	1.7	0.6	0.18

Constants	
Wall type	recurve
T_p (s)	12
Water level above LLD (m)	2

6.3.3 Beach levels

The results of the four beach level tests are shown in Figure 71. The overtopping initially increased when the beach level was increased from LLD to LLD +1 m but then decreased significantly when the beach level was adjusted to LLD +1.5 m. This is because the initial waves were pulsating and increased in wave height due to shoaling up to the beach level of +1 m LLD, after which the waves started to break before they reached the wall resulting in a much smaller wave at the toe of the structure.

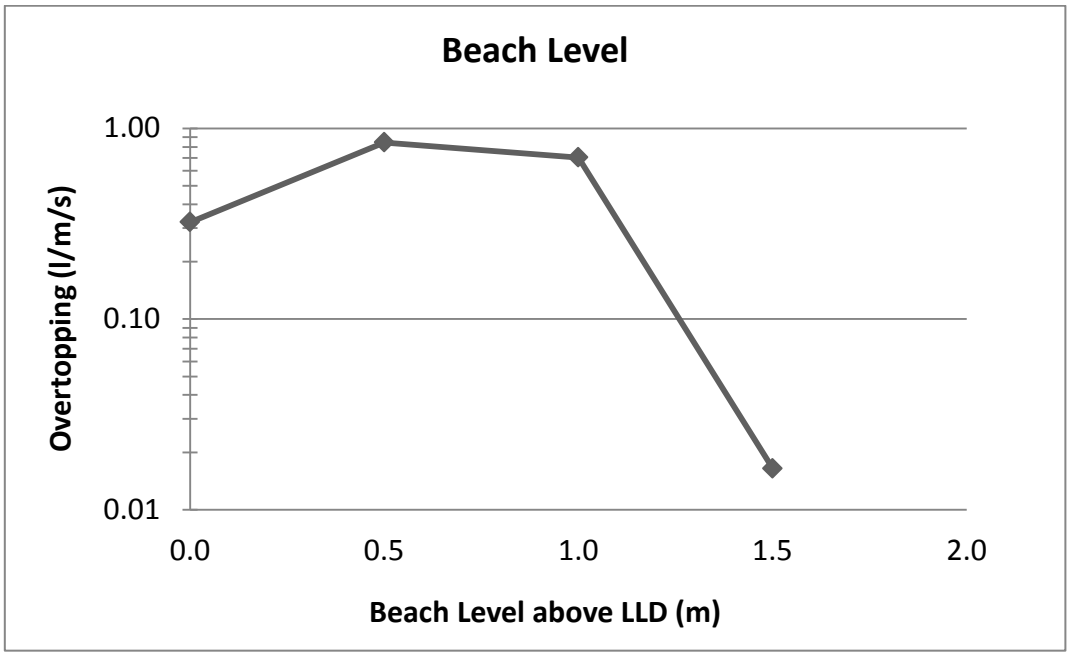

Figure 71: Effect of changing the beach level

The results showed that maintaining the beach between LLD to LLD +1 m does not influence the overtopping much with a water level of LLD +2 m but if the beach level could be maintained at LLD +1.5 m the overtopping could be reduced significantly below the threshold of 1 l/s/m. This would allow for the height of the wall to be reduced significantly. Further details about the results in Figure 71 can be found in Table 25.

Further tests should be done with a wider variety of water levels, wave heights and crest levels in order to optimise the beach level that is required at different water levels.

Table 25: Beach level results

		Prototype		
Test	**Date**	**Beach level above LLD (m)**	**H_{mo} measured (m)**	**q (l/s/m)**
30	10/04/2012	0.0	0.60	0.323
31	10/04/2012	0.5	0.60	0.844
15	03/04/2012	1.0	0.58	0.704
32	11/04/2012	1.5	0.56	0.016
Constants				
Wall type			recurve	
Slope			1/50	
T_p (s)			12	
Water level above LLD (m)			2	
R_c (m)			1.4	

6.3.4 Sensitivity to period

It was found that the overtopping increased as the wave peak period increased up to 12 seconds after which the overtopping decreased again. This is as a result of the wave height increasing from shoaling since longer period waves have a longer wave length and start shoaling in deeper water. The tests with 14 and 16 seconds wave periods started to break before they reached the recurve wall because they were reaching the depth-induced breaking limit. This caused the waves to lose energy and resulted in smaller broken waves reaching the wall. The model tests are therefore very sensitive to wave height and wave period. Further details about the results in Figure 72 can be found in Table 26.

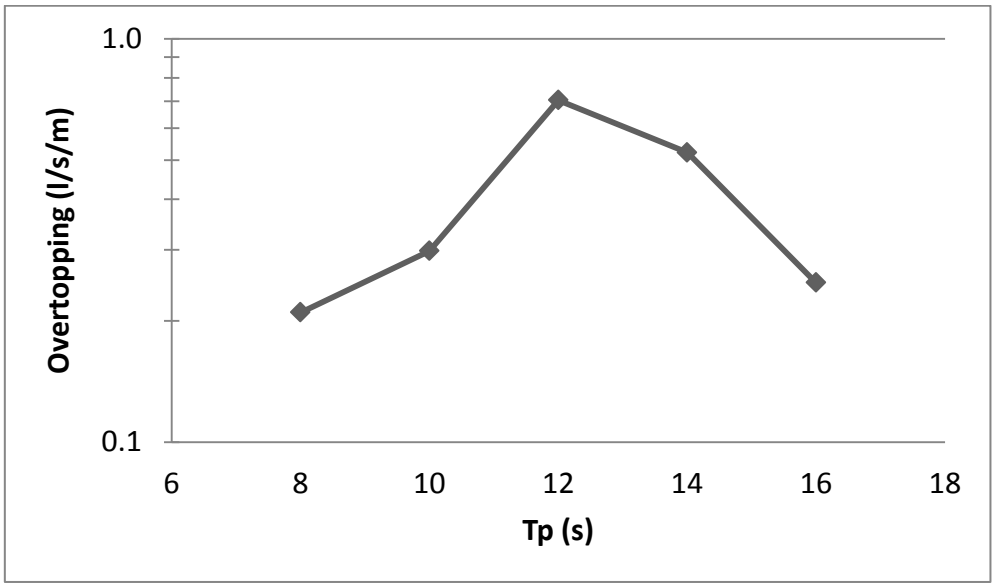

Figure 72: Effect of variation period on overtopping

The tests show that in depth-limited areas waves with a smaller period could cause more overtopping than the longer wave periods associated with extreme wave conditions. It is therefore important to not only test the expected worst case scenarios when designing a coastal defensive structure.

The results show that using T_p of 12 seconds to model the Strand is a good choice since it is the most frequently occurring wave peak period in False Bay and it resulted in the highest overtopping rate.

Table 26: Peak period sensitivity results

		Prototype		
Test	**Date**	**T_p (s)**	**H_{mo} measured (m)**	**q (l/s/m)**
23	03/04/2012	8	0.56	0.21
33	10/04/2012	10	0.56	0.298
15	03/04/2012	12	0.58	0.704
24	03/04/2012	14	0.56	0.523
25	03/04/2012	16	0.6	0.249

Constants	
Wall type	recurve
Slope	1/50
T_p (s)	12
Water level above LLD (m)	2
R_c (m)	1.4

6.3.5 Comparative and accuracy testing

Test US29 and Test US28 from the previous physical modelling (IWEE, 2011) were repeated to determine if direct comparisons could be made between the results. The accuracy of the physical modelling in the tests which formed part of this study was also tested. Repeat tests of Test 9 and Test 12 were done.

Figure 73 and 74 shows the results of the comparative and accuracy tests plotted. All the tests showed a high level of accuracy and repeatability. Therefore, the previous physical modelling results are comparable to the physical modelling results of this study. The results and set-up parameters for the comparative and accuracy tests can be found in Table A 1-3 in the Appendix.

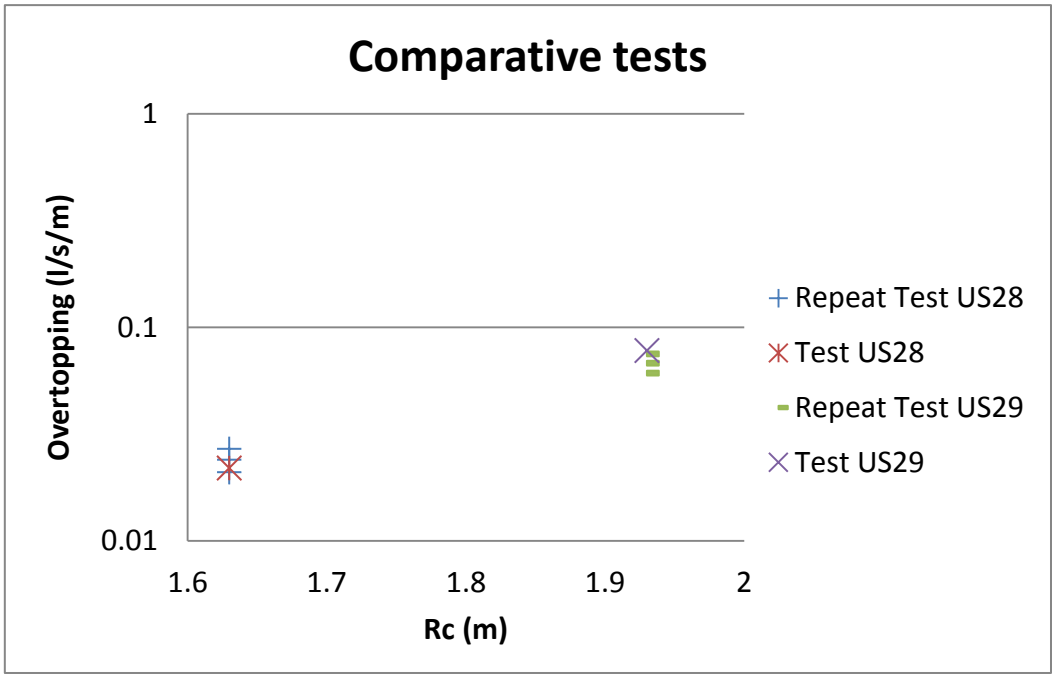

Figure 73: Comparative tests

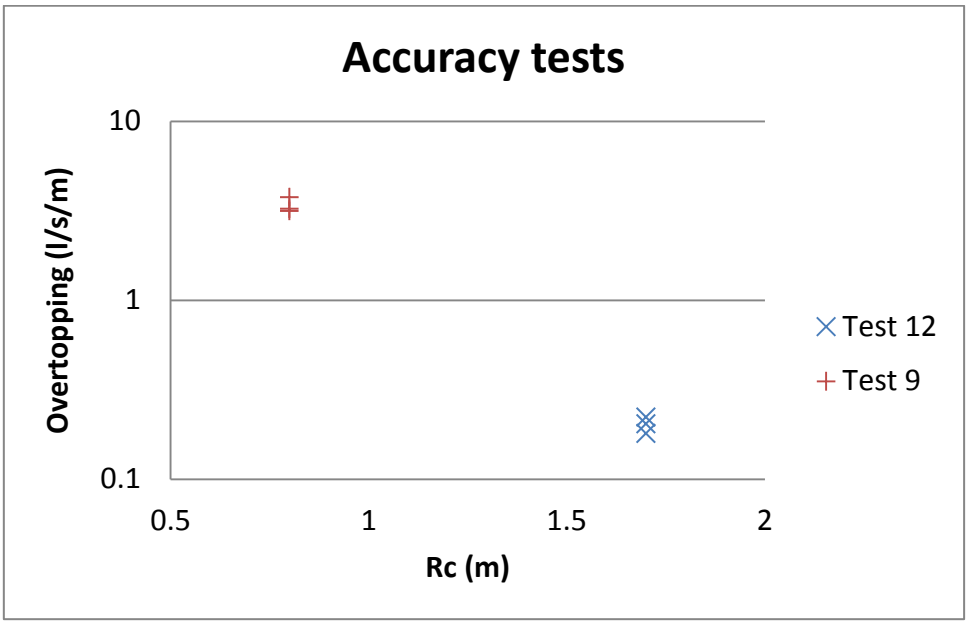

Figure 74: Accuracy tests

7 Interpretation of results

The results of the physical modelling are compared to overtopping estimation methods for vertical walls. The predicted recurve reduction factor is compared with the actual reduction factor from the physical modelling.

Several comparisons are made between the results of the physical modelling of this study and the previous study. This includes beach level, water level and freeboard comparisons. Trends in the results are also discussed.

7.1 Comparison of overtopping estimation methods

7.1.1 Vertical wall

A comparison between the empirical equation for vertical walls, the estimated values from the CRESS overtopping calculation tool and the measured values from the vertical wall tests was done. The CRESS tool selected was the Van der Waal overtopping equation (Van der Waal, 1992). Details about the parameters used for the tests and results can be seen in Table A 4 in the Appendix.

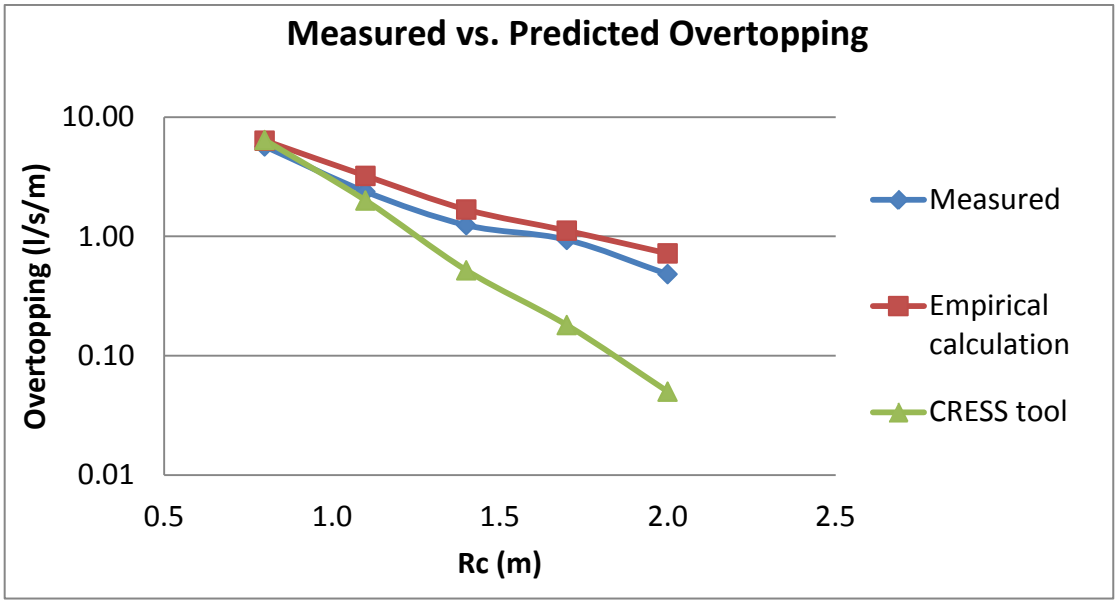

Figure 75: Comparison of predicted and measured overtopping of a vertical wall

In Figure 75 it can be seen that the empirical calculation using Equation 17 (Pullen et al. 2007) is a good estimate for overtopping in this model. The CRESS tool is only accurate in predicting overtopping at relatively low freeboard levels.

The impulsiveness parameter (h_*) of the wave condition that is used in the empirical formula was smaller than 0.2 which suggests that the waves are breaking (Equation 17) but the waves were found to be pulsating. Kim (2009) determined that this could happen when the wave period is long while the wave height is relatively low. The impulsiveness parameter should rather be seen as an indicator for which equations are valid and not necessarily the breaking conditions of the wave.

The Neural Network (NN) overtopping tool was also investigated for this case but it was found that the wave steepness fell outside the testable range of the programme. The testable range of wave steepness is between 0.005-0.07 while the vertical wall tests of this study have a wave steepness of 0.003. A comparison was made between the NN overtopping tool, CRESS overtopping tool and the associated empirical equation for the following input parameters which fall within the testable wave steepness range: $T_{m-1.0}$ of 8.7 seconds, water depth of 1 m and H_{mo} of 0.6 m. Details regarding the results can be found in Table A 5 in the Appendix.

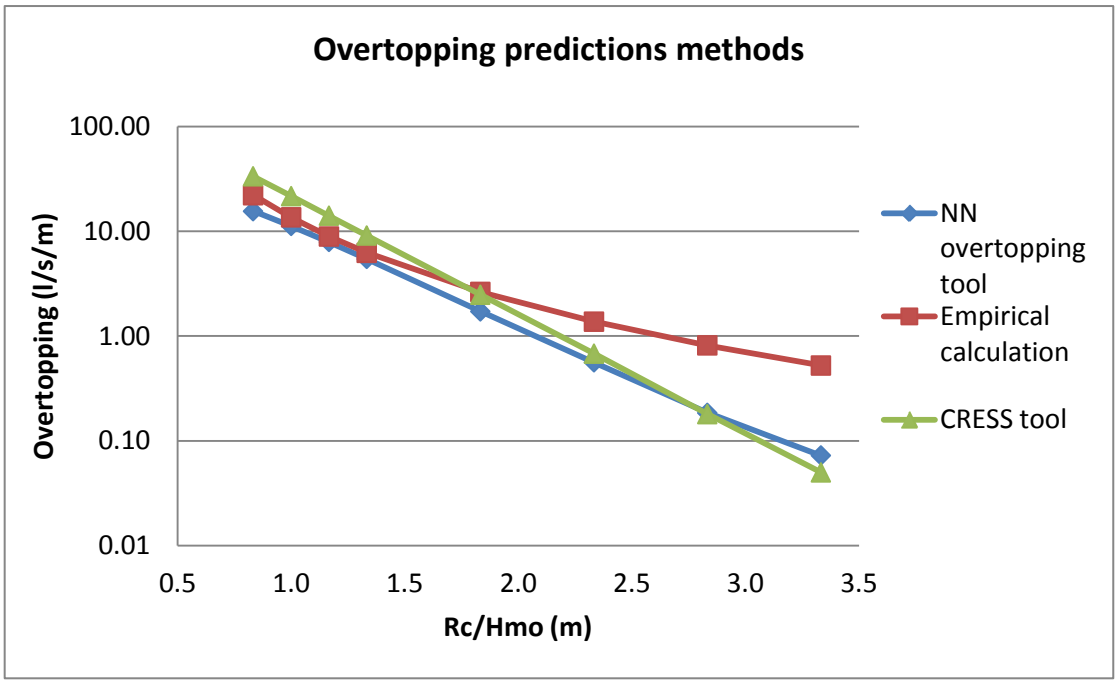

Figure 76: Overtopping prediction methods

It was found that the results of the NN overtopping tool, CRESS tool and empirical calculations converge when the ratio of R_c/H_{mo} is less than 1.83. The results of the NN overtopping tool and the CRESS tool are both very similar within the tested range while the empirical calculation produced much larger overtopping values than the prediction tools at high freeboard levels. This is very similar to Figure 75 which also

showed that the CRESS tool underpredicted the overtopping rate of empirical calculations and the measured overtopping from the physical modelling.

It is therefore important to ensure that the ratio of R_c/H_{mo} is no greater than 1.83 when using the prediction methods.

7.1.2 Empirical reduction factor

The actual reduction factor achieved by the recurve wall was determined by dividing the measured overtopping of the recurve wall with the measured overtopping of the vertical wall. The results are shown in Table 27. The average reduction factor that was achieved is 0.46 which is a 54% reduction in overtopping. The highest reduction factors (k) were found at the lowest ratio of R_c/H_{mo}. This indicates that the recurve wall is most effective in reducing overtopping when the ratio of R_c/H_{mo} is greater than 2.5.

The results correspond well to Cornett et al. (1999) who tested chamfered parapets on vertical seawalls. He found that the mean reduction in overtopping for the range of tests ($0.67<R_c/H_{mo}<3.33$) was 60%.

Table 27: Actual recurve reduction value (k)

R_c/H_{mo}	1.43	1.90	2.41	2.83	3.33
Recurve wall	Test 13	Test 14	Test 15	Test 16	Test 17
Overtopping measured (l/s/m)	3.015	1.132	0.704	0.314	0.180
Vertical wall	Test 22	Test 18	Test 19	Test 20	Test 21
Overtopping measured (l/s/m)	5.670	2.368	1.242	0.936	0.481
k	0.53	0.48	0.57	0.34	0.38

The generic overtopping reduction factor that was determined by Kortenhaus et al. (2003) was not effective in predicting the expected overtopping. The generic method was derived by making use of the results of a limited number of parapet and recurve seawall designs. The differences between the generic overtopping reduction factor and the actual reduction factor could be as a result of the geometric design of the recurve wall used in this study does not fit the geometric designs that were used to derive the generic method.

7.2 Comparison with previous physical modelling

Comparisons are made between the previous physical modelling and the physical modelling of this study. The results of the effect of beach level and freeboard on overtopping are compared for different water levels and wave heights.

7.2.1 Beach level comparison

The effect that a varying beach level has on overtopping is compared for the results of the tests of this study and the tests of the previous physical modelling. The objective is to determine if the same type of response to the changes in beach level is visible in both physical modelling studies. Table 28 contains the variables of the two test series. There is a difference in water level, wave height and freeboard for the two test series.

Table 28: Beach level comparison

	Series 1 (previous study)			**Series 2 (current study)**			
Beach level (m above LLD)	0.0	0.5	1.0	0.0	0.5	1.0	1.5
R_c (m)	2.33	2.33	2.33	1.4	1.4	1.4	1.4
H_{mo} input (m)	1.7	1.7	1.7	0.6	0.6	0.6	0.6
Water level (m above LLD)	1.67	1.67	1.67	2.0	2.0	2.0	2.0
Overtopping (l/s/m)	2.540	0.205	0.022	0.323	0.844	0.704	0.016

The results of the tests are shown in Figure 77. The overtopping was found to decrease again as the beach level was increased but Series 1 was much more sensitive to the increase in beach level than Series 2. This is as a result of the waves breaking and reducing in size as the wave depth at the back of the beach decreases when the beach level increases. Series 1 had larger waves approaching the beach than Series 2 and therefore reached the depth induced breaking limit before Series 2.

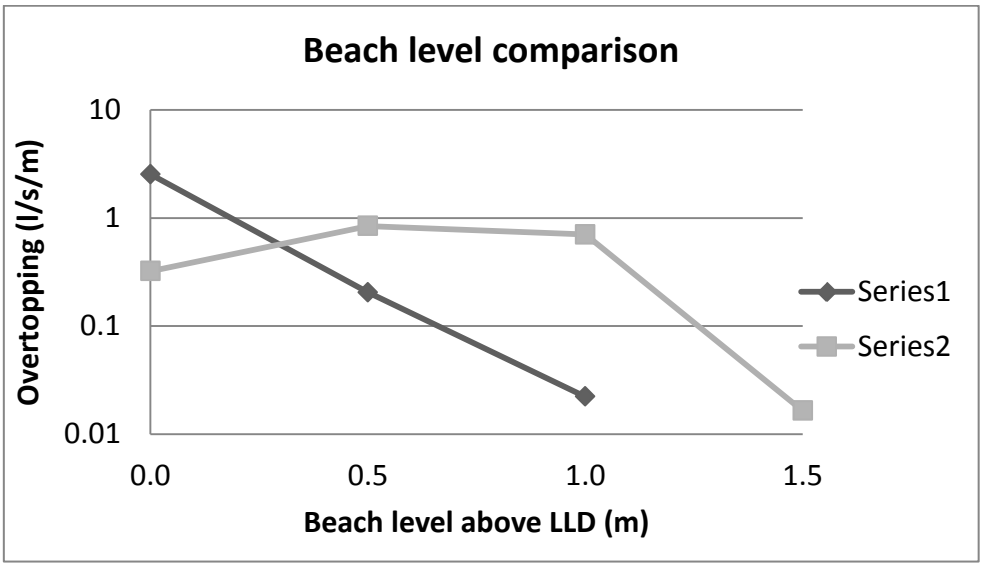

Figure 77: Beach level comparison

A comparison of overtopping and water depth at the back of the beach in Figure 78 shows that similar overtopping is experienced at a shallow depth since the waves from both Series 1 and Series 2 are broken and depth limited. Series 2 produced more overtopping in a water depth of 1 m than Series 1 even though Series 2 has a smaller wave input than Series 1. This is because Series 2 is no longer depth limited in 1 m water depth and the waves reach the recurve wall without breaking.

Series 1 remains depth limited and the overtopping increases linearly as the water depth increases while the overtopping of Series 2 decreases slightly towards a depth of 2 m since the wave height decreases in deeper water because the waves are less affected by wave shoaling.

As expected, the numerical modelling showed that for the same water level the offshore extreme wave conditions all produced the same wave height at the back of the beach. These physical model tests show that a smaller offshore wave height which would occur more frequently could produce more overtopping than the extreme wave heights for the same water level, if the beach level does not cause the smaller waves to break before they reach the back of the beach.

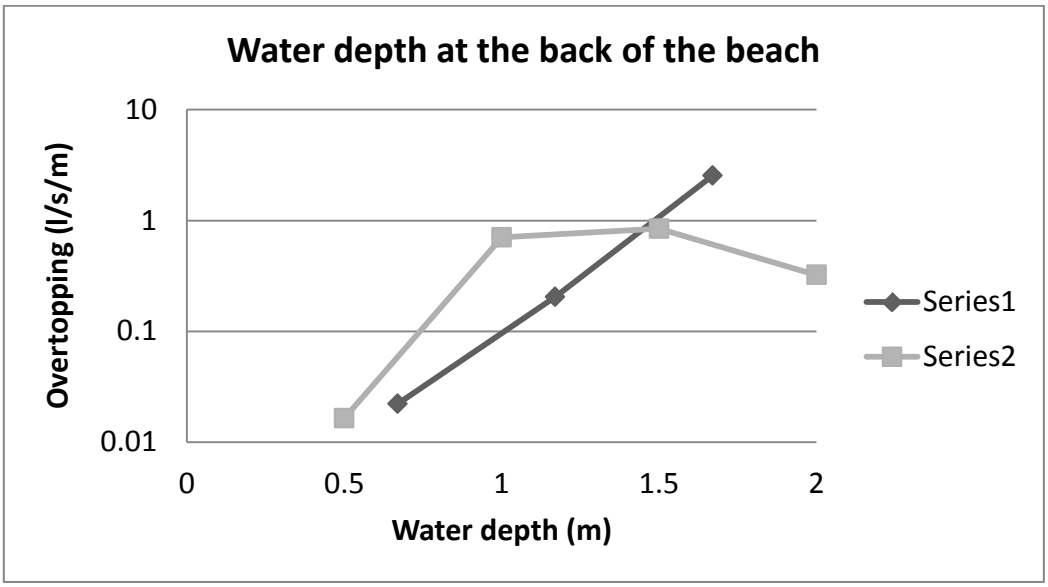

Figure 78: Comparison of water level

It is therefore important for beach maintenance purposes to know which beach level will result in a water depth at the back of the beach which would reduce overtopping for not only extreme wave conditions but also the more frequently occurring wave conditions.

7.2.2 Comparison of freeboard level

A comparison is made between different water levels and input wave conditions with varied freeboard levels. Tests of the previous study were done at a water level of LLD +1.67 m and LLD +2.16, and an input significant wave height of 1.7 m and 2 m respectively was used. The beach level for all the tests was kept constant at LLD +1 m. The water level of this study was kept at LLD +2 m and the input significant wave height of 0.6 m was used. The results of the tests are shown in Figure 79.

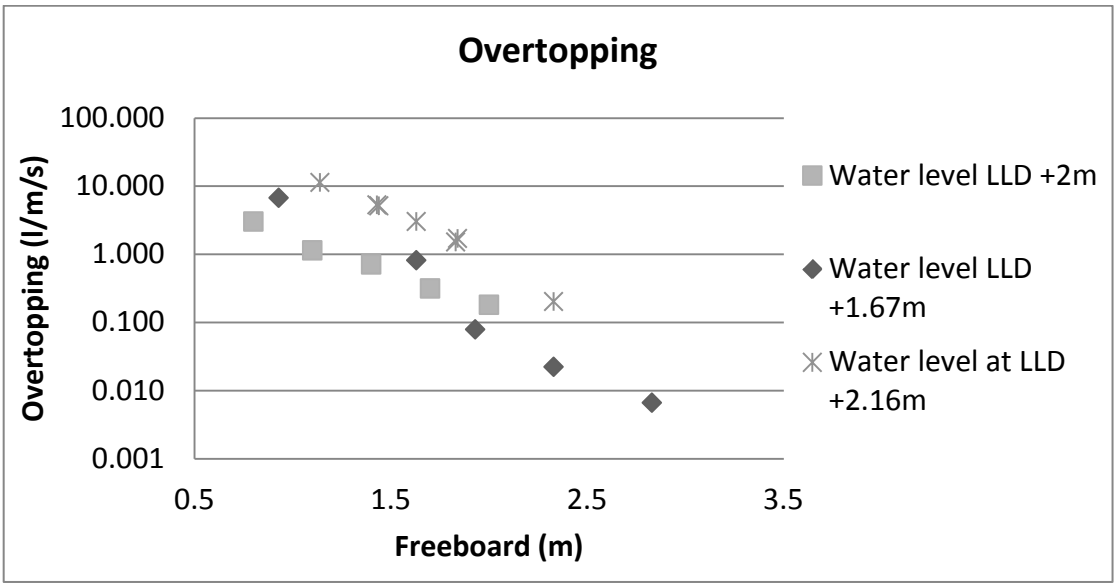

Figure 79: Overtopping of impulsive and pulsating waves

The overtopping results of the different tests are very similar but the rate of change in overtopping for varying freeboard differs between the previous tests and the tests of this study.

The waves of the previous tests were breaking and reforming before they reached the wall and were reduced in size but also ensured that a mixture of pulsating and impulsive waves reached the wall. It is well-known that impulsive waves of the same magnitude as pulsated waves produce more overtopping. This can be seen in Figure 79 as the overtopping results of the mixed waves conditions of the previous study are more sensitive to changes to the freeboard than the pulsating wave conditions of this study. This confirms that different overtopping equations should be used to calculate the overtopping rate based on the impulsiveness characteristics of the waves.

7.3 Trends

Overtopping is highly sensitive to changes in wave height. The wave height is influenced by the water depth at the back of the beach. Overtopping can be reduced by increasing the beach level which in turn reduces the water depth and limits the size of the waves that reach the back of the beach.

Using empirical calculations to determine overtopping can provide a good first estimate in determining the overtopping of vertical walls. Caution should be taken when using overtopping prediction tools to determine estimates of overtopping at

high ratios of R_c/H_{mo} since the results of the empirical calculations and prediction tools started to diverge from each other when the ratio was larger than 1.83.

Changes to the geometry of a vertical seawall can reduce overtopping significantly. The recurve wall used in this study showed a 54% average reduction of overtopping compared to a vertical wall. The recurve wall reduction calculated using Figure 11 was not accurate in estimating the actual reduction factor. Increasing the freeboard decreases the overtopping of both the vertical and the recurve seawall by the same rate. The reduction in overtopping was most effective with high ratio of R_c/H_{mo}.

Changes to beach level are only effective in reducing overtopping if they cause the waves to break before they reach the seawall. The beach level comparison between the previous study and this study showed that smaller offshore wave conditions that remain unbroken up to the seawall could produce more overtopping than extreme wave conditions which decrease in wave energy caused by wave breaking before they reach the seawall.

Differences were found in the rate of increase of overtopping between non-broken pulsating waves and a mixture of impulsive and pulsating waves. The overtopping rate of pulsating waves was less sensitive to changes of freeboard than a mixture of pulsating and impulsive wave conditions.

8 Overtopping solution for the Strand

Preventing overtopping while minimising the visual impact on pedestrians, residents and local businesses is difficult. A soft solution using beach maintenance on its own will not prevent the wave runup from reaching the area behind the seawall. A combination of beach maintenance and with an adequate seawall would reduce the severity and frequency of overtopping. The desired level of protection that is required depends on the amount of risk the public and the municipalities are willing to take.

According to Headland (2012), building a defensive structure for a 1:20 year overtopping event and then upgrading the structure after 20 years, would be cheaper than building now for a 1:100 year overtopping event. This would allow for adjustments to be made in accordance with the predicted rise in sea levels which has proved to be extremely difficult to quantify and predict with certainty.

The preferred solution for the Strand, purely from an overtopping point of view, would be to increase the beach level and adding a small recurve wall to the back of the beach to prevent wave runup from reaching the infrastructure behind the beach. It might not always be possible to increase the beach level if sand erosion is high or if it is not possible to source the necessary sand. However issues such as safety and aesthetics need to be taken into account in a broader study.

The wave height distribution along the Strand is not uniform and differs along the back of the beach. Therefore the crest level of the recurve wall is varied in order to offer only the required levels of protection. The significant wave height distribution was determined from the numerical modelling for different water and beach levels and results are shown in Figures 80-83. The average reduction factor for the recurve wall was used in combination with the empirical calculations (Equations 15, 16 and 17) from the EuroTop Manual (Pullen et al. 2007) to determine the wall crest level for each of the sections along the Strand for 1:20 and 1:100 year water levels with the beach level at LLD +1 m and LLD +1.5 m.

Based on the tests of this study, the recommended recurve wall crest height for allowing a maximum overtopping of 1 l/s/m to pass over the structure, at the given return period water levels, is shown in Table 29. The overtopping threshold was selected in order to allow trained staff to walk safely behind the seawall and for vehicles to drive slowly on the road.

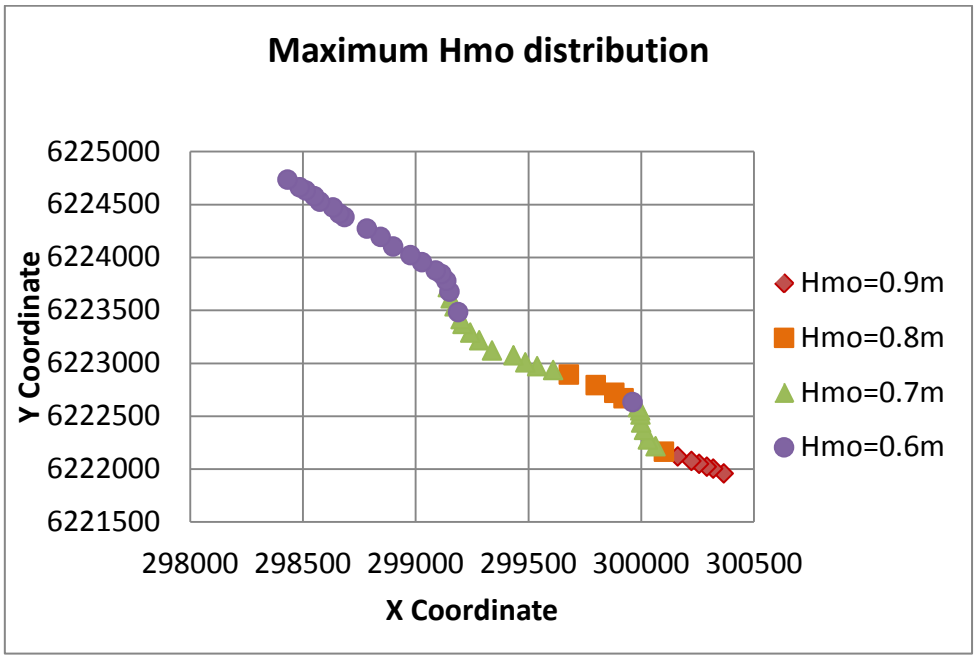

Figure 80: Beach level LLD +1 m and 1:20 year water level

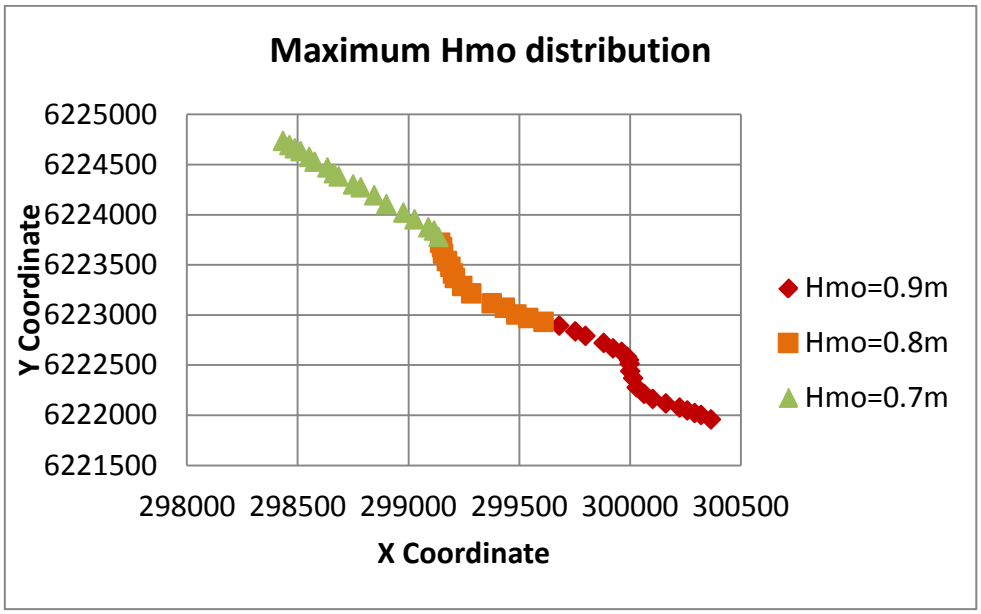

Figure 81: Beach level LLD +1 m and 1:100 year water level

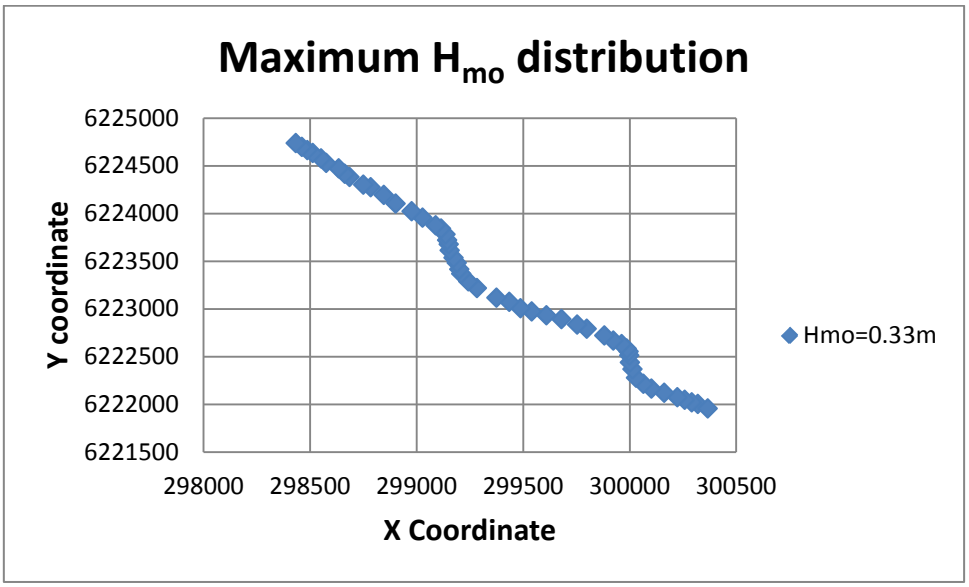

Figure 82: Beach level LLD +1.5 m and 1:20 year water level

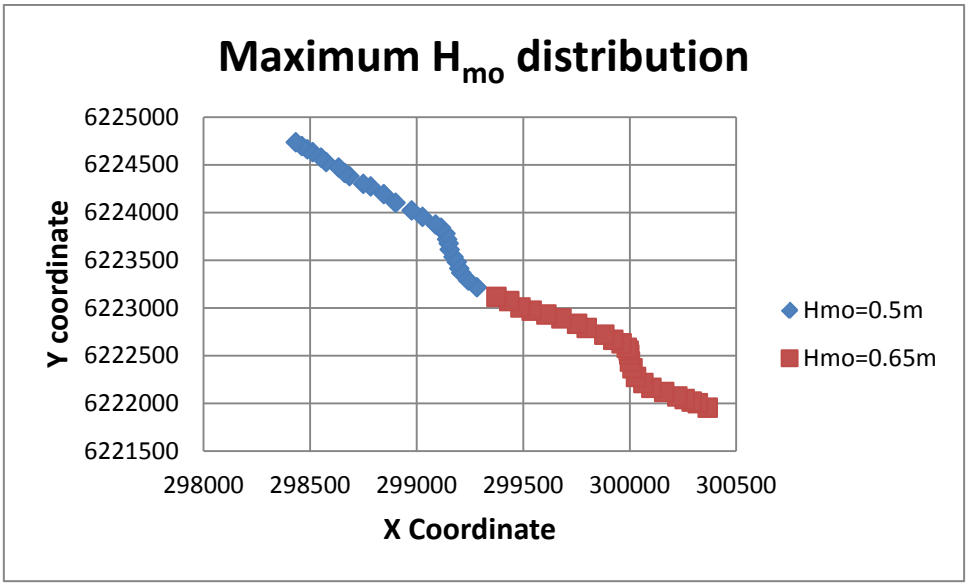

Figure 83: Beach level LLD +1.5 m and 1:100 year water level

Table 29: Recommended recurve wall crest level

1:20 year water level return period			
Beach level	**Location**	**Minimum recurve wall crest level above LLD (m)**	**H_{mo} max (m)**
LLD +1 m	A-D	3.1	0.60
	D-F	3.4	0.70
	F-G	3.7	0.80
	G-H	3.4	0.70
	H-I	4.0	0.90
LLD +1.5 m	A-I	2.4	0.33
1:100 year water level return period			
Beach level	**Location**	**Minimum recurve wall crest level above LLD (m)**	**H_{mo} max (m)**
LLD +1 m	A-D	3.1	0.70
	D-F	3.4	0.80
	F-I	4.2	0.90
LLD +1.5 m	A-F	2.9	0.50
	F-I	3.3	0.65

Figure 84: Reference locations A-I

9 Conclusion

This study confirmed that it is possible to reduce the overtopping considerably at the Strand by making use of a low recurve wall at the back of the beach. Factors that influence the overtopping rate were identified by making use of numerical modelling, overtopping calculations and physical modelling.

The numerical modelling revealed that the waves at the Strand are depth limited and therefore very sensitive to changes in water depth. The water depth could be reduced by increasing the beach level which would result in smaller waves reaching the back of the beach. The results of the numerical modelling related well with known areas that experience overtopping. It showed that the wave heights differ along the back of the beach of the Strand and the largest waves were found in those areas with the lowest beach level.

The extreme wave heights that were determined with an extreme value analysis were modelled with Delft3D-Wave and resulted in the same wave height at the back of the beach. This shows that at the same water level the regularly occurring wave height conditions are just as likely to cause overtopping as the extreme wave conditions.

The overtopping prediction tools and calculations could predict the measured overtopping of the vertical seawall when $R_c/H_{mo} \leq 1.83$ but the results of the methods began to differ when this ratio was increased. The empirical calculations showed that the overtopping is expected to increase with longer periods. Overtopping was also found to be very sensitive to changes in freeboard level.

The physical modelling showed that the measured overtopping of the vertical wall was reduced (by using the recurve wall) by an average of 54% for the tested range of $1.33<R_c/H_{mo}<3.33$. For the tested water level, the freeboard of the recurve wall was able to be approximately 25% lower than that of the vertical wall for the same overtopping rate. The recurve wall was found to be most effective in reducing overtopping at high freeboard levels.

The overtopping was again found to increase as the wave peak period increased but only up to a limit of 12 seconds, after which the waves started to break and cause a decrease in wave height which resulted in less overtopping. This indicates that extreme offshore wave conditions associated with longer wave periods are not expected to cause more overtopping than normal wave conditions on a similar water level.

The beach width and slope were tested with pulsating waves and it was found that the beach profile does have an influence on the overtopping rate. The beach profiles that were gently sloped (1:50) and wide produced more overtopping than the beach profiles that were steep (1:10) and narrow for non-breaking waves.

The physical modelling showed that increasing the beach level could increase the overtopping if the waves do not break because the wave height at the back of the beach will increase as a result of shoaling. Increasing the beach level will only decrease the overtopping when it causes the waves to break before they reach the back of the beach. Therefore, beach maintenance (replenishment of sand) needs to increase the low-lying areas along the Strand beach in order to restrict the maximum wave height that will reach the back of the beach.

10 Further research

A rise in sea levels will increase the severity of future storm conditions. Studies should be done to determine optimum recurve wall design ratios and how modifications could be made to existing seawalls to improve their efficiency in reducing overtopping.

More physical modelling should be done using recurve walls with large ratios of R_c/H_{mo} to improve the recurve reduction factor diagram of Pearson et al. (2004). This would be of great use when making first estimates of overtopping. A study should be done to determine if separate overtopping equations are required for seawalls with parapets and seawall with recurves.

A greater variety of beach slope and beach level tests are required for different wave breaking conditions to verify the results of this study. Additional physical modelling is required to distinguish between the influences that beach width and beach slope have on the overtopping results. For these tests the wave height should be measured at the toe of the structure to give additional information about how the wave is affected by these variables. It is also necessary to test both breaking and non-breaking wave conditions.

11 References

Abarbanel, H., Koonin, S. & Levine, H., 1992. Statistics of extreme events with application to climate. , 3481(703).

Allison, I. et al., 2009. *The Copenhagen Diagnosis*, The University of New South Wales Climate Change Research Centre (CCRC).

Allsop, N. et al., 2005. Hazards to people and property from wave overtopping at coastal structures. In *Proc. International Conference on Coastlines, Structures and Breakwaters*. pp. 153–165.

Allsop, N.W.H., 2009. Coastal Defence and Harbour Structures. *University of Southhampton*, (Supporting notes), pp.1–44.

Battjes, J., 1974. Surf similarity. In *Proc. 14th Coastal Engineering Conference, Am. Soc.* American Society of Civil Engineers, pp. 466–480.

Battjes, J. & Stive, MJ, 1985. Calibration and Verification of a Dissipation Model for Random Breaking Waves. *Journal of Geophysical Research*, 90(5), pp.9159–9167.

Besley, P., 1999. Overtopping of seawalls: design and assessment manual. *Environment Agency. Bristol, R & D Technical Report*.

Besley, P., Stewart, T. & Allsop, N., 1998. Overtopping of vertical structures: new prediction methods to account for shallow water conditions. In *Coastlines, structures and breakwaters: proceedings of the international conference organized by the Institution of Civil Engineers and held in London, UK, on 19-20 March 1998*. Thomas Telford, p. 46.

Booij, N., Ris, R.C. & Holthuijsen, L.H., 1999. A third-generation wave model for coastal regions: 1. Model description and validation. *Journal of Geophysical Research*, 104(C4), p.7649.

Bosboom, J. & Stive, Marcel, 2012. Coastal Dynamics I. *Delft University of Technology. VSSD.*, (Version 0.3), pp.161–163.

Bouws, E. & Komen, G., 1983. On the balance between growth and dissipation in an extreme depth-limited wind-sea in the southern North Sea. *Journal of Physical Oceanography*, 13, pp.1653–1658.

British Standards Institution, 2000. *British standard: maritime structures BS 6349*, British Standards, United kingdom.

CIRIA; CUR; CETMEF, 2007. *The Rock Manual. The use of rock in hydraulic engineering (2nd edition)*, C683, CIRIA, London.

Cape Town Collectables, 2012. Seawall with parapet at Cape Town [online image]. Available at: http://capetowncollectables.wordpress.com/2012/03/06/sea-point-promenade-where-the-city-and-the-ocean-meet/ [Accessed October 19, 2012].

References

Cape Town Gazette, 2008. Cape Town Storms in Helderberg Photos 2008 [online image]. Available at: http://capetowngazette.com/cape-town-storm-in-helderberg-photos-2008-953 [Accessed February 20, 2012].

Chawla, A., Spindler, D. & Tolman, H., 2011. WAVEWATCH III R Hindcasts with Re-analysis winds. *U. S. Department of Commerce National Oceanic and Atmospheric Administration National Weather Service*, pp.4–9.

Cornett, A., Li, Y. & Budvietas, A., 1999. Wave overtopping at chamfered and overhanging vertical structures. *Proceedings of the International Workshop on Natural Disasters by Storm Waves and Their Reproduction in Experimental Basins, Kyoto, Japan*, p.14.

DEFRA, 2006. Flood and Coastal Defence Appraisal Guidance FCDPAG3 Economic Appraisal Supplementary Note to Operating Authorities – Climate Change Impacts. *Department for Enviroment, Food and Rural Affairs*, pp.1–9.

DHI, 2009. EVA–Extreme Value Analysis–Technical Reference and Documentation. *Danish Hydraulic Institute Water and Environment. Denmark*, pp.8–69.

Deltares, 2011. Delft3D-WAVE. *Simulation of Sort-Crested Waves with SWAN User Manual*, 3.04, pp.10–120.

EAK, 2002. Ansätze für die Bemessung von Küstenschutzwerken. Die Küste, Archive for Research and Technology on the North Sea and Baltic Coast.

Edge, B.L., 1988. Coastal engineering. In Coata del Sol-Malaga: ASCE, pp. 899–913.

FireflyAfrica, 2012. Vertical seawall at P.E [online image]. Available at: http://2.bp.blogspot.com/_Dt7LueKRwF0/TMCk4AaocYI/AAAAAAAAEpQ/zkIAtvOt3YU/s1600/2010_10200009.jpg [Accessed October 19, 2012].

Franco, L., De Gerloni, M. & Van der Meer, J., 1995. Wave overtopping on vertical and composite breakwaters. In *Coastal Engineering Conference Proceedings*. ASCE AMERICAN SOCIETY OF CIVIL ENGINEERS, pp. 1030–1030.

Gayton, J., 2010. Vertical wall at Teignmouth [online image]. Available at: http://members.virtualtourist.com/m/pb/4a50e/9d51c/ [Accessed October 19, 2012].

Goda, Y, 2009. Derivation of unified wave overtopping formulas for seawalls with smooth, impermeable surfaces based on selected CLASH datasets. *Coastal Engineering*, 56(4), pp.385–399.

Goda, Y, 2010. Random Seas and Design of Maritime Structures Volume 33 of Advanced Series on Ocean Engineering. *Yokohama National University. World Scientific*, 33, pp.560–732.

Goda, Yoshimi & Kishira, Y., 1975. Laboratory investigation on the overtopping rates of seawalls by irregular waves. *Ports and Harbour Research*, 14(4), pp.4–39.

References

Hadewych, V., 2005. Neural network preddiction of wave overtopping at coastal structures. *PhD Thesis. University of Gent. Civil Department. ISSN 1377-0950*, pp.61–97.

Headland, J.R., 2012. Coastal/Port Structures & Sea Level Rise: Adaptive Management Approach. In *8th International Conference On Cosatal And Port Engineering In Developing Countries*. pp. 52–63.

Hedges, T.S., 2009. Wave Breaking and Reflection. *University of Liverpool. Department of Civil Engineering*, pp.1–3.

Hughes, S.A., 1993. *Physical models and laboratory techniques in coastal engineering*, London: World Scientific Pub Co Inc.

Hunter, I.T., 2005. Cape of Storms - August 2005. *Mariners Weather Log. South African Weather Service*, 43(3).

IPCC, 2007. *IPCC Fourth Assessment Report (AR4) - Working Group III: Climate Change 2007* S. Solomon et al., eds., Intergovernmental Panel on Climate Change.

IWEE, 2011. Physical Model Tests of the Strand Seawall Options. *Institute of Water and Environmental Engineering, Stellenbosch University. Report submitted to PD Naidoo & Associates for CoCT*.

Jury, M.R., 1984. Wind Shear And Differential Upwelling Along S W Tip Of Africa. *PhD Thesis. University of Cape Town. Department of Physical Oceanography*.

Kaminsky, G. & Kraus, N., 1993. Evaluation of depth-limited wave breaking criteria. In *2nd International Symposium on Ocean Wave Measurement and Analysis*. New Orleans, pp. 180–193.

Kim, Y., 2009. *Handbook of coastal and ocean engineering*, Los Angeles: World Scientific Pub Co Inc.

Kobelco, 2012. Flaring seawall at Kunigami [online image]. Available at: http://www.kobelco.co.jp/english/about_kobelco/csr/environment/2012/img/03_02.jpg [Accessed October 19, 2012].

Kortenhaus, A. et al., 2003. Influence of parapets and recurves on wave overtopping and wave loading of complex vertical structures. *ASCE 2004*, pp.369–381.

Marine Insight, 2012. Rock revetment and seawall at Galveston [online image]. Available at: http://marineinsight.com/wp-content/uploads/2010/12/galveston-seawall.jpg [Accessed October 19, 2012].

Metz, B. et al., 2007. Summary for policymakers. *Working Group I Report to the Fourth Assessment Intergovernmental Panel on Climate Change*, pp.1–18.

Miche, A., 1944. Mouvements ondulatoires de la mer en profondeur croissante ou decroissante. *Annales des Ponts et Chaussées*, Tome 114, pp.42–78.

References

Murakami, K., Irie, I. & Kamikubo, Y., 1996. Experiments on a non-wave overtopping type seawall. In *Coastal Engineering Conference Proceedings*. ASCE American Society of Civil Engineering, pp. 1840–1851.

NRC, 1987. Responding to Changes in Sea Level: Engineering Implications. *Committee on Engineering Implications of Changes in Relative Mean Sea Level. National Academy Press. Washington .D.C.*, pp.33–71.

PRDW, 2010. Climate Change Think Tank - Marine Inputs to Salt River Flood Model. *Prestedge Retief Dresner Wijnberg (Pty) Ltd Report Submitted to CoCT. No 1063/1*.

Patrick, M., 2005. Slope seawall with recurve at Nice [online image]. Available at: http://www.alpix.com/nice [Accessed October 19, 2012].

Pearson, J., Bruce, T. & Allsop, W., 2004. Effectiveness of Recurve Walls in Reducing Wave Overtopping on Seawalls and Breakwaters. *International Conference Coastal Engineering*, pp.4404–4416.

Pierson, W.J. & Moskowitz, L.A., 1964. Proposed Spectral Form for Fully Developed Wind Seas Based on the Similarity Theory of S. A. Kitaigorodskii. *Journal of Geophysical Research*, 69, pp.5181–5190.

Pullen, T. et al., 2007. *EurOtop Wave Overtopping of Sea Defences and Related Structures: Assessment Manual*, Die Küste. Online: www.overtopping-manual.com.

De Rouck, Julien, Verhaeghe, H. & Geeraerts, Jimmy, 2009. Crest level assessment of coastal structures — General overview. *Coastal Engineering*, 56(2), pp.99–107.

SANHO, 2011. False Bay survey data submitted to Stellenbosch University by South African Navy Hydrographic Office. *Unpubished. Cape Town*.

SANHO, 2012. *South African Tide Tables* A. Kampfer, ed., Tokai: South African Navy Hydrographic Office.

SAWS, 2011. Wind measurements for the Strand and Cape Town International Airport 2001-2011.

Smith, G. & Luger, S., 2003. EIA specialist study on the impacts of the container terminal expansion on shoreline stability. *CSIR Environmentek. ENV-S-C 2003-087*, pp.13–17.

Steel, K., 2011. Vertical seawall at Durban [online image]. Available at: http://www.kurtsteelphotography.com/photo_7611247.html#photos_id=7611192 [Accessed October 19, 2012].

The Telegraph, 2012. Vertical seawall at Weston-super-Mare [online image]. Available at: http://www.telegraph.co.uk/news/uknews/law-and-order/9241062/Pensioner-fell-to-death-over-sea-wall-after-council-deputy-

leader-brands-railing-plan-health-and-safety-gone-mad.html [Accessed October 19, 2012].

US, 2011. *Nearshore Wave Data of False Bay* J. Joubert, ed., Stellenbosch: University of Stellenbosch. Department of Civil Engineering.

USACE, 2006. *Coastal Engineering Manual* A. Morang, ed., Mississippi: US Army Corps of Engineers.

USACE, 1984. *Shore Protection Manual* 2nd ed., Vicksburg: Dept. of the Army, Waterways Experiment Station, Corps of Engineers, Coastal Engineering Research Center.

USACE, 2009. Water Resource Policies and Authorities Incorporating Sea Level Change Considerations in Civil Works Programs. *U.S. Army Corps of Engineers*, 1165-2-211, pp.10–21.

Van Doorslaer, K. & De Rouck, J., 2010. Reduction of wave overtopping on a smooth dike by means of a parapet. In *Proceedings of Conference on Coastal Engineering*. pp. 1–15.

Van Gent, M.R.A., Smale, A.J. & Kuiper, C., 2003. Stability of rock slopes with shallow foreshores. *Coastal Structures*, pp.100–112.

Van der Meer, J., 2002. Technical report wave run-up and wave overtopping at dikes. *Technical Advisory Committee on Flood Defence, Delft, The Netherlands*, p.43.

Van der Meer, J.W., Verhaeghe, H. & Steendam, G.J., 2009. The new wave overtopping database for coastal structures. *Coastal Engineering*, 56(2), pp.108–120.

Van der Waal, J.., 1992. Influence Of Wind On Overtopping. *Delft Hydraulics WL*, H1635WP, pp.10–23.Van der Meer, J., 1988. Rock slopes and gravel beaches under wave attack. *Ph.D. Thesis. Technical University of Delft. Delft Hydraulics Communication No.306. The Netherlands*.

Verhagen, H. & Mertens, M., 2009. Riprap stability for deep water, shallow water and steep foreshores. *ICE Coasts, Marine Structures and Breakwaters*, pp.1–10.

WJM, 2011. Topographical Survey-Beach Road. Plan number 1851/2. *Submitted to PD Naidoo & Associates for CoCT*.

WML Coast, 2011. Coastal Protection Works Strand. *Report submitted to PD Naidoo & Associates for CoCT. Cape Town*.

WSP, 2008. *Design drawings of temporary seawall protection (Provided by City of Cape Town)*, Cape Town.

Appendix

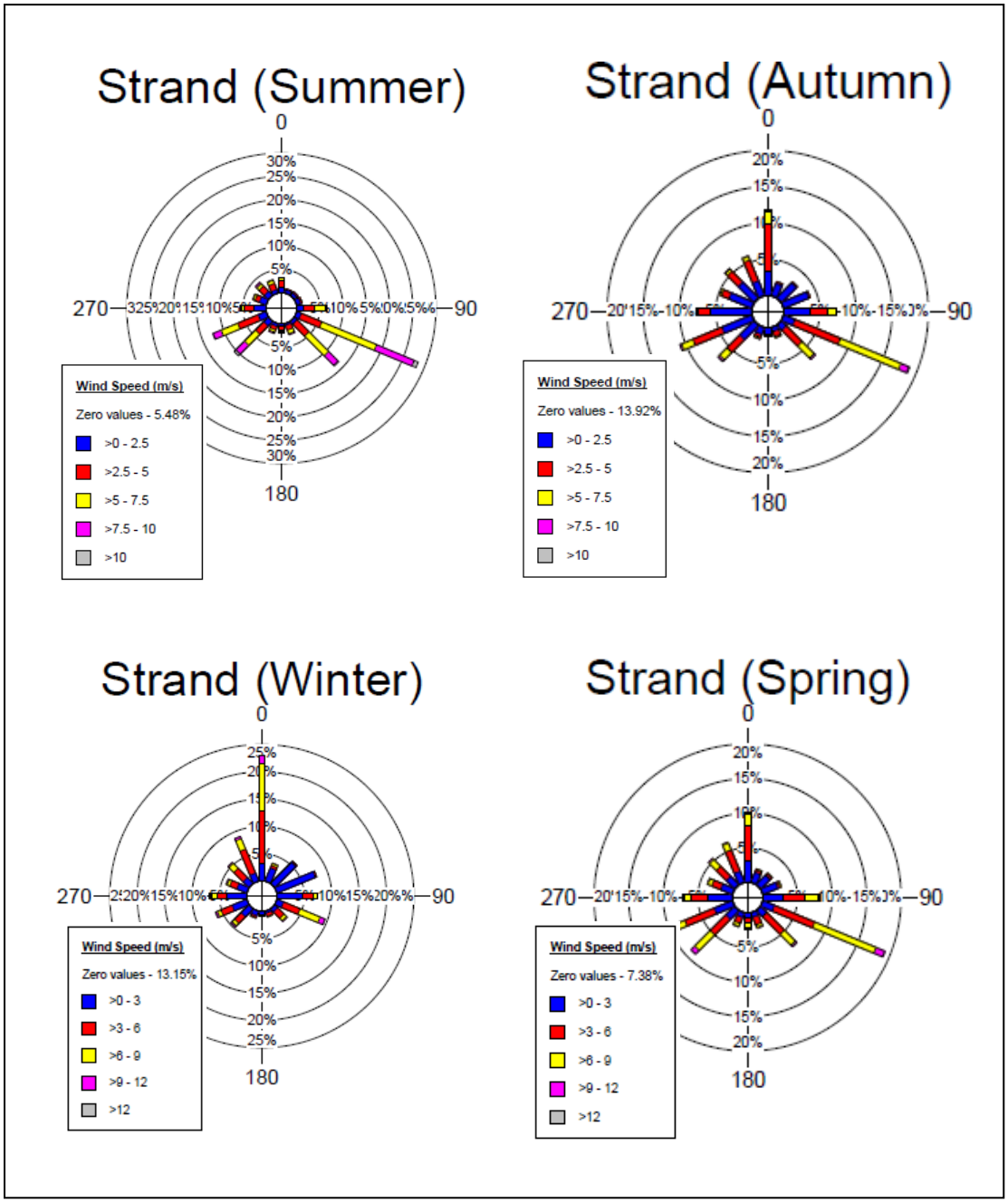

Figure A 1: Seasonal wind roses of the Strand

Appendix

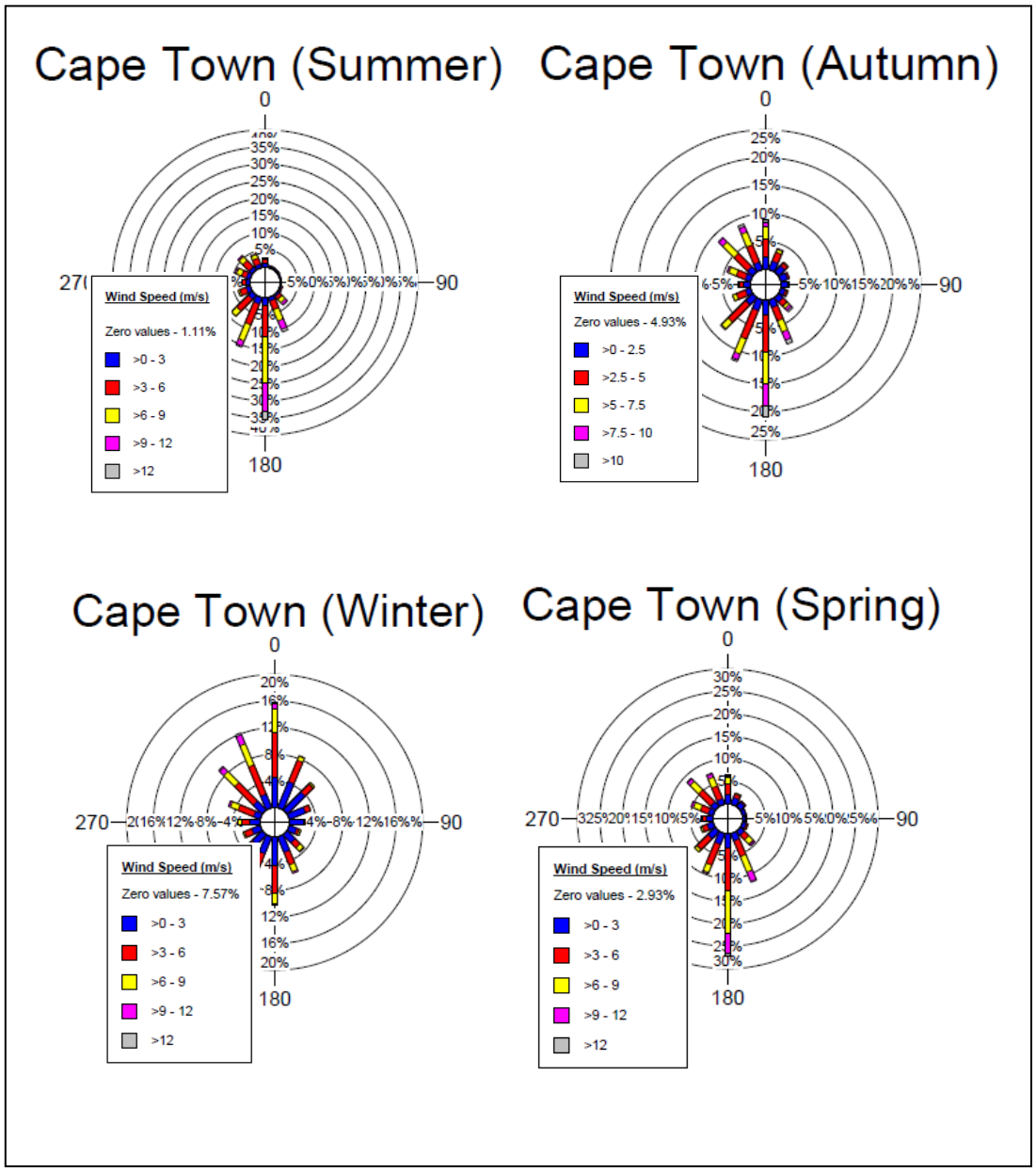

Figure A 2: Seasonal wind roses of Cape Town International Airport

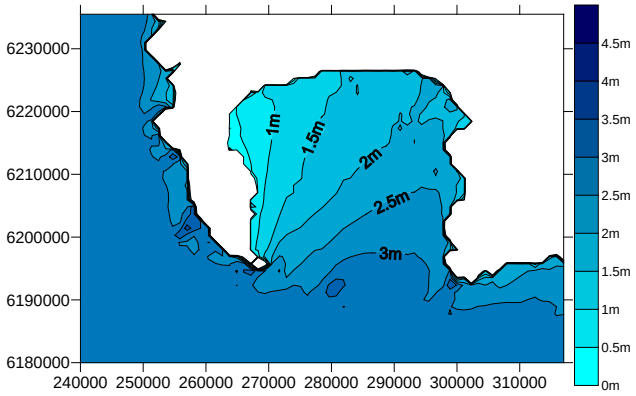

Figure A 3: Wave height distribution with 5 m/s SW wind

Appendix

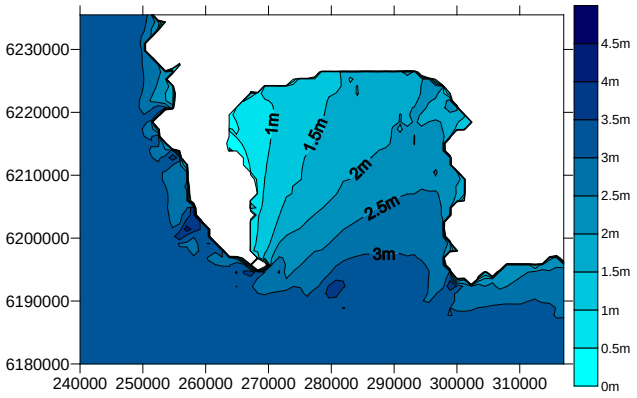

Figure A 4: Wave height distribution with 5 m/s S wind

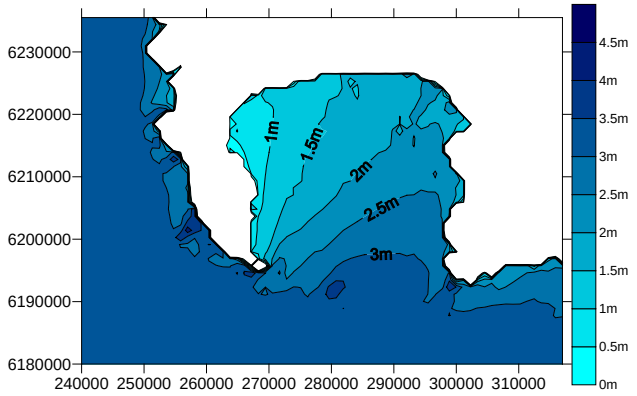

Figure A 5: Wave height distribution with 5 m/s SE wind

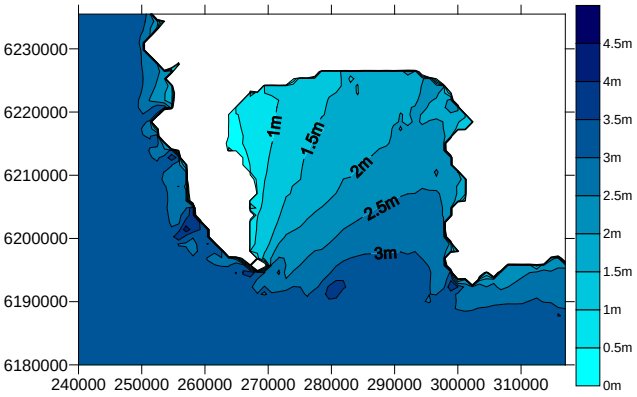

Figure A 6: Wave height distribution with 5 m/s N wind

Appendix

Table A 1: Accuracy Tests

	Test	Test 9.1	Test 9.2	Test 9.3	Test 12.1	Test 12.2	Test 12.3
	Period (s)	12	12	12	12	12	12
	Wall Type	Recurve	Recurve	Recurve	Recurve	Recurve	Recurve
	Slope	1/10	1/10	1/10	1/10	1/10	1/10
Prototype	**Beach level above LLD (m)**	1.00	1.00	1.00	1.00	1.00	1.00
	Crest level above LLD (m)	2.80	2.80	2.80	3.70	3.70	3.70
	Water level above LLD (m)	2.00	2.00	2.00	2.00	2.00	2.00
	Time (s)	12007	1200	12007	12007	12007	12007
	Wave height (m)	0.56	0.56	0.56	0.56	0.56	0.56
	Overtopping (l/s/m)	3.240	3.147	3.759	0.180	0.204	0.222

Table A 2: Comparative Test US20

	Test	Test US20	Test 28.1	Test 28.2	Test 28.3
	T_p (s)	12	12	12	12
	Wall Type	Recurve	Recurve	Recurve	Recurve
	Slope	1/50	1/50	1/50	1/50
Prototype	**Beach level above LLD (m)**	1.00	1.00	1.00	1.00
	Crest level above LLD (m)	3.30	3.30	3.30	3.30
	Water level above LLD (m)	1.67	1.67	1.67	1.67
	Time (s)	12003	12008	12008	12008
	Wave height (m)	1.70	1.70	1.70	1.70
	Overtopping (l/s/m)	0.022	0.024	0.021	0.027

Appendix

Table A 3: Comparative Test US19

	Test	Test US19	Test 29.1	Test 29.2	Test 29.3
	T_p (s)	12	12	12	12
	Wall Type	Recurve	Recurve	Recurve	Recurve
	Slope	1/51	1/50	1/50	1/50
Prototype	**Beach level above LLD (m)**	1.00	1.00	1.00	1.00
	Crest level above LLD (m)	3.60	3.60	3.60	3.60
	Water level above LLD (m)	1.67	1.67	1.67	1.67
	Time (s)	12008	12008	12008	12008
	Wave height (m)	1.70	1.70	1.70	1.70
	Overtopping (l/s/m)	0.078	0.075	0.068	0.061

Table A 4: Results of measured, CRESS and empirical calculations

	Test	Test 22	Test 18	Test 19	Test 20	Test 21
	Date	04/04/12	04/04/12	04/04/12	04/04/12	11/04/12
	Wall Type	Vertical	Vertical	Vertical	Vertical	Vertical
	Slope	1/50	1/50	1/50	1/50	1/50
Prototype	**Tp**	12	12	12	12	12
	Tmo-1	10.91	10.91	10.91	10.91	10.91
	Beach level above LLD (m)	1	1	1	1	1
	Crest level above LLD (m)	2.8	3.1	3.4	3.7	4
	Water level above LLD (m)	2	2	2	2	2
	Time (s)	12008	12008	12008	12008	12008
	Hmo measured (m)	0.55	0.58	0.58	0.6	0.6
	d or hs	1	1	1	1	1
	h*	0.013	0.013	0.013	0.012	0.012
	h*.Rc/Hmo	0.019	0.024	0.030	0.034	0.040
	Rc	0.8	1.1	1.4	1.7	2
	q Equ17 (l/m/s)	6.35	3.22	1.68	1.12	0.72
	q CRESS (l/s/m)	6.4	2	0.52	0.18	0.05
	q measured (l/s/m)	5.670	2.368	1.242	0.936	0.481

Table A 5: Results for NN overtopping tool, CRESS tool and empirical equations

		NN tool	Empirical calculation (Equation 17)	CRESS tool
R_c/H_{mo}	R_c (m)	Overtopping (l/s/m)		
0.83	0.5	15.54	22.14	33.35
1.00	0.6	11.20	13.53	21.62
1.17	0.7	7.88	8.93	14.02
1.33	0.8	5.43	6.22	9.09
1.83	1.1	1.72	2.63	2.48
2.33	1.4	0.56	1.37	0.68
2.83	1.7	0.18	0.81	0.18
3.33	2	0.07	0.52	0.05